University of Sussex

Impact of Radiative Decay on Cosmic String Dynamics at Small Scales

Stephanie Stuckey

Submitted for the degree of Master of Philosophy

University of Sussex

September 2010

Declaration

I hereby declare that this thesis has not been and will not be submitted in whole or in part to another University for the award of any other degree.

Signature:

Stephanie Stuckey

UNIVERSITY OF SUSSEX

Stephanie Stuckey, Master of Philosophy

Impact of Radiative Decay on Cosmic String Dynamics at Small Scales

Summary

Cosmic strings are topological defects appearing as extended solutions in many high energy physics scenarios. Observation of signatures expected due to the presence of cosmic string networks could provide critical evidence in distinguishing and constraining fundamental cosmological and particle physics theories.

Large scale evolution of cosmic string is well understood but the dynamics influenced by small scale structure remains unclear. Radiation back-reaction is expected to smooth strings, setting the scale of small structure and the size of loops produced. We undertake an investigation of cosmic strings numerically simulated from their underlying field theories, in particular we use the $U(1)$ gauge theory of the Abelian-Higgs model which radiates to massive modes and the global $U(1)$ theory of the Goldstone model which additionally radiates into the massless mode of the Goldstone field. By comparison to the emission of Goldstone bosons we can infer the effects of gravitational radiation, a further important energy loss mechanism for cosmological string, but difficult to simulate. We analyse the scaling properties of the string tangent vector correlation function and loop number density distributions which are expected to follow related power law forms and compare the results for gauge and global strings with a view to deciphering the influence of a massless degree of freedom on these attributes of network evolution. We find that the change in correlation function due to a massless mode can be incorporated by an effective value for the exponent of time by which the scale factor evolves whereby the smoothing due to back-reaction behaves like additional causal damping. From long gauge strings we find no evidence for direct 'core'-sized loop production, finding instead that our simulations favour radiation into the gauge and Higgs modes and fragmentation of horizon-sized loops.

Acknowledgements

Thanks to STFC for funding this degree and to my supervisor Mark Hindmarsh.

For the simulations I acknowledge use of the Sussex Archimedes HPC cluster and Cosmos, the UK national cosmology supercomputer. Additional thanks to Neil Bevis for allowing me to adapt the LAH algorithm and providing the LATfield library.

Contents

Chapter 1

Introduction

Despite the origins of time and space being shrouded in mystery, cosmology has become a mature subject and we have many observationally consistent theories to explain our beginnings. Much of what we know about cosmology comes from our understanding of gravitational physics on large astronomical/ cosmological scales. The very high energies needed for experiments to verify theories of the early universe are well out of reach of todays technology though with each passing decade we manage to get closer. So we look to the skies for data. From observational cornerstones like recession of galaxies, the smoothness of the cosmic microwave background (CMB) and primordial abundances of the light elements we are able to confirm or exclude our ideas. From such observations we are able to work with models that insist that our universe is expanding, is close to homogeneous and isotropic, that it has undergone an accelerated expansion in the past and that the geometry of our spacetime today is flat. The Einstein equations and our increasing collection of observations lead us to the standard model of cosmology, based on the Big Bang theory, and a working description of how our universe has evolved.

In the past when the universe was hotter, symmetries were unbroken and the field theories of particle physics were united. As Wienberg-Salam-Glashow have shown for the electroweak theory, the electromagnetic and weak forces are described by a combined theory at high energy. As our universe cooled and expanded the forces decoupled in a symmetry breaking phase transition and the bosons which mediate the forces acquire mass by the Higgs mechanism. It is possible that there is further unification in a single grand unified theory (GUT) at the energy scale

where the quantised theory of electrodynamics (QED) and the strong interactions, quantum chromodynamics (QCD) are expected to unite, $10^{16}GeV$. But we have not been able to extend the classical theory of general relativity at very high energy and microscopic length scales to fit the framework of a quantum theory so unifying gravity with the rest of the forces would require a new formulation. For this string theory is a strong contender, since all the forces and particles are encompassed and quantised by the one theory.

In many cases the physics behind the unification of forces and Big Bang cosmology lead naturally to topological defects. The cosmic string is one such class. They are extended solutions arising from the spontaneous symmetry breaking (SSB) of a non-simply connected vacuum manifold and found in many field theory particle physics and condensed matter models. In cosmology, the production of strings in this manner is called the Kibble mechanism. In string theory, it has more recently been recognised that the production of superstrings, shown to take on the role of cosmic strings in our visible 1+3 dimensional spacetime, can occur at the end of brane or hybrid inflationary models. As such, strings are a generic feature of the physics we use to describe our universe and observation of string signatures can lead to constraints on a variety of cosmological models and one of string theory's possible hopes of verification.

Cosmic strings have unique gravitational attributes which if detected could provide a window to high energy theories. Many gravitational observation experiments, both land and sky based, have and will be providing data over the coming years. From observations we hope to distinguish between signals from cosmic strings and the background of other gravitational perturbations but first we must identify what attributes and strengths of signals to look for. Fortunately the gravitational effects of strings are not model dependent so simple examples suffice as a starting point for theorists.

Simple networks of strings are formed in SSB of gauge and global U(1) field theories. They reach a scaling evolution where dynamical length scales evolve linearly with cosmic time so that the energy density in string becomes a constant small fraction of the total energy density. It is widely accepted that the energy density achieves this scaling regime through the formation of loops which detach from the

long string network, oscillate and decay. Sharp cusps are formed at sites where loops have broken off and kinks are formed when strings self intersect sending small waves moving out along the string. Oscillations of decaying loops emit gravitational radiation and their collapse produces bursts of particles, both providing possibilities for detection and constraints for cosmological models. Gravitational radiation bursts are also expected at cusps and as kinks of small scale structure interact.

Scaling is a very important aspect of cosmic string dynamics and evolution. One implication is that the typical size of loops produced will be a fixed fraction of the cosmological horizon but it is as yet inconclusive what this fraction is. If tiny loops are produced by the interaction of small scale structure on long string then the nature of the structure will determine the typical size and abundance of these loops. Gravitational radiation back reaction is expected to smooth out small scale structure on scales at a power of the dimensionless string tension $G\mu$ determined by the power spectrum of fluctuations on long strings, thus setting the scale for loop production. Once the loop size distribution is established, a picture of the possible observational signatures emerges. Overall, the large scale properties of simulated string networks scale without needing to include gravitational effects and here we develop a more precise understanding of small scale structure and the radiative processes which determine how strings in a realistic cosmological background might lose energy and reach a scaling evolution. From field theory simulations, that rely on few approximations especially at small scales, we begin to discover differences from this conventional scenario.

Motivated by the success of the approach by Polchinski and collaborators in the analytic modelling of small scale structure [70, 35], we inspect the structure of strings using field theory simulations that with ever improving computational power are now able to attain useful dynamical range. We study gauge strings of the Abelian Higgs model and global strings of the Goldstone model through the two-point tangent vector correlator and the loop distribution function. We find excellent agreement for the two-point tangent vector correlator for gauge strings, showing that its slope at short distances and the mean square velocity are related as predicted by their model. To increase our understanding of the radiative processes we look to global string which produces a massive Higgs and a massless Goldstone boson. The

backreaction from this massless radiation should be akin to effects from gravitons emitted when cusps annihilate and kinks collide, making strings smoother. However we are then intrigued by the similar nature of the small scale structure on global strings to their gauge counterparts. An extension to this model by Refs.[26, 54], hopes to explain the deviation at the smallest of scales found by other simulations and we discuss this in the context of our results. We also investigate the speed with which the network relaxes to scaling, and in particular how quickly the small scale structure appears.

Radiation from loops is independent of their size so it is important to know how many of them there are. For field theory simulations we calculate the number density distributions of loops from which the loop production function can be derived. The predicted form of the loop production function [70] is unfortunately less successful than the tangent vector correlation function, even after taking into account the fact that in field theory simulations loops lose energy and shrink at a constant rate.

Through their appearance in so many high energy physics and cosmological models there is a strong motivation on many fronts for a study of cosmic strings. We proceed by reviewing some fundamental large scale physics; the Einstein equations and some salient aspects of the standard model of cosmology which sets the scene for the production and large scale evolution of topological defects. We then discuss the finer details of cosmic strings as learned from both a full field theoretic approach and from useful approximations which help with analytic investigations of these non-linear problems. Finally we present the results of small scale structure and loop distributions in cosmic string networks able to radiate in both massive and massless modes.

1.1 Particle Physics

Particle physics is very successfully described with field theories and symmetry groups. The powerful Lagrangian formulation is commonly used to write down such theories, from which the action and Euler-Lagrange equations of motion can be calculated and particles are produced via the Higgs phenomenon, a symmetry breaking mechanism. When a symmetric configuration becomes unstable due to

a physical parameter reaching a critical value, the system moves to a new state randomly chosen from a set of degenerate states which are related by a symmetry transformation under which the Lagrangian density is invariant. In the broken symmetry state the fields are redefined and different physics is observable.

1.1.1 Topological Defects

Topological defects are formed if the vacuum manifold in a theory, the ground state at the minimum of the potential, has certain topological properties described by its homotopy groups. A homotopy group π_n is a set of mathematical mappings of an n-dimensional sphere onto the manifold. If π_n is non-trivial then the group can be spit into homotopy classes where the mappings can either be shrunk to a point or not. Where paths cannot be shrunk, the manifold is not simply connected, and defects can form where the path is trapped winding around the disconnected region.

The production of 1 dimensional strings will come from the symmetry breaking of some group G to a smaller group H such that the manifold $M = G/H$ has a homotopy group π_1 which maps a circle onto the manifold. π_1 is non-trivial if mappings of S^1 can encircle a hole in the manifold space so the mapping cannot be shrunk to a point and here the string is realised. $\pi_1(S^1) = Z$ since the mapping of S^1 on to the manifold can wind around the unconnected region an integer number of times.

So, a string can form when a complex scalar field ϕ in a $U(1)$ rotationally symmetric potential acquires a non-zero expectation value. For a quartic potential like shown in Fig. [1.1], the expectation value lies on a circle of degenerate minima, $\phi = \eta e^{i\theta}$. But the phase, θ, is not invariant under the U(1) symmetry of the theory under the transformation $\phi \to e^{i\alpha}\phi$ since $\theta \to \theta + \alpha$. Thus the symmetry is spontaneously broken and the defect forms as the phase of the field winds through 2π with the zeros of the field located in the middle forming an extended string-like configuration Fig. [1.2]. Topological defects are real physical phenomena observed in condensed matter systems, produced in spontaneous symmetry breaking (SSB) phase transitions just as cosmological evolution may have experienced. The standard model of particle physics is described by the gauge groups $G_{SM} = SU(3)_C \times SU(2)_L \times U(1)_Y$ with our current vacuum state $G_{vac} = SU(3)_C \times U(1)_{EM}$ having gone through a

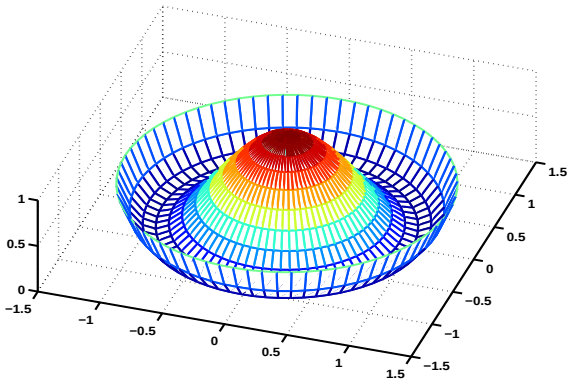

Figure 1.1: A ϕ^4 potential has a circular manifold of degenerate minima mapping trivially to S^1.

Figure 1.2: The string is a flux tube trapped as the phase of the field ϕ rotates through 2π.

cosmological phase transition. Therefore some large grand unified particle physics group G_{GUT} must be of at least rank four to undergo symmetry breaking into G_{SM}. A survey of grand unified gauge groups up to rank 8 showed that that all phenomenologically acceptable ones lead to the production of cosmic strings, [45].

Field theory cosmic strings produced in spontaneous symmetry breaking are solitonic, that is, objects which are solutions to the classical field equations. Their mass per unit length is fixed by the symmetry breaking energy scale η. When Abelian strings collide it is well established from studying the field theory dynamics that they always break and rejoin with opposite partners, resulting in an intercommutation. Thus their intercommutation probability is approximately unity. This process is a key contributor to the scaling energy attribute since intercommutation of a string with itself leads to the production of a loop which decays away.

The collision of cosmic superstrings on the other hand is a quantum-mechanical process. The intercommutation probability is less than one and depends on relative speed and angle. Despite this notable difference, cosmic superstrings have many properties in common with their solitonic cousins, with similar foundations for their dynamics and observational signatures.

1.2 Cosmology

1.2.1 Observation

The basis of modern cosmology is the Hot Big Bang hypothesis which relies fundamentally on the Copernican or cosmological principle that no point in the universe is in any way special. Galaxies outside our local group have been shown to be moving away from us and indeed all other points in space, which is the fundamental observation behind the notion of cosmological expansion. That everything in the universe is moving apart leads to the idea of a Big Bang.

The expansion of our universe is quantified by Hubble's law which simply relates the the velocity of the recession of a galaxy as proportional to the distance from its observer with Hubble parameter H. From the Hubble law $\mathbf{v} = H\mathbf{r}$ for a distance $\mathbf{r}$ comoving with the expansion rate $\mathbf{r} = a(t)\mathbf{x} \Rightarrow H = \frac{1}{a}\frac{da}{dt}$ where a is the scale factor of the stretching. As the universe expands, the maximum distance that photons can travel in a time t with a constant speed $c = 1$ is called the horizon distance and defined by

$$d_h = a(t) \int_0^t \frac{dt'}{a(t')}. \tag{1.1}$$

It is the largest distance over which events can affect each other. On scales large compared to d_h, the universe is smooth, homogeneous and isotropic and feels the effect of this expansion. On small scales that fall within the Hubble radius there is an obvious gravitational clumping of matter. How this happened, holds the key to our search for cosmological models today.

An important validation of hot big bang cosmology is its successful prediction of the abundances of the light element isotopes, in a theory known as Big Bang Nucleosynthesis (BBN). BBN marks the boundary of our testable knowledge of the early universe, but is highly predictive, simple physics. The relic abundances depend only on the baryon to photon ratio and the expansion rate at a temperature of around 1 MeV, and using wel-established nuclear physics, BBN predicts the abundances of D, ^{3}He and ^{4}He with great accuracy and to a lesser extent, though within reasonable bounds, ^{7}Li.

Another important prediction of hot big bang cosmology is the cosmic microwave background (CMB). At early times the universe was hot and ionised, and interactions

were rapid enough to keep most species of particle in thermal equilibrium. As the universe expanded and cooled, electrons and nuclei combined into neutral atoms and the universe became transparent to radiation, leaving a black-body thermal distribution of photons visible to us today at a temperature of 2.7K.

The CMB is smooth over the whole surface of last scattering which is far larger than the horizon at that time, approximately 380,000 years after the Big Bang. While justifying the homogeneity assumption of the cosmological principle, it is a puzzle how this homogeneity came about. This puzzle, known as the horizon problem, can be resolved by a period of accelerated expansion with $\ddot{a} > 0$ or inflation. This would have the effect of greatly increasing the horizon distance. To account for the volume over which the photons have equilibrated at last scattering, the universe must have inflated by about 60 e-folds, [56].

There are also small anisotropies in the CMB at a level of about 1 part in 10^5. Describing our universe requires that we understand these deviations from homogeneity as it is likely that gravitational instability acting on small initial fluctuations have generated cosmological structure. Inflation offers an explanation as it generates and amplifies scalar perturbations that could lead to structure formation and tensor perturbations in the metric which produce relic gravitational waves. In trying to determine these important signatures to understand inflation, it is vital to distinguish signals from the perturbations generated by inflation from other sources such as cosmic strings.

1.2.2 Friedmann-Robertson-Walker Universe

The spacetime of our universe is believed to follow the Einstein equations relating local space-time curvature to the energy-momentum of a matter source.

$$G_{\mu\nu} = R_{\mu\nu} - \frac{1}{2} g_{\mu\nu} \mathcal{R} = 8\pi G T_{\mu\nu} \tag{1.2}$$

where the Ricci curvature tensor $R_{\mu\nu}$ is defined as a summation over two indices of the Riemann curvature tensor,

$$R_{\mu\nu} = R^{\alpha}_{\mu\alpha\nu} = \partial_\alpha \Gamma^{\alpha}_{\mu\nu} - \partial_\nu \Gamma^{\alpha}_{\mu\alpha} + \Gamma^{\alpha}_{\beta\alpha}\Gamma^{\beta}_{\mu\nu} - \Gamma^{\alpha}_{\beta\nu}\Gamma^{\beta}_{\mu\alpha}, \tag{1.3}$$

The homogeneity of the universe coupled to the observed expansion leads directly to the simplest model for the spacetime metric of the universe, the Friedmann-

Robertson-Walker (FRW) metric

$$ds^2 = dt^2 - a^2(t)\, d\mathbf{x^2} \tag{1.4}$$

where $d\mathbf{x^2}$ is the metric of a 3-dimensional space with constant curvature.

A matter source is well described by a perfect fluid, whose energy-momentum tensor can be written $T^{\mu\nu} = \mathrm{diag}(\rho, -p)$. The cosmological constant, Λ, can be thought of as a contribution from some cosmological fluid with energy-momentum tensor $T_{\mu\nu} = \Lambda g_{\mu\nu}/(8\pi G)$, i.e. with negative pressure and equation of state $p = -\rho$. Current observations indicate that our universe is presently in a state of accelerated expansion, consistent with there being a non-zero cosmological constant.

CMB observations are also consistent with the 3-dimensional metric being flat, so that the metric is $g_{\mu\nu} = \mathrm{diag}(1, -a^2, -a^2, -a^2)$. Substituting this metric into the Einstein equations with a perfect fluid provides the cornerstone equations of standard cosmological evolution. The time-time components give the Friedmann equation

$$\left(\frac{\dot{a}}{a}\right)^2 = \frac{1}{3}\left(8\pi G\rho + \Lambda\right) \tag{1.5}$$

the space-space components give the acceleration equation,

$$\frac{\ddot{a}}{a} = -\frac{4\pi G}{3}\left(\rho + 3p\right). \tag{1.6}$$

and the covarient conservation of energy momentum is

$$\dot{\rho} + 3\frac{\dot{a}}{a}\left(\rho + p\right) = 0. \tag{1.7}$$

1.2.3 Inflation

As mentionsed in the previous section, inflation resolves the horizon problem, and it can also explain why the universe is so flat. The simplest model of inflation postulates that the energy-momentum of the universe was dominated at a very early stage by a homogeneous scalar field or inflaton with potential V. Its equation of motion is

$$\ddot{\phi} + 3H\dot{\phi} + V'(\phi) = 0 \tag{1.8}$$

where the Hubble parameter H is determined by the Friedman equation, which takes the form

$$H^2 = \frac{1}{3m_{pl}^2}\left(\frac{1}{2}\dot{\phi} + V(\phi)\right). \tag{1.9}$$

When the friction term dominates, $\ddot{\phi} \ll 1$, the inflation is slow and with a flat enough potential the rolling time $\frac{\phi}{\dot{\phi}}$ is long compared to the the expansion time $\frac{1}{H}$. In this case the energy density of the scalar field is dominated by the potential. From the Friedman equation it can be seen that the Hubble parameter is approximately constant for a slowly changing field, and thus behaves as if it had a cosmological constant (see Eq. (1.5)) of $8\pi GV$ and accelerates. The conditions for the potential to be flat enough to allow so-called 'slow-roll' inflation can be summarised as

$$\epsilon = \frac{m_{pl}^2}{16\pi}\left(\frac{V'}{V}\right)^2 \ll 1 \quad \text{and} \quad |\eta| = \left|\frac{m_{pl}^2}{8\pi}\frac{V''}{V}\right| \ll 1.$$

The number of e-folds, N, of inflation required to produce the observed smoothness and flatness of the universe, must be at least about 60 as mentioned in the last section.

Near the minimum of the potential, the slow-roll conditions fail so the inflaton overshoots and oscillates around the minimum. The oscillations of ϕ create particles and add a damping term to the equations of motion of $\Gamma_\phi \dot{\phi}$ where Γ_ϕ is the total decay width. The particles created as ϕ decays interact and thermalise, a process known as reheating.

Inflation can also explain the origin of density fluctuations observed in the CMB. Fluctuations produced by inflation are a mixture of scalar perturbations and gravitational tensor perturbations to the spacetime metric, which in a suitable gauge can be written, [13]

$$g_{ij} = a^2[(1-2\mathcal{R})\delta_{ij} + h_{ij}]$$

with $h_i^i = 0$ and $\partial_i h_{ij} = 0$. Here, $\mathcal{R}$ is called the curvature perturbation, describing the scalar metric perturbation, and h_{ij} is the tensor perturbation.

The curvature perturbation measures the spatial curvature of a comoving slice of spacetime and the power spectrum of fluctuations specifies the amplitude of each mode as it crosses the horizon,

$$\Delta_{\mathcal{R}}^2(k) \simeq \frac{1}{24\pi^2}\left(\frac{V}{m_{pl}^4}\right)\frac{1}{\epsilon}\bigg|_{N_k} = \Delta_{\mathcal{R}}^2(k_0)\left[\frac{k}{k_0}\right]^{n_s-1} \tag{1.10}$$

where n_s is the spectral index and k_0 is a reference or 'pivot' scale. The potential V and ϵ are evaluated at the e-fold number when the scale of interest is equal to the Hubble length (often called horizon-crossing), or $k = aH(N_k)$.

Gravitons are propagating modes associated with transverse ($h_{ii} = 0$) traceless ($\partial_j h_{ij} = 0$) tensor metric perturbations and each of the two polarisations (h_+ and $h_\times$) behave like minimally coupled scalar fields. The equations of motion follow from the Einstein equations and the two polarisations evolve independently according to

$$\ddot{h_\times} + 3H\dot{h_\times} + \left(\frac{h}{a}\right)^2 h_\times = 0, \tag{1.11}$$

and similarly for h_+. The spectrum of tensor perturbations due to inflation is

$$\Delta_T^2(k) \simeq \frac{2}{3\pi^2}\left(\frac{V}{m_{pl}^4}\right) = \Delta_T^2(k_0)\left[\frac{k}{k_0}\right]^{n_T} \tag{1.12}$$

and the tensor to scalar ratio of perturbations $r = \frac{\Delta_T^2(k)}{\Delta_{\mathcal{R}}^2(k)} = 16\epsilon$.

The spectral index for the scalar modes is related to the slow roll parameters by $n_s = 1 - 6\epsilon + 2\eta \sim 1$ and for the tensor mode by $n_T = -2\epsilon$.

A curvature perturbation can be equivalently described as an adiabatic perturbation in the energy density, where matter and radiation are effected equivalently. In higher density regions when the matter and radiation are coupled, compressing the radiation increases the temperature. The temperature of the universe is measurable in the Cosmic Microwave Background (CMB), which is relic radiation from when the matter and radiation decoupled: electrons and nuclei combined into neutral atoms, became stable and the universe became transparent to radiation. Competing with the instrinsic temperature fluctuations is the redshifting of photons as they climb out of potential wells from the high density regions. These fluctuations in temperature are seen as small perturbations in the intensity of the CMB, which are a very sensitive probe of the parameters of inflation [52]. For example, observations show that $n_s \sim 1$ [52], indicating that perturbations are scale invariant. This is consistent with slow roll inflation. The tensor mode contributions, detectable in priciple from CMB polarisation data, have not yet been seen and it is here that an understanding of the contributions from cosmic strings will be important.

Inflation is important in the chronology of defect formation. If strings are formed before inflation, they would be so dilute now that there would be little chance of finding any within our Hubble volume or of detecting any effect from them. This is a good thing for other topological defects such as domain walls or monoploes as they do not lose energy like strings so their energy density would grow, tipping the scales

of the Einstein equations to overclose the universe. Any symmetry breaking that produces this kind of defect are constrained to have occurred before the inflationary epoch. Conversely, a phase transition producing strings must be produced after inflation.

Chapter 2

Cosmic Strings

Cosmic strings formed as topological defects as a result of spontaneous symmetry breaking are complicated non-linear systems fully described by their underlying field theories. We will discuss two simple $U(1)$ theories with a single complex scalar field, one with a global symmetry and one with the scalar field coupled to a gauge field whereby the symmetry is local. Studying the complexity of their evolution thereafter can be simplified by making approximations, a vital approach for simulations before computing power was sufficient for full field theoretic evolutions with useful dynamic range. Extensive analysis of the Nambu-Goto approximation for gauge strings has yielded much understanding and here we bring together these results with field theory simulations. We outline some aspects of string evolution for which the approximations reflect the true evolution of the fields and where they seem to differ.

2.1 Field Theories

2.1.1 The Goldstone Model

The underlying field theory of a simple global string network in a cosmology with metric $g_{\mu\nu}$ is described by the Goldstone model with action,

$$S_G = \int \mathrm{d}^4x \sqrt{-g}\, \left[\partial_\mu\phi\partial^\mu\phi^* - V(\phi)\right], \tag{2.1}$$

for a complex scalar field ϕ in a potential $V(\phi) = \frac{\lambda}{4}(|\phi|^2 - \eta^2)^2$ where the self coupling is λ. The action of this theory is invariant under the global transformation

$$\phi \to e^{i\Lambda}\phi$$

for a constant Λ and has degenerate vacua with $|\phi| = \eta$ related by this global symmetry transformation. We say that the the vacuum state breaks the global symmetry. By decomposing ϕ into two real scalar fields, f and α such that $\phi = f(x)e^{i\alpha}$, we see that the Lagrangian density

$$\mathcal{L} = (\partial_\mu f)^2 + f^2(\partial_\mu \alpha)^2 - V(f) \tag{2.2}$$

Fluctuations of f around $\langle 0|f|0\rangle = \eta$ represent a massive field with $m \sim \sqrt{\lambda}\eta$ while α is a massless Goldstone boson. In the solution representing a straight sting, the phase of the field completes a "winding" of 2π at large distances from the string, and the sting is located where the field rises over the peak in the potential at $|\phi| = 0$. The region where the field departs from the minimumof the potential defines the core of the string whose width δ is determined by the Compton wavelength of the massive field m^{-1}.

The mass per unit length μ of the string is given by

$$\mu = \int \mathrm{d}^2x\, T_{00} \tag{2.3}$$

where the energy momentum tensor is calculated by variation of the action with respect to the metric

$$\begin{aligned} T_{\mu\nu} &= -2\frac{\delta\sqrt{-g}\mathcal{L}}{\delta g^{\mu\nu}} && (2.4)\\ &= \partial_\mu\phi\partial^*_\nu\phi - g_{\mu\nu}\mathcal{L}. && (2.5) \end{aligned}$$

Hence with large radius cut-off R

$$\mu = \eta^2 + \int_0^R \mathrm{d}r\, 2\pi r \left[\left(\frac{\partial f}{\partial r}\right)^2 + V(f)\left(\frac{1}{r}\frac{\partial \alpha}{\partial \theta}\right)^2\right], \tag{2.6}$$

where θ is the azimuthal angle. In the static string solution $\alpha = \theta$, and the third term gives a dominant divergent piece, which is

$$\mu \simeq 2\pi\eta^2 \ln\left(\frac{R}{\delta}\right) \tag{2.7}$$

2.1.2 The Abelian Higgs Model

The Abelian Higgs model is the simplest gauge field theory to admit conventional "solitonic" cosmic strings. The Lagrangian density is

$$\mathcal{L} = (D_\mu \phi)^* (D^\mu \phi) - \frac{1}{4g^2} F_{\mu\nu} F^{\mu\nu} - \frac{\lambda}{4}(|\phi|^2 - \eta^2)^2, \tag{2.8}$$

where ϕ is the complex scalar Higgs field, A_μ is the gauge field, $D_\mu = \partial_\mu + iA_\mu$ is the gauge covariant derivative, $F_{\mu\nu} = \partial_\mu A_\nu - \partial_\nu A_\mu$ is the field strength tensor, and λ and g are coupling constants. The Lagrangian is invarient under the gauge transformation $\phi \to e^{i\Lambda(x)}\phi$.

We can define gauge invarient fields $f = |\phi|$ and $\alpha_\mu = A_\mu + \partial_\mu \alpha$ in terms of which the Lagrangian density can now be written

$$\mathcal{L} = -\frac{1}{4g^2} F_{\mu\nu} F^{\mu\nu} + \frac{1}{2}\eta^2 A_\mu A^\mu (\partial_\mu f)^2 - V(f) \tag{2.9}$$

which reveals the gauge field acquiring a mass via the Higgs mechanism.

String solutions in this model [64] are well known and well studied. The phase of the Higgs field winds around $2\pi n$ ($n \in \mathbb{Z}^{\pm}$) as a closed loop is traversed through space and ϕ is forced to depart from the vacuum manifold over a tube of radius $\sim 1/\sqrt{\lambda}\eta$, inversely proportional to the linear mass density which is finite for Abelian Higgs string,

$$\mu = \int \mathrm{d}^2x \, T_{00} \sim \eta^2. \tag{2.10}$$

The gauge field, A_θ acts to compensate the winding, resulting in a pseudo-magnetic flux tube of radius $\sim 1/g\eta$. It is common to study the Abelian Higgs model at the Bogomol'nyi value of the couplings $\lambda = g^2$ [23] where the ratio of the scalar to vector masses is unity. The Goldstone model can be viewed as the extreme limiting case with the gauge coupling g going to 0.

The Euler-Lagrange equations of motion in a flat FRW universe,

$$g_{\mu\nu} = a^2 \mathrm{diag}(+1, -1, -1, -1),$$

are obtained from the variational principle in the temporal gauge, $A_0 = 0$

$$\ddot{\phi} + \frac{2\dot{a}}{a}\phi - D_j D_j \phi = -\frac{a^2\lambda}{2}\phi\left(|\phi|^2 - \eta^2\right) \tag{2.11}$$

$$\dot{F}_{0j} - \partial_i F_{ij} = \frac{2g^2}{a^2} Im\left(\phi D_j \phi^*\right) \tag{2.12}$$

where differentiation is with respect to comoving coordinates.

Clearly, there is great significance in the value of η, which is the field expectation value, the symmetry breaking scale and the string tension. As an example, strings produced at the Grand Unification energy scale have $\eta \sim 10^{16}$GeV, and gravitational coupling $G\mu \sim (\eta/m_{pl})^2 \sim 10^{-6}$. Cosmic string models are heavily constrained by their possible tensions with observations setting limits on the dimensionless parameter $G\mu$ and therefore the symmetry breaking scale of the models in which they are produced.

2.2 Effective Actions

2.2.1 Nambu-Goto Approximation

Ignoring radiation, relativistic gauge string can be described by the Nambu-Goto equations if the width of the string is assumed much less than the radius of curvature. On scales the size of the radius of curvature of the string, especially at later cosmological times, the string width is many orders of magnitude smaller. The action can then be approximated by the worldsheet traced out by the trajectory of a one dimensional object, the so-called Nambu-Goto action. Parameterising the worldsheet by a conformal time coordinate τ and a spatial coordinate σ along the string and denoting its spacetime coordinates $X^\mu(\sigma,\tau)$, the proper area element is the determinant of the worldsheet metric $\gamma_{ab} = g_{\mu\nu}\partial_a x^\mu \partial_b x^\nu$

$$\mathrm{d}A = \sqrt{-\gamma}\,\mathrm{d}\sigma\mathrm{d}\tau \tag{2.13}$$

For example in a non-expanding spacetime with $g_{\mu\nu} = \eta_{\mu\nu}$

$$\gamma = \det \begin{pmatrix} \dot{X}^2 & \dot{X}\cdot X' \\ \dot{X}\cdot X' & X'^2 \end{pmatrix}$$

where dot is differentiation with respect to the time-like coordinate, prime denotes differentiation with respect to the spatial coordinate and

$$dA = \sqrt{\dot{X}^2 \cdot X'^2 - (\dot{X}\cdot X')^2}\,\mathrm{d}\sigma\mathrm{d}\tau.$$

A relativistic string with mass per unit length μ has tension $T \sim \mu$ and the action for the string is

$$S_{NG} = -\mu \int \mathrm{d}A = -\mu \int d\sigma d\tau\, \sqrt{-\gamma} \tag{2.14}$$

Aligning the parameterisation so that the velocity $\dot{\mathbf{X}}$ is tangent to lines of constant σ, $\mathbf{X}'$ and $\dot{\mathbf{X}}$ are perpendicular and so $\dot{\mathbf{X}} = \mathbf{v}_\perp$. We adopt this transverse gauge to allow the string trajectory to be written in terms of the 3-vector $\mathbf{X}$. In a flat spacetime the worldsheet metric is conformally flat

We may choose the parameterisation of the worldsheet such that the worldsheet time $\tau = t$, where t is the coordinate time, and the 3-velocity $\dot{\mathbf{X}}$ is perpendicular to the 3-tangent vector $\mathbf{X}'$. In a flat spacetime we can also arrange that the interval $d\sigma$ has fixed energy $\mu d\sigma$, which turns out to be equivalent to $\dot{\mathbf{X}}^2 + \mathbf{X}'^2 = 1$. The flat spacetime action is then

$$S_{NG} = -\mu \int d\sigma dt \sqrt{(\mathbf{X}')^2(1 - \dot{\mathbf{X}}^2)} \tag{2.15}$$

and the equations of motion found from varying the action is a simple wave equation with constraints summarised as

$$\dot{\mathbf{X}}^2 + \mathbf{X}'^2 = 1 \tag{2.16}$$

$$\ddot{\mathbf{X}}^2 - \mathbf{X}''^2 = 0 \tag{2.17}$$

$$\dot{\mathbf{X}} \cdot \mathbf{X}' = 0 \tag{2.18}$$

In an expanding FRW universe, it is not possible to maintain the condition 2.16 and the equations of motion in the transverse gauge $\dot{\mathbf{X}} \cdot \mathbf{X}' = 0$ are

$$\ddot{\mathbf{X}} + 2\frac{\dot{a}}{a}\left(1 - \dot{\mathbf{X}}^2\right)\dot{\mathbf{X}} = \frac{1}{\epsilon}\left(\frac{\mathbf{X}'}{\epsilon}\right)' \tag{2.19}$$

where

$$\dot{\epsilon} = -2\frac{\dot{a}}{a}(1 - \dot{\mathbf{X}}^2)\epsilon$$

The legitimacy of the Nambu-Goto action as an approximation can be established more formally [39], with corrections only important when the extrinsic curvature is of order the string width, for example at cusps.

2.2.2 Kalb-Ramond Effective Action

For global string the situation is more complicated since there is no Higgs mechanism with the breaking of the global symmetry, leaving a long range interaction from the massless Goldstone boson. The energy in the massless field is high and the energy per unit length of the string is logarithmically divergent.

The massless scalar field of the boson can be related to a 2-index antisymmetric axion field [48, 55], $B^{\lambda\rho} = -B^{\rho\lambda}$ via Eq. (2.20) which will behave like a gravitational field.

$$\eta\partial_\mu\alpha = 1/2\,\epsilon_{\mu\nu\lambda\rho}\partial^\nu B^{\lambda\rho} \tag{2.20}$$

with field strength tensor

$$H^{\mu\nu\lambda} = \partial_\mu B^{\nu\lambda} + \partial_\lambda B^{\mu\nu} + \partial_\nu B^{\lambda\mu} \tag{2.21}$$

and action

$$S_H = \frac{1}{6}\int \mathrm{d}^4x\, H^2. \tag{2.22}$$

Approximating the string as a zero width world-line $X(\sigma,\tau)$ in string coordinates σ and τ, the Kalb-Ramond action describes global U(1)-string [48, 55, 99, 93]

$$S = S_{NG} + \frac{1}{6}\int \mathrm{d}^4x\, H^2 + 2\pi\eta \int \mathrm{d}\sigma^{\mu\nu} B_{\mu\nu} \tag{2.23}$$

where $\mathrm{d}\sigma^{\mu\nu} = \epsilon^{ab} X^\mu_{,a} X^\nu_{,b} \mathrm{d}\sigma\mathrm{d}\tau$, and the first term, S_{NG} is the effective action for Nambu-Goto string. This reveals that at large radius of curvature, the global string action becomes that of a Nambu-Goto string interacting with a massless field.

2.3 Evolution of Gauge Strings

2.3.1 Scaling

Since the original string scenario was introduced [49, 50, 91] a broad picture of the cosmological evolution of string networks has emerged, using a mixture of calculation, numerical simulation, and analytic modelling. Local cosmic strings form networks of infinitely long string and loops, where a string can be called "infinite" in cosmological terms if it is larger than the horizon. Infinite string takes the form of a random walk with correlation length $\xi \sim \xi$. The network evolves in a self-similar manner, keeping ξ at about the horizon scale, the important dynamical feature known as *scaling*. Scaling means that the energy density of infinite strings decreases as $1/t^2$, (t is cosmic time), and thus constitutes a constant fraction of the total. Yet, a major unsolved problem is the eventual destination of the energy in the infinite strings. This is of notable importance and greatly limits our ability to

constrain string scenarios via their decay products, such as gravitational waves or energetic particles. As the network evolves with string intersecting itself or crossing other strings, intercommutation occurs leading to loops of string being chopped out. Since the correlation length of the string is of order the horizon size, the loops of string chopped from the network, typically thought to be a small fixed fraction of the horizon size $\langle l \rangle = \alpha t$ will proceed to oscillate and decay. The problem is agreement on the value of α.It is often argued that it is determined by the typical size of small-amplitude oscillations on the long string network, called small-scale structure.[1]

Important generic features on strings are kinks and cusps. Kinks are sharp changes in the tangent vector, which are formed when strings intercommute. These discontinuities then resolve themselves into kinked waves travelling in both directions away from the intercommutation site. Cusps are points where the string instantaneously reaches speed of light, $|\dot{\mathbf{X}}| = 1$, producing a singularity in the shape of the string where the tangent vector vanishes, $\mathbf{X}' = \mathbf{0}$. The string is bent back on itself and has the opportunity to interact with itself over the length of the cusp region.

A string moves in its own gravity field which will affect the motion, a process known as back-reaction. The local self interactions result in a renormalisation of the string tension, completely analogous to the classical electron mass renormalisation. The remaining self interactions result in the emission of gravitational radiation and the damping of high-frequency waves on the string, with the result that kinks are rounded off, [41, 73]

2.3.2 Decay Mechanisms

Conventionally, three main energy loss mechanisms have been considered for gauge strings, all of which take place on loops which have broken off from the long string network.

The power emitted through gravitational radiation, P_g, from a sizeable oscillating string loop of length l and mass $m \sim \mu l$ can be estimated from its quadrupole moment $I \sim ml^2$ [98, 88].

$$P_g \sim G\left(\frac{d^3 I}{dt^3}\right)^2 \sim G\omega^6 I^2 \propto G\mu^2. \tag{2.24}$$

[1] We will return to this point repeatedly as the picture unfolds.

A defect core is a state of unbroken symmetry or 'false vacuum' and everywhere else the symmetry is broken. The Higgs and gauge fields are in their true vacuum states. The ultra high energy 'quanta' of Higgs and gauge field in the string, with $m_s = \sqrt{\lambda}\eta$ and $m_v = g\eta$ respectively, are released from the string if the topological stability of the string is removed causing the string to unwind. These conditions can occur at intercommutation, as loops evaporate or as cusps annihilate. During an intercommutation the string overlaps on a scale of order the width of the string $\delta \sim m^{-1}$, releasing energy $\mu\delta \propto \mu m^{-1}$. Then since $\mu \sim \eta^2$ the energy of $\frac{1}{g^2}$ particles of mass $g\eta$ is released per intercommutation. Thus the flux from this particular mode is down to the rate of intercommutation. Similarly, $\frac{1}{g^2}$ particles are released when a collapsing loop finally reaches a length $l \sim \delta$. The flux from this will depend on the fragmentation of loops as they die. Loops born with high harmonic number (e.g with kinks) are expected to rapidly fragment into core loop sized debris in a timescale of order L = length of the loop produced.

Perturbative production of particles from the coupling to the Higgs field for strings with $m \ll \mu^{1/2}$ can be calculated to produce a flux of high energy particles with power [83]

$$P_p = \mu(\eta l)^{-1}, \tag{2.25}$$

where l is the size of the loop.

Where string is overlapping in cusp regions, it can annihilate releasing energy in the form of high energy particles. The energy released depends on the length of the overlapping region which forms the cusp $l_c \sim (L\delta)^{1/2} = (L/\mu)^{1/2}$ creating a flux [22]

$$P_c \propto \mu(\eta l)^{-1/2}. \tag{2.26}$$

Purely based on the length dependence of these relations for the power output, gravitational radiation P_g is the dominant decay channel for loops of length $l > \delta(G\mu)^{-2}$, where δ the string core width. Below this length, cusp annihilation would be dominant. Much additional work has been done on the production of gravitational wave bursts at the sites of cusps on strings with and without additional small scale structure [31, 32, 80, 81]. Cusps on strings with small-scale structure are also sources of intense loop production [81, 35].

Numerical simulations using the Nambu-Goto approximation [4, 14, 5], seem to support this picture. Copious loop production was observed at scales a small fraction

of the cosmological horizon, $\langle l \rangle \sim \alpha t$. In the standard scenario α_{st} is determined from the power emitted in gravity waves such that $\alpha_{st} \sim \Gamma G\mu$ and also determines the characteristic wavelength of the small scale structure along the string as found in Nambu-Goto simulations in the presence of small-scale structure in the correlation functions of the long string. The small-scale structure is related to the creation of small-scale loops, but progress on understanding the connection has been slow.

It is crucial to establish the dominant length scale of loop production, as it controls both the amplitude and frequency of the gravitational wave signal, and the fraction of energy going into ultra-high energy cosmic rays. But there is a great deal of uncertainty over the loop population of cosmic string networks and Minkowski space Nambu-Goto simulations have been used to argue that loop production might even peak on the scale of the string width [97]. In light of this controversy, the typical loop length at birth is commonly parameterised by $\epsilon = \alpha/\alpha_{st}$ so that $\langle l \rangle = \epsilon\Gamma G\mu t$ though it is still under debate whether ϵ is dimensionless or itself a function of $G\mu$ or time.

Although it is clear that in the presence of kinks and cusps, the Nambu-Goto approximation is strictly not justified, it is assumed that gravitational radiation back-reaction will act to smooth the strings on a scale $l \sim (G\mu)^{1+2\chi}t$ [71], where χ is a small parameter defined below, and that large-scale properties will be reproduced correctly.

In the absence of back-reaction, Nambu-Goto simulations show that loops are produced at a small constant physical scale, which is most likely the initial correlation length of the network [75, 61, 67]. In Ref. [61] there is a claim that there are signs that this scale is growing, while Ref. [67] emphasises the significance of an apparently stable population of loops with sizes $l \sim 0.1t$, arguing that the peak at the initial correlation length will eventually disappear.

To resolve the kinks and cusps correctly, and include classical radiation as a form of energy loss, one uses the underlying field theory. While the conventional arguments given above emphasise gravitational radiation, omitted from all simulations, one should be able to see the other forms of energy loss and to check their scaling with loop size. However, previous field theory simulations [95, 62] found a scaling infinite string network without a significant population of loops. There appears to

be an energy-loss mechanism allowing the strings to scale, which has a different length dependence to any of those outlined above.

To see this, consider a string network whose spatial distribution scales with the horizon size such that the length of string in an horizon volume is $\sim t$. The energy density of the string network hence varies as $\rho_s \sim \mu/t^2$, which then requires the network to lose energy at a rate $|\dot{\rho}_s| \sim \mu/t^3$. Hence the rate of energy loss from a piece of string of size $\sim t$ is $P_s \sim \mu$. Thus a scaling network requires an energy loss mechanism which is independent of the size of the string, like gravitational radiation, but a factor $(G\mu)^{-1}$ stronger. One implication of the mechanism is that the length of a loop of string will shrink at a constant rate of order unity. This is verified in Sec. [4.1.2] and illusrated in Fig. [4.2] for Abelian Higgs string.

The detailed mechanism for this strong energy loss is not well understood. Attention has been focused on the production of 'core' sized protoloops [95, 62], which would nicely connect the Nambu-Goto and field theory simulations. Protoloops produced at the size of the string core width would quickly evaporate into classical radiation, and despite a large production rate would have a very low number density, which is easily estimated to be a few per Hubble volume [62]. In this scenario, field theory strings are behaving like Nambu-Goto strings in that loops are being produced at the smallest physical scale, which is in one case the string width, and the other the initial correlation length. While we see protoloops, we would expect them to be associated with long string, and as we will show, we are unable to find such a correlation. Their number density is also too low to account for the energy loss from long string. It may be that energy is being broken off in lumps which are too small to register as loops at all.

The idea of direct radiation raises a puzzle though. In order to create radiation in a mode with mass M, the field must be oscillating at a frequency $\omega \sim M$. A smooth string curved on the horizon scale H^{-1} is constructed from field modes with frequencies $\omega \sim H$. In view of the mismatch it was argued that gauge and Higgs radiation must be negligible [37]. Numerical simulations of smooth strings [66] show that radiation is indeed suppressed by a factor exponential in the ratio of the curvature radius to the string width. Nevertheless, simulations exhibit scaling behaviour at times when the network length scale exceeds the string width by a factor

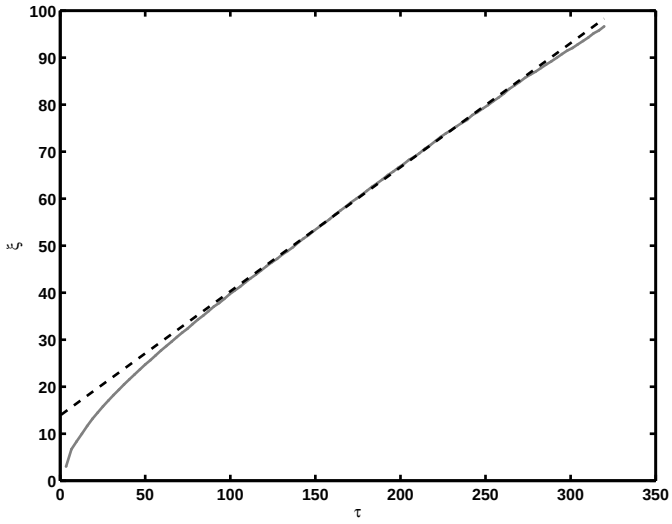

Figure 2.1: The comoving network length scale ξ (roughly corresponding to the radius of curvature of long string) for a 1024^3 lattice simulation in the matter era. The linear behaviour with conformal time τ is evidence for scaling extending to values of ξ nearly two orders of magnitude greater than the string width, which is of order unity in simulation units.

~ 50 [95, 62, 17], for example in Fig. [2.1] we see that this is confirmed to ~ 100 in our larger simulations. It should be noted that a similar puzzle was presented by the small size (compared with the horizon scale) of loops in Nambu-Goto simulations. Recent work by Polchinski and collaborators [70, 71, 35] has resolved the problem by showing how small-scale structure can give rise both to apparently smooth strings and to loop production at the small-scale cut-off on the string network.

Going beyond the Nambu-Goto approximation, which breaks down at the string width scale, we calculate with the underlying theory which for solitonic strings is its quantum field theory. Fortunately, quantum corrections appear to be small [24], and classical field theory should be a good approximation. Numerical simulations in the classical Abelian Higgs model [95, 62] showed that infinite string does indeed scale by losing energy into gauge and Higgs radiation (see Fig. [2.2]), although it was not established whether the decay proceeded via short-lived loops at the size of the string core width, or directly from the long strings themselves. In any case, no sign of copious loop production was found. In Ch.6 we present evidence that direct radiation is much more important than small loop production for Abelian Higgs

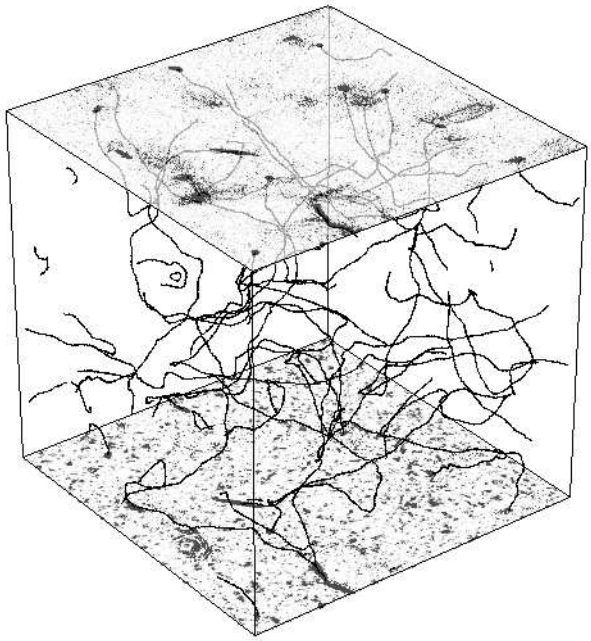

Figure 2.2: A snapshot from a simulation of a string network in the Abelian Higgs model. Lines show the centres of the strings, and the shading on the top and bottom faces represents magnetic field energy density and Higgs field potential energy density respectively.

string networks.

2.3.3 Kinks, Cusps and the Back Reaction Scale

As mentioned above, the intercommutation process generates kinks where the tangent vector changes sharply. Although the kinks are rounded off by Hubble friction and radiation reaction, we would expect the long string to experience a build up of small scale structure.

The interaction of the left and right moving ripples along the string are the source of gravitational radiation. This is seen from the linearised Einstein equations in the harmonic gauge $g^{\mu\nu}\Gamma^{\alpha}_{\mu\nu} = 0$, for a perturbation $h_{\mu\nu}$ to the flat metric

$$\Box\bar{h}^{\mu\nu} = -16\pi G T^{\mu\nu} \tag{2.27}$$

where $\bar{h}_{\mu\nu} = h_{\mu\nu} - 1/2\eta_{\mu\nu}h$. The energy momentum tensor for Nambu-Goto string as the source

$$T^{\mu\nu} = \mu \int \mathrm{d}\sigma\, \mathrm{d}\tau\, \left(\dot{X}^{\mu}\dot{X}^{\nu} + X^{\mu}X^{\nu}\right) \delta^4(x - X) \tag{2.28}$$

with $X^\mu(\sigma,\tau)$ the string position parameterised by worldsheet coordinates σ and τ.

Introducing null coordinates $u=\sigma-\tau$ and $v=\sigma+\tau$ we can decompose the string into left and right movers

$$X^\mu = \frac{1}{2}\left(a^\mu(u)+b^\mu(v)\right). \tag{2.29}$$

The Fourier transform of the energy-momentum tensor for the wave vector $k^\mu=(\omega,\mathbf{k})$ for a string loop of invariant length $L(=E/\mu)$ oscillating with period $2\pi/\omega=L/2$ is

$$T^{\mu\nu}(k) = \frac{\mu}{L}\int \mathrm{d}u\,\mathrm{d}v\,(\partial_u X^\mu \partial_v X^\nu + \partial_v X^\mu \partial_u X^\nu) exp(-ik\cdot X)$$

and we see that the waveform can be factorised so that

$$T^{\mu\nu} = \frac{\mu}{2}(U^\mu V^\nu + V^\mu U^\nu)$$

with

$$U^\mu(k) = \frac{2}{L}\int_0^L \mathrm{d}u \partial_u X^\mu exp(ik\cdot a) \tag{2.30}$$

and similarly

$$V^\nu(k) = \frac{2}{L}\int_0^L \mathrm{d}v \partial_v X^\nu exp(-ik\cdot b) \tag{2.31}$$

for the oppositely moving modes, which can be calculated separately.

Hence it is through the interaction of the left and right modes that gravitational radiation is produced. It is also apparent from the form of $T_{\mu\nu}$ that the length scale of the loops produced by a string network determines both the amplitude and frequency of the gravity waves produced.

The energy radiated per unit solid angle by a loop of string [77]

$$\frac{dP}{d\Omega} = 2G\omega\left(T^{\mu\nu}(k)T^*_{\mu\nu}(k) - \frac{1}{2}|T(k)|^2\right) \tag{2.32}$$

then using the left and right mover equations Eqs. (2.30-2.31) this can be expressed as [41]

$$\frac{dP}{d\Omega} = \frac{G\mu^2}{16\pi^2}\int_0^\infty d\omega\,\omega^2\{|U|^2|V|^2 + |U^*\cdot V|^2 - |U\cdot V|^2\} \tag{2.33}$$

$$\simeq \frac{G\mu^2}{16\pi^2}\int_0^\infty d\omega\,\omega^2|U|^2|V|^2 \tag{2.34}$$

since the last two terms will cancel when averaged over the short scale structure for real V^μ.

For an approximately straight infinite string the total power of gravitational radiation per unit length of string emitted by two colliding perturbations with small perturbations $\mathbf{U}_\perp(k_a)$ and $\mathbf{V}_\perp(k_b)$ of different wavelength with wavenumbers k_a and k_b is then given by [77, 41]

$$\frac{dP}{dl} \simeq \pi G\mu^2 \int \frac{\mathrm{d}k_a}{2\pi} \int \frac{\mathrm{d}k_b}{2\pi}(k_a + k_b)|\mathbf{U}_\perp(k_a)|^2|\mathbf{V}_\perp(k_b)|^2. \tag{2.35}$$

and the sum of the wavenumbers can be split such that

$$\frac{dP}{dl} = \frac{dP_a}{dl} + \frac{dP_b}{dl}, \tag{2.36}$$

where

$$\frac{dP_a}{dl} = \pi G\mu^2 \int \frac{\mathrm{d}k_a}{2\pi} k_a|\mathbf{U}_\perp(k_a)|^2 \int \frac{\mathrm{d}k_b}{2\pi}|\mathbf{V}_\perp(k_b)|^2, \tag{2.37}$$

with a similar expression for dP_b/dl.

Defining the wavelength to amplitude ratios as

$$\varepsilon_U^2(k_a) = |U(k_a)|^2, \quad \varepsilon_V^2(k_b) = |V(k_b)|^2 \tag{2.38}$$

we see that

$$\dot{\varepsilon}_{U(k_a)} \sim -\pi G\mu k_a \varepsilon_{U(k_a)} \bar{\varepsilon}_V^2. \tag{2.39}$$

where $\bar{\varepsilon}_V^2 = \frac{\mathrm{d}k_b}{2\pi}\varepsilon_V^2(k_b)$. A similar expression applies for $\dot{\varepsilon}_V(k_a)$. Comparing the lifetime of these modes to the Hubble time in that

$$\frac{\dot{\varepsilon}_U}{\varepsilon_U} \sim -\frac{1}{\tau_g}, \tag{2.40}$$

the mode with wavenumber k_b will be damped by expansion if $\tau_g < t$. If the integration extends to $k_b \sim 1/t$ where the amplitude and the wavelength are similar, then $\varepsilon_V^2 \sim 1$, leading to the original naive estimate that only wavelengths $\lambda > \mathcal{O}(G\mu t)$ will survive.

This is inconsistent, however, as there is an implicit assumption in the formula (2.35) that

$$\frac{\varepsilon^2_{U^2(k_a)} k_b}{k_a} \ll 1\,, \quad \frac{\varepsilon^2_{V^2(k_b)} k_b}{k_a} \ll 1 \tag{2.41}$$

otherwise gravitational radiation will be suppressed, [82]. This means that there is a lower cut-off in the integral defining $\bar{\varepsilon}_V^2$

Refs. [82] and [71] differ as to what the lower cut-off should be, and derived

$$\lambda > (\Gamma G\mu)^{(1+2\beta)/2} t \tag{2.42}$$

$$\lambda < (G\mu)^{1+2\chi} t \tag{2.43}$$

respectively, where the indices β and χ are defined from the power spectra as $\varepsilon_U^2(k_a) \sim k_a^{2\beta}$ or $\varepsilon_U^2(k_a) \sim k_a^{1+2\chi}$ in the two approaches.

2.4 Evolution of Global String

Global string evolves very differently from Abelian Higgs string. Most of the global string energy is contained in the Goldstone field rather than the string cores and they are able to decay via massless boson radiation. They experience a long range interaction with force $\propto \frac{1}{\xi}$, since no gauge field is present to compensate.

A mixture of Kalb-Ramond effective action and small field theory simulations [33, 29, 40, 101, 12] have established that dynamics of global string networks are strongly influenced by massless radiation, with lower densities, faster decay rates and higher velocities than Abelian Higgs string networks but that scaling was nonthe-less achieved. In simulations of Refs. [103, 100, 102], scaling was observed with loops typically produced at $\sim 0.48t$ in both radiation and matter eras.

2.4.1 Local Back Reaction Approximation

There remains the question of the influence of back reaction on the string evolution. Numerical calculations of the power of massless radiation from long global strings [9], show that strings emit radiation at the frequency at which they oscillate. Analytically, one can use the Kalb-Ramond effective action

$$\mu_0 \partial_a \left(\sqrt{-\gamma}\gamma^{ab}\partial_b X^\mu\right) = F^\mu = 2\pi\eta H^{\mu\alpha\beta}\epsilon^{ab}\partial_a X_\alpha \partial_b X_\beta \tag{2.44}$$

$$\partial_\mu H^{\mu\alpha\beta} = -2\pi\eta \int \mathrm{d}\sigma \mathrm{d}\tau\, \epsilon^{ab}\partial_a X_\alpha \partial_b X_\beta\, \delta^4(x - X). \tag{2.45}$$

By separating the force density, $F^\mu = (f^0, \mathbf{f})$, into a radiation and self field in order to absorb the self field, which diverges close to the string core, the equations of motion can be renormalised [27, 30]. Battye et al [10, 11], then calculate a form for the local back reaction force density due to the radiation field.

The massless scalar Green's function satisfie $\Box D = \delta^4(x)$ whereby the solution to an equation of the form $\Box F(x) = S(x)$ is given by

$$F(x) = \int \mathrm{d}^4x' D(x - x')S(x').$$

In flat space one can define the retarded, $D_{\rm ret}(x) = \frac{1}{2\pi}\theta(x^0)\delta(x^2)$, and advanced, $D_{\rm adv}(x) = \frac{1}{2\pi}\theta(-x^0)\delta(x^2)$, functions on the backward and forward light cones respectively where the Heavyside function $\theta(x^0) = 1$ for $x^0 > 0$ and 0 otherwise. Since the radiation field is 'free', a homogeneous Greens function can be used such that

$$D_{\rm rad}(x) = \frac{1}{2}(D_{\rm ret}(x) - D_{\rm adv}(x)) = \frac{1}{4\pi}\left(\theta(x^0) - \theta(-x^0)\right)\delta(x^2) \tag{2.46}$$

and the self field

$$D_{\rm self}(x) = \frac{1}{2}(D_{\rm ret}(x) + D_{\rm adv}(x)) = \frac{1}{4\pi}\delta(x^2). \tag{2.47}$$

In the Lorentz antisymmetric tensor gauge where $\partial_\mu B^{\mu\nu} = 0$, $\Box B_{\alpha\beta} = \partial_\mu H^{\mu\alpha\beta}$, the form for the separated fields ${H_{\mu\alpha\beta}}^{\rm self}$ and ${H_{\mu\alpha\beta}}^{\rm rad}$ can be calculated and lead to approximations for the force density:

$$f^{0,{\rm rad}} \simeq \frac{4\pi\Delta\eta^2}{3}\left[\epsilon^2\left(\frac{(\dot{\mathbf{X}}\cdot\dddot{\mathbf{X}})}{1-\dot{\mathbf{X}}^2}\right)\right] \tag{2.48}$$

$$\mathbf{f}^{\rm rad} \simeq \frac{4\pi\eta^2\Delta}{3}\left[\epsilon\ddddot{\mathbf{X}} - \frac{1}{\epsilon}\left(\frac{(\mathbf{X}'\cdot\dddot{\mathbf{X}})}{1-\dot{\mathbf{X}}^2}\right)\mathbf{X}'\right] \tag{2.49}$$

$$f^{0,{\rm self}} = -2\pi\eta^2\log\left(\frac{\Delta}{\delta}\right)\dot{\epsilon} \tag{2.50}$$

$$\mathbf{f}^{\rm self} = -2\pi\eta^2\log\left(\frac{\Delta}{\delta}\right)\left(\ddot{\mathbf{X}} - \frac{1}{\epsilon}\left(\frac{\mathbf{X}'}{\epsilon}\right)'\right) \tag{2.51}$$

The equations of motion can then be redefined in terms of the renormalised string tension

$$\mu(\Delta) = \mu_0 + 2\pi\eta^2\ln\left(\frac{\Delta}{\delta}\right) \tag{2.52}$$

for a cutoff of order the radius of curvature Δ. In the temporal transverse gauge, $X^0 = \tau$, $\dot{\mathbf{X}}\cdot\mathbf{X}' = \mathbf{0}$, the string equations of motion in flat spacetime, including backreaction, become

$$\mu(\Delta)\left(\ddot{\mathbf{X}} - \frac{1}{\epsilon}\left(\frac{\mathbf{X}'}{\epsilon}\right)'\right) = \mathbf{f}^{\rm rad} \tag{2.53}$$

$$\mu(\Delta)\dot{\epsilon} = f^{0,\ {\rm rad}} \tag{2.54}$$

with energy

$$E = \frac{\mu(\Delta)}{L}\int_0^L {\rm d}\sigma\epsilon$$

and the power radiated can be approximated by

$$\frac{{\rm d}P}{{\rm d}l} = -\dot{E} = \frac{1}{L}\int_0^L {\rm d}\sigma f^{0,\ {\rm rad}}.$$

We will apply this formula to the global string dynamics demonstrated in our simulations in Section 5.4.

Chapter 3

Detection

Testing for cosmic string is an indirect way to test high energy physics and cosmology models. Actually finding cosmic string would be a more direct way of constraining models but so far we have to be content with those arising from a distinct lack of any cosmic string signal and bounds then placed on the dimensionless parameter $G\mu$ which determines string tension and the energy scale of string production.

Cosmic string, if found, is likely to reveal itself through distinctive gravitational effects or by its radiated by products. Loops of string oscillate and decay, shrinking due to their tension, an energy loss mechanism producing gravitational waves, but we need to understand what is distinctive about a cosmic string compared to strong signals arising from inflationary perturbations or other strong emitters of gravitational waves.

Perturbations to the linearised metric due to a 'stiff' $T_{\mu\nu}$ to describe the defect can be decomposed into scalar, vector and tensor components which in turn decomposes the Einstein equations and all perturbation modes evolve independently.

Perturbations produced in the scalar modes by cosmic string produced at the GUT scale with $G\mu \sim 10^{-6}$ were initially thought to provide the right amplitude for large scale structure formation. Data from the CMB anisotropies subsequently showed that string tensions were restricted to $G\mu < 10^{-7}$ and that primordial density perturbations were more likely seeded by inflation. If there is a cosmic string presence it is likely they are formed at the end of SUSY hybrid inflation or Brane inflation at energy scales determined by a range of allowed $G\mu$, set by the available data and our understanding of possible string models. For instance, inflation that

occurred in the radiation dominated epoch that produced loops of cosmic string that decay predominantly gravitationally would have to have very low tensions to have survived to the present day.

Strings also emit massive particles and the balance of decay mechanisms constrains possible values for $G\mu$. If the tension is very low and the strings are very light, there is less gravitational radiation, bounded by avoiding overproduction of massive particles whose flux must be consistent with cosmic ray observations and BBN. Loops and long string causing vector perturbations in spacetime, could also potentially be observed through gravitational lensing or induced anisotropies in the CMB from vector and tensor perturbations.

There is a great deal of available and forthcoming astrophysical data to make use of. CMB anisotropies (WMAP and the awaited Planck), gravitational wave detectors (LIGO and LISA), weak lensing surveys (CLASS, LOFAR and SKA), pulsar timing experiments and BBN. In this section we discuss how a variety of data sets can be used to obtain constraints on possible string tensions. Here we keep our focus on vanilla cosmic string with intercommutation probability $p = 1$ rather than cosmic superstrings since the model dependant parameters begin to multiply. Even with these simple string models constraints are based on parameters in string scenarios such as the typical size of loop production or density distributions which remain ambiguous between models. The discrepancy in predictions for these in Nambu-Goto and Abelian Higgs field theory strings means the constraints on $G\mu$ can differ between these models, highlighting the importance of continued work on the basic but crucial aspects of these simple cosmic string models.

3.1 CMB

The Cosmic Microwave Background provides a window to the surface of last scattering. Combined data from WMAP (Wilkinson Microwave Anisotropy Probe), sub-orbital experiments and soon the Planck satellite can be mapped as a power spectrum of amplitudes over multipole moment $\ell \leq 3500$. The amplitudes of fluctuations perfectly describe the seeds for large scale structure formation with unique features of scale invariance, near gaussianity and synchronicity of formation sup-

porting the inflationary paradigm. Through seeking an insight into the energy scale or era of the production of these seeds for structure formation, we may meet new physics from GUTs, SUSY, dark energy, extra dimensions, quantum gravity or string theory. So along the way we can draw upon the physics of cosmic strings and their likelihood in so many of the predicted models for early universe evolution to help constrain the plethora.

Primordial gravity waves will appear as quadrupole anisotropies as they perturb the space in which electrons and photons are interacting at recombination, leaving an observable polarisation from Thompson scattering. Density perturbations can only affect the E mode polarisation but the B mode is dominated by the gravitational wave background with peaks in the spectrum at large angular scales and at decoupling though the amplitude is as yet undetermined. Calculations show that a distinctive signal due to cosmic strings in the polarisation B-mode is likely to peak at multipole $\ell \sim 600 - 1000$ [16, 69] and cannot be confused with inflationary tensor perturbations.

Cosmic strings can also create temperature variations though gravitational interactions with radiation and matter. A cosmic string moving across the sky with transverse velocity v will redshift protons moving in front of the string and blue shift photons moving behind it causing a discontinuity in the CMB temperature, known as the Gott-Kaiser-Stebbins effect Ref. [38, 46]

$$\delta T \sim 8\pi G \mu v T_{CMB}.$$

The spectrum produced by cosmic strings is wide and flat, clouded by contributions from the inflation model which follows the shape of the CMB spectrum with a large peak. However their total power contribution could account for as much as 10% [18, 68].

A strong signal due to cosmic strings is expected at high $\ell \approx 3500$ as has been recently calculated in [19] in light of forthcoming data at small angular scales from Planck. New CMB data will also be able to detect non-guassianities from gravitational instabilities evident in the bi- and tri-spectrum of temperature correlation functions. Non-gaussianity in the CMB is measured in terms of the non-linearity parameters $f_{NL} \sim \frac{\langle\zeta\zeta\zeta\rangle}{\langle\zeta\zeta\rangle^2}$ for the bi-spectrum and $\tau_{NL} \sim \frac{\langle\zeta\zeta\zeta\zeta\rangle}{\langle\zeta\zeta\rangle^3}$ for the tri-spectrum where ζ is the dimensionless primordial curvature fluctuation and these are ex-

tremely small. Contributions due to a cosmic string presence is expected to be strong [43, 42, 74] with non-linearities in the temperature correlation functions scaling with $G\mu$ as $f_{NL} \propto (G\mu)^{-1}$ and $\tau_{NL} \propto (G\mu)^2$.

3.2 Gravitational Waves

Loops, kinks and cusps are all sources of radiation. As the loops oscillate with frequency inversely proportional to their radius they create a stochastic background of gravitational waves and features like cusps and kinks emit radiation in bursts. A stochastic background from the superposition of incoherent bursts at cusps and kinks has also been calculated [65].

The power emitted in gravitational radiation by oscillating loops can be roughly estimated from the quadrupole formula as outlined in Sec. [2.3.2] at a rate $P = \Gamma G\mu^2$ with $\Gamma \sim 50 - 100$ expected.

Bounds are placed on $G\mu$ by finding a parameter space of excluded models depending on loop size distribution at production $\langle l \rangle = \epsilon(G\mu)t$. ϵ is a parameter that possibly depends on $G\mu$ but with an exponent that is still a matter of contention as discussed in Sec. [2.3.3] and essentially $\epsilon = 0$ in field theory simulations.

Pulsar timing experiments are measures of gravitational waves through the Kaiser-Stebbins effect induced by a string crossing the line of sight to a pulsar. Limits placed on the string tension are model dependant on string loop densities and gravitational radiation frequencies but data from Parkes Pulsar timing array, Arecibo and the Green Bank telescope have been combined [72] for the latest constraint by direct measure though this remains weak compared to the CMB constraints.

A cluster of small loops within the galactic halo could also create a gravitational wave background in the sensitivity band for LISA (0.1Hz - 10mHz) [34]

3.3 Lensing

Lensing due to strings can be classified either as strong lensing creating a variability in flux from objects like Galaxies, Quasars and Compact Radio sources or weak lensing in the vector modes which create image distortions or rotations.

A conical deficit, with characteristic Einstein angle $\Theta_E = 8\pi G\mu$, is produced around a straight cosmic string since the spacetime is locally flat but globally conical. Consequently, light from a source with a cosmic string in the way would be seen around both sides of the string thus appearing as a double image with its flux doubled. As the source passes through the Einstein angle, the flux varies. Due to the unusual nature of flat space around a string (or nearly flat, due to some small scale structure), the images would not be magnified plus further lensed objects would likely be seen along the string and therefore distinguish cosmic string from other gravitational lenses.

Lensing by loops depends on its size. If the loop is large compared to the deficit angle then on scales comparable to the image separation, the string acts like a straight string. For small loops much less than the size of the deficit angle, it acts like a point source with a Schwartzchild metric. Low tension/light strings gravitationally decay slower and therefore loops which decay predominantly by gravitational radiation have a longer lifetime. Smaller loops of light string ($G\mu < 10^{-12}$) with lengths less than a galactic size $\sim 0.1 d_{\rm h}$ will have their centre of motion damped by the expansion and are predicted to cluster [53, 25] much like cold dark matter and could exist in areas like the centres of galaxies with densities higher than their cosmological average. Then stellar sources with small angular size compared to the Einstein angle of the string will act as point sources with oscillations and relativistic motion of the string inducing fluctuations in the observed brightness of those stars. The latest results analysing variability in quasar brightness over many years from the Sloan Digital Sky Survey SDSS [85] has found no cosmic string like signal; setting a bound on $G\mu < 2.3 \times 10^{-6}$ which is weak compared to other observations but also set limits on the possible galactic density of loops at $\Omega_{loop} < 0.01$.

If clustering of loops increases densities sufficiently in the galactic halo then it may be possible to detect them via radio interferometer, [57]. Detection of lensing due to small cosmic string loops in the radio frequency by experiments like LOFAR and SKA could further constrain the parameter space of cosmic string models. According to Ref.[57], CLASS already rules out a large swathe of parameter space though their analysis relies on loop densities behaving according to the one scale model which has been shown not to be predictive of loop densities in field theory

simulations, [44].

A string with structure is longer than a smooth sting so that its mass per unit length, μ is reduced. String with a smaller tension would still still induce a weak lensing effect without the local spacetime around it being flat, causing a gravitational potential near the string. This could be seen as an elliptical distortion in the shape of background galaxies in the direction the projection of string onto the sky [36].

The distinctive vector perturbations of a moving wiggly string will also create rotations in the lensed image of background galaxies and create a specific power spectrum in the weak lensing of background galaxies that will not be generated by standard density perturbations [84].

3.4 Cosmic Rays

Ultra high energy cosmic rays have been detected and their origin is undetermined. Massive particles can be produced from string directly or during cusp and kink annihilations as outlined in Sec. [2.3.3]. This decay of topological defects in the early universe into massive particles which lose energy could account for some of the cosmic ray flux as described by the 'top-down' model in [21]. Experiments detecting cosmic rays, γ-rays and neutrinos can be used in comparisons to cosmic string models to set bounds.

The tension of cosmic string appears in a simple rate equation describing the flux of massive particles injected by string. The rate equation is model dependant relying on the string tension, as mentioned, the fraction of energy lost to massive particle production and the fractional size of the correlation length of the network compared to the horizon.

For a string network in a scaling regime, the correlation length $\xi = x_* t$ where $\dot{\xi} = x_*$ is constant. The energy injection rate per unit volume released in the form of particles emitted from cusps ρ_c as a fraction f_c of the total radiation $\dot{\rho_T} \propto \frac{\mu\dot{\xi}}{\xi^3}$ is

$$Q(t) = \frac{1}{a^3}\frac{\mathrm{d}}{\mathrm{d}t}\left(a^3\right) \sim \frac{f_c \mu}{t^3 x_*^2} \tag{3.1}$$

The model

$$Q(t) = Q_0 \left(\frac{t}{t_0}\right)^{-4+p}$$

where

$$Q_0 = \mu \left(\frac{t_0^3 f_c}{x_*^2} \right) \tag{3.2}$$

$$\Rightarrow \quad p = 1 \tag{3.3}$$

Digressing from vanilla string briefly, an important aspect of particle production from superstring networks is baryon production. For instance the U(1) symmetry breaking of $B - L$ at a scale η_{B-L} to produce strings light enough to form particles that can produce leptons in an out of thermal equilibrium CP[1] asymmetric decay. For $\eta_{B-L} > 10^{11} GeV$ and Yukawa coupling $h_1 > 0.01$, the particles produced by the strings have been shown to be able to account for the baryon asymmetry of the universe.

[1] charge-parity

Chapter 4

Simulations

The evolution of the equations of motion to simulate gauge and global string networks is outlined below. For the most part we show the intricate detail using the more complicated Abelian Higgs model since the Goldstone model can be considered as a limiting case with the gauge coupling set to zero. The code used to simulate the strings on the lattice will be referred to as LAH (Lattice Abelian Higgs) [17]. From the simulations we investigate small scale structure by extracting, over time, the values of the fields, the physical location on the lattice of zeroes in the scalar field at coordinates of non-trivial winding and the transverse velocity here. From the string coordinates we identify individual loops, calculating their lengths and number density distribution. For the topological core loops which are the smallest lengths of string that can be identified as a loop we calculate their proximity to other loops and long string. For long string we calculate the decay rate and the tangent vector correlations and fit them to the model of Eq. (5.17). We then compare the results for gauge strings where there is no massless mode for radiative decay with global string evolution which mimics gravitational effects through the ability to emit Goldstone bosons and suffer massless radiation backreaction.

4.1 Gauge Strings

The two fixed physical length scales determining the width of the string core, $1/\sqrt{\lambda}\eta$ and $1/g\eta$, must be resolved in any simulation of the string network but, in an expanding Friedman-Robertson-Walker universe, they rapidly fall away from the

other length scales that must also be resolved. Using comoving coordinates the horizon size is given simply by the conformal time τ and is the relevant length scale at which the super-horizon tangle of string begins to straighten and decay. However, the comoving string width decays as the reciprocal of the cosmic scale factor a and therefore as τ^{-1} in a radiation-dominated universe and τ^{-2} under matter- domination. We therefore need to resolve two scales which diverge as τ^3 under matter domination, which would, in principle, limit us to very short periods of simulation[1].

However in Ref. [17], a technique was demonstrated via which the coupling constants g and λ can be raised to time dependent variables:

$$\lambda = \lambda_0 a^{-2(1-\kappa)} \tag{4.1}$$

$$g = g_0 a^{-(1-\kappa)} \tag{4.2}$$

in order that the comoving string width r behaves as:

$$r \propto a^{-\kappa}. \tag{4.3}$$

That is, $\kappa = 1$ gives the true dynamics while $\kappa = 0$ yields a comoving string width, which is particularly convenient for simulation. The dynamical equations derived upon variation of the action become

$$\ddot{\phi} + 2\frac{\dot{a}}{a}\dot{\phi} - D_j D_j \phi = -a^{2\kappa}\frac{\lambda_0}{2}(|\phi|^2 - \eta^2)\phi \tag{4.4}$$

$$\dot{F}_{0j} + 2(1-\kappa)\frac{\dot{a}}{a}F_{0j} - \partial_i F_{ij} = -2a^{2\kappa} g_0^2 \mathcal{I}m[\phi^* D_j \phi] \tag{4.5}$$

(in the gauge $A_0 = 0$) with the A_0 variation yielding the quasi-Gauss' Law constraint:

$$-\partial_i F_{0i} = -2a^{2\kappa} g_0^2 \mathcal{I}m[\phi^* \dot{\phi}]. \tag{4.6}$$

Although these field equations do not conserve energy if $\kappa \neq 1$ (because the action is not time- translation invariant), the dynamics were shown in Ref. [17] to be insensitive to κ. Indeed the difference in their results for the two-point correlation

[1] That our simulations resolve the string width limits them in size to being far smaller than the horizon size at matter-radiation equality and therefore our simulations are also limited to much earlier times. However, we can simulate a matter dominated universe at very early times and use scaling to make statements about a matter dominated era at later times.

functions of the energy-momentum tensor between $\kappa = 1$ and $\kappa = 0$ in the radiation era, where $\kappa = 1$ was achievable, were found to be slight while their results for the CMB power spectra, which are dominated by the matter era, were found to be similarly insensitive to κ over the range 0 to 0.3, with the latter being the largest value at which reliable CMB results could be obtained.

Here we use the equations of motion Eqs. (4.4) and (4.5) with $\kappa = 0$ throughout, although we also check our results using simulations with $\kappa = 1$ for the radiation era (only), and find changes that are negligible. Note also that our equations of motion at $\kappa = 0$ are not precisely the same as those used in Ref. [62]. There the coefficients in the equations of motion that depend on the scale factor are changed independently but they do not relate those coefficients via a single parameter as we do. They keep the coefficient for the F_{0j} term fixed at 0.

4.1.1 Simulation Specifics

Eqs. (4.4) and (4.5) are discretised onto a lattice using the procedure described in Ref. [17] and referred to here as LAH.

Scalar field values lie on the vertex of the lattice and the tensor field values lie centred on the plaquette side joining two vertices. Time and space derivatives are taken in a standard numerically discrete way, the space derivatives then also sit half way along lattice sides. In the following, note that the index notation represents position on the lattice. The covariant gauge derivative is calculated

$$D_j\phi^{x+\frac{1}{2},j} = \sum_j \frac{\phi^{x+j} - \exp[i\Delta x A_j^{x+\frac{1}{2}j}]\phi^x}{\Delta x} \tag{4.7}$$

$$\sim \sum_j \left(\frac{\phi^{x+j} - \phi^x}{\Delta x} - iA_j^{x+\frac{1}{2}j}\phi^x \right). \tag{4.8}$$

This approximation allows it to be written in terms of a phase rotation θ

$$\theta_j^{x+\frac{1}{2}j,t} = \Delta x A_j^{x+\frac{1}{2}j,t}, \tag{4.9}$$

$$\theta_0^{x,t+\frac{1}{2}} = \Delta t A_0^{x,t+\frac{1}{2}} \tag{4.10}$$

so that in the temporal gauge with $A_0 = 0$ the field strength terms become

$$F_{0j} = \partial_0 A_j = \frac{1}{\Delta x}\sum_j \left(\frac{\theta_j^{x+\frac{1}{2}j,t+1} - \theta_j^{x+\frac{1}{2}j,t}}{\Delta t}\right), \tag{4.11}$$

$$F_{ij} = \partial_i A_j = \frac{1}{\Delta x}\sum_i\sum_j \left[\left(\frac{\theta^{x+\frac{1}{2}j+i} - \theta^{x+\frac{1}{2}j}}{\Delta x}\right) - \left(\frac{\theta^{x+\frac{1}{2}i+j} - \theta^{x+\frac{1}{2}i}}{\Delta x}\right)\right]$$
$$= \frac{1}{(\Delta x)^2}\sum_i\sum_j \Delta_{ij}^{x+\frac{1}{2}i+\frac{1}{2}j}. \tag{4.12}$$

The product is written

$$F_{ij}F_{ij} \sim \frac{2}{(\Delta x)^4}\sum_i\sum_j (1-\cos\Delta_{ij}), \tag{4.13}$$

since $1-\cos x \longrightarrow x^2$ as $x \longrightarrow 0$. The discretised fields ϕ, Π, θ and ϵ where

$$\Pi^{x,t+\frac{1}{2}} = \frac{\phi^{x,t+1} - \phi^{x,t}}{\Delta t}, \tag{4.14}$$

$$\epsilon^{x+\frac{1}{2}j,t+\frac{1}{2}} = \frac{\theta^{x+\frac{1}{2}j,t+1} - \theta^{x+\frac{1}{2}j,t}}{\Delta t}. \tag{4.15}$$

comprise all the required components to evolve the system according to the equations of motion using a 'leap-frog' algorithm outlined in Appendix A.

LAH is an extension from Minkowski space-time to flat FRW universes of the standard approach of Ref. [63]. This preserves the Gauss' law constraint to machine precision. Initial conditions were chosen following Ref. [17] in order for a string network to emerge rapidly and the Gauss constraint obeyed. To achieve the latter, we set to zero the gauge field and the time derivatives of both the gauge and Higgs fields. To achieve the former, we set the simulation start time such that the horizon is comparable to the (uniform) lattice spacing Δx and therefore the phase of the scalar field is an independent random variable on each lattice site, while we set $|\phi| = \eta$. We employ periodic boundary conditions and therefore the fields can be evolved forward reliably until the half-box crossing time for light.

We use a lattice spacing of $\Delta x = 0.5$ and set $\eta = 1$, $\lambda_0 = 2$ and $g_0 = 1$, which together guarantee that strings are resolved for all a when $\kappa = 0$ and for $a \lesssim 1$ in the radiation era when we double ckeck against the true equations of motion with $\kappa = 1$. Note that the above scalings leave the ratio $\lambda/2g^2$ constant and we study the model at the Bogomol'nyi value [23], which yields equal scalar and gauge masses. The simulations were performed using the UK National Cosmology supercomputer

[1], with parallel processing enabled via the LATfield library [15], using a lattice size of 512^3 for Abelian Higgs simulations and averaging over 20 realisations. Global string and additional Abelian Higgs simulations using a 768^3 lattice were performed on the University of Sussex HPC Archimedes cluster.

We have been able to access a dynamic range of similar order to Nambu-Goto simulations performed by other groups working on small scale structure issues but due to the differences between the simulations the measures for dynamic range that are suitable in one case are ambiguous in another, making this a difficult comparison. On N^3 lattice volumes with $\Delta x = 0.5$, a network of strings of width $\delta \sim 1$ is fully formed from conformal time $\tau_i \sim 20$ and is simulated until $\tau_f = N\Delta x/2$, when the periodic boundary conditions of the simulation volume can potentially be felt. Checks of the full energy-momentum tensor indicate that scaling is achieved at around $\tau_{sc} \sim 64$ for lattices with $N = 512$, [17].

One measure of dynamic range is $\xi(\tau_f)/\delta \sim 50$, which contains measurable quantities in our simulation. This can be compared with the ratio of the initial and final correlation lengths, (~ 100 [75, 67]) in Nambu-Goto simulations although the initial correlation length has no straightforward meaning in our simulation. Another measure is the ratio of the final time to the time at which the network achieves scaling. For us, $\tau_{sc} \sim 64$ gives us a dynamic range of about 2 (in conformal time) for our 512^3 simulations and about 3 for 768^3 lattices. Nambu-Goto simulations [75] estimate a dynamical range of 5 from the scaling of the energy density of long string in the radiation era.

4.1.2 String length measurements

At intervals during the evolution we record the coordinates of lattice plaquettes around which the phase of ϕ has a net winding number.[2] As a first approximation we then take it that a segment of string having length Δx threads through each plaquette of 2π winding and joins the centres of the lattice cells on either side. From these segments we can then construct the path of the string, although since it is composed of an array of perpendicular lengths the string length is overestimated.

[2]While a winding of the phase is gauge-invariant in the continuum, on a lattice it can be removed by a finite gauge transform. Therefore we employ the gauge- invariant measure of Ref. [47].

At this stage, we do not attempt to smooth the paths in order to compensate, as in Refs. [95, 62, 20], but instead apply a Scherrer-Vilenkin correction of $\pi/6$ [79] to such length measurements.This factor is the ratio between the lattice approximation and the true length of the line $\phi = 0$ for a two-component Gaussian random field ϕ. The scalar field is not a Gaussian random field, and so the estimate will not be completely accurate for our dynamic string network. However, the results for the average string length density are in approximate agreement with that measured using the Lagrangian density Fig. [4.1]. This second method makes use of the fact that perturbative radiation makes zero contribution to $\mathcal{L}$, while a static straight string contributes at $-\mu$ per unit length density. Since $\mathcal{L}$ is a four-scalar and length density picks up a γ-factor upon a Lorentz transform, then $-\int \mathcal{L} d^3x/\mu$ is a measure of the (invariant) string length [17].

Rather than use the (comoving) string length density directly, we instead compare with the network length scale ξ, defined as:

$$\xi = \sqrt{\frac{V}{L}}, \tag{4.16}$$

where V is the reference volume and L the string length within it. For a scaling network $\xi \propto \tau$. In Fig. [4.1], we plot both the Lagrangian measure result $\xi_{\mathcal{L}}$ and the winding measure result ξ (with no subscript since it is our default measure), which reveal a linear behaviour $\xi \propto (\tau - \tau_{\xi=0})$ after an initial transient, consistent with the expected scaling. As pointed out in Ref. [17], there is nothing fundamental about the value of $\tau_{\xi=0}$ and it is simply an artefact of the initial conditions. Indeed, this can be seen in Fig. [5.7], which shows additional results from two runs in which an artificial damping phase (similar to that used in Ref. [96]) was employed for an extended time. As can be seen in the figure, when the damping is released, both these runs show ξ rapidly reverting to approximately the same gradient as the undamped run. In Ref. [17] scaling with $\tau - \tau_{\xi=0}$ was also observed in the two-point correlation functions of the energy-momentum tensor, so there is no evidence from the simulations that this scaling is a transient. These energy-momentum correlators show that the network demonstrates scaling in a 512^3 simulation over the conformal time range $64 < \tau < 128$, which will be referred to as the scaling epoch.

We also verify that Abelian Higgs strings lose energy at a constant rate of order unity by running 256^3 radiation era simulations for a very long time until there

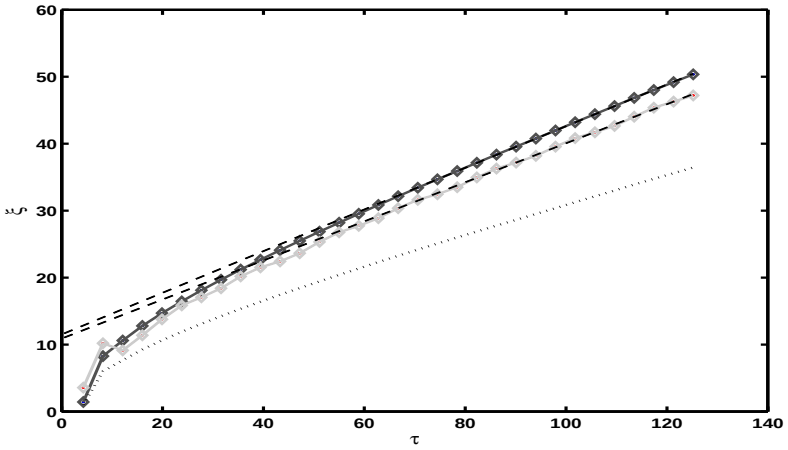

Figure 4.1: Network length scale ξ in a radiation era simulation calculated from Eq. (4.16) is in solid dark grey with fit over scaling times ($\tau \in [64, 128]$) giving $d\xi/d\tau = 0.31$ (the dotted line shows ξ before rescaling total string length using the Scherrer-Vilenkin factor). $\xi_{\mathcal{L}}$ calculated directly from the Lagrangian is in solid light grey with fit $d\xi_{\mathcal{L}}/d\tau = 0.29$.

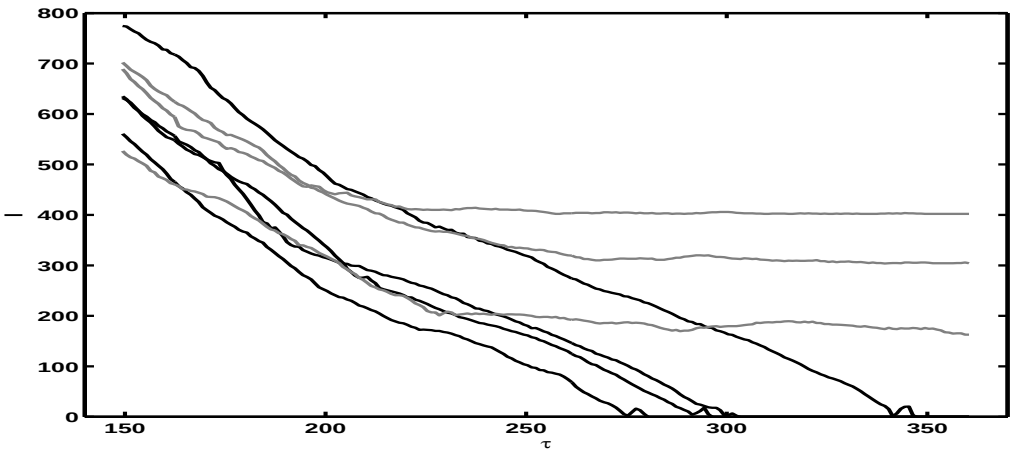

Figure 4.2: Change of total comoving length of string l with conformal time τ for late time Abelian Higgs simulations in the radiation era with box side size $L = 256\Delta x$ and $\Delta x = 0.5$. The energy loss from a loop of string is linear with constant gradient $\mathcal{O}(1)$ until the loop fragments and evaporates (examples shown in black). Once only pairs of straight strings remain in the box (3 examples shown in grey), the linear energy loss stops and the string length oscillates around the box crossing length; L, $L\sqrt{2}$ or $L\sqrt{3}$ depending on the direction it wraps the box.

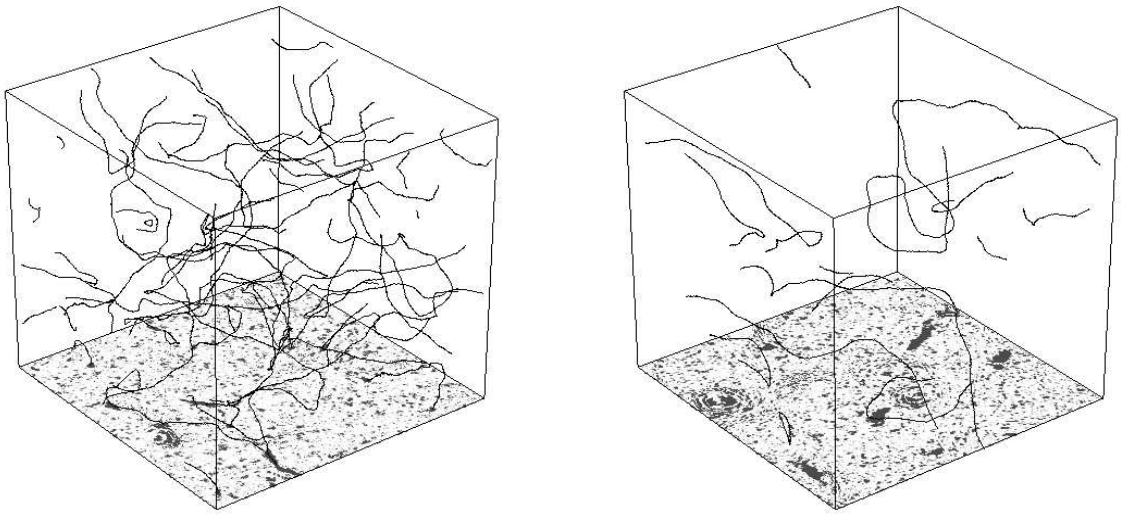

Figure 4.3: Comparison of the simulations of Abelian Higgs string (left) and global string (right) in the same size simulation after the same time

is only a single shrinking loop or a pair of straight strings winding around one or more directions in the simulation volume, which has periodic boundary conditions. The change in total comoving string length with conformal time is shown in Fig. [4.2] to be linear. By inspection one can see that for strings that are shrinking, $dl/d\tau \sim \mathcal{O}(1)$. Once two strings in the box become straight their length oscillates around the box crossing distance, which is the behaviour expected in the Nambu-Goto approximation.

4.2 Global Strings

The equations of motion for global string are the same as for the Abelian Higgs model but with the gauge coupling set to zero. Using LAH, with $g = 0$, we need only to remove the field configurations θ and ϵ in the discretised equations describing the gauge field (Sec. [4.1.1]). This modification allows for larger simulations to be performed as the gauge fields require large amounts of memory.

As expected, the density of global string is noticeably lower than gauge string after the same evolution time Fig. [4.3]. The interstring distance, ξ, is therefore larger for global string simulations and its linear growth with time during the scaling regime is higher than gauge string networks, Fig. [4.4]. The correlation length $\bar{\xi}$ defined in Eq. (5.19) is found to be lower for global strings such that the correlation

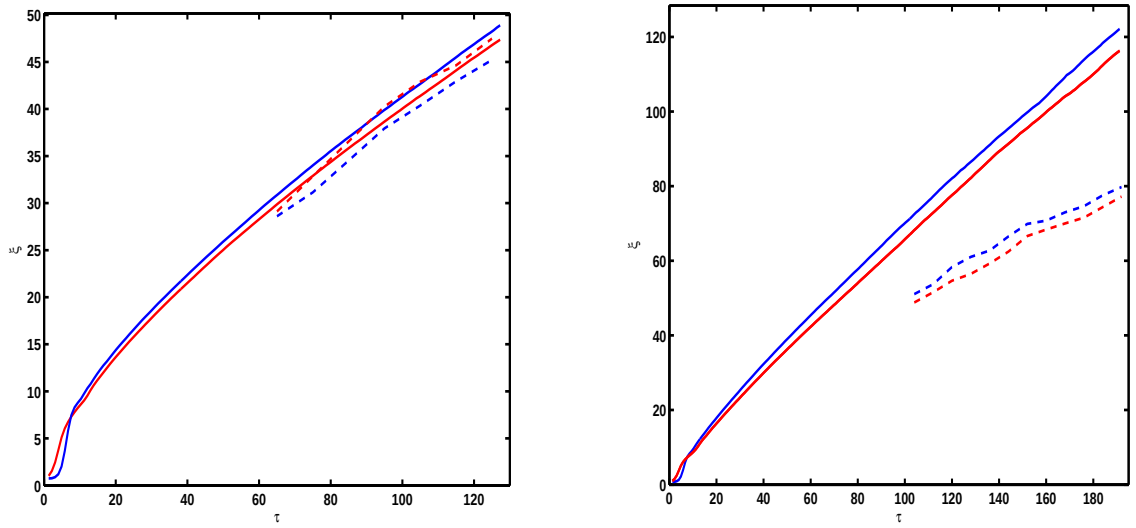

Figure 4.4: Comparison of the network lengthscale ξ (solid lines) according to Eq. (4.16) with Smith-Vilenkin smoothing and the correlation length $\bar{\xi}$ (dash lines) calculated from Eq. (5.19) for Abelian Higgs strings on a 512^3 lattice (left) and global strings on a 768^3 lattice (right). Matter era is in red and radiation era in blue.

	AH radiation	AH matter	G radiation	G matter
$\frac{d\xi}{d\tau}$	0.29	0.28	0.57	0.55
$\frac{d\bar{\xi}}{d\tau}$	0.30	0.28	0.32	0.32

Table 4.1: Summary of the evolution of the network lengthscale ξ and string correlation length $\bar{\xi}$ for Abelian Higgs (AH) and global (G) string networks. Values are averaged over 5 simulation realisations.

lengths for gauge and global strings are very similar. Values for $d\xi/d\tau$ and $d\bar{\xi}/d\tau$ are summarised in Table. 4.1.

The increased rate of change in ξ indicates that Goldstone radiation is making a considerable difference to the decay rate of global string. At late time when a single loop or pair of straight strings remain wrapping the lattice, we find the rate of change of string length with time to be considerably higher; $\mathcal{O}(10)$ as shown in Fig. [4.5]. The long range interaction between global strings causes them to eventually collide and annihilate preceded by plateaux in the decay as the remaining strings move toward their fate.

The proportion of energy density in the massless mode, ρ_G, is considerable,

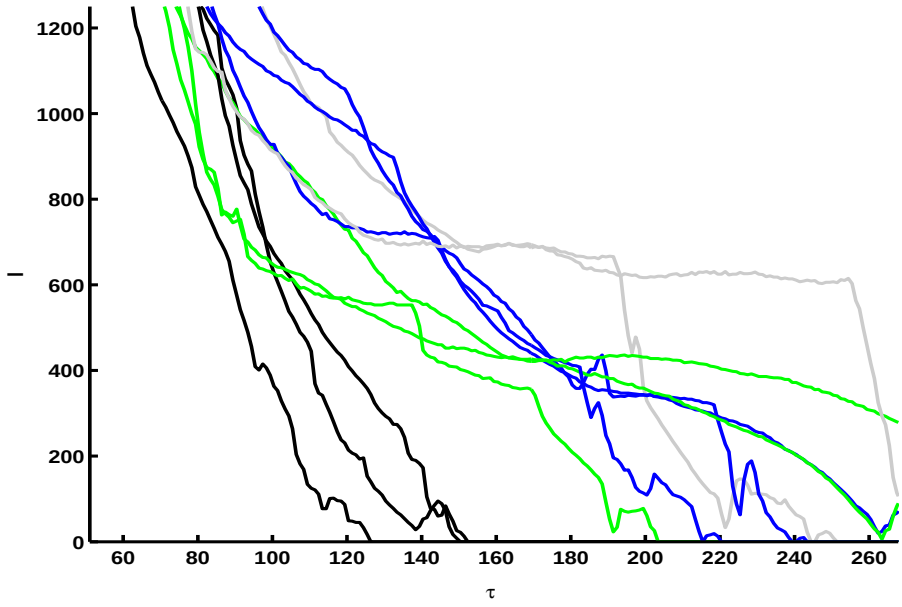

Figure 4.5: Change of comoving global string length, l, in late time radiation era simulations with box side $L = 256\Delta x$ and $\Delta x = 0.5$. A single loop (black) shrinks at a rate $\mathcal{O}(10)$. Plateaux are seen when pairs of straight strings of length L, $L\sqrt{2}$ and $L\sqrt{3}$ remain then the long range interaction pulls the string together and annihilation occurs.

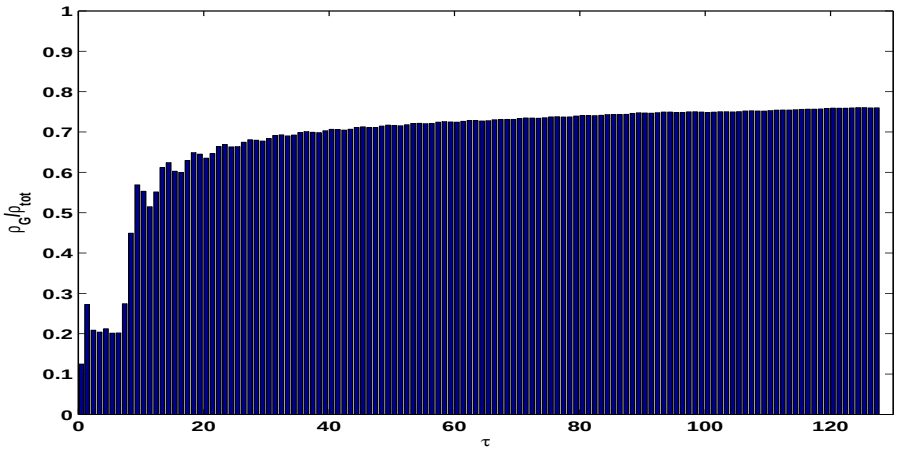

Figure 4.6: Proportion of energy density in the massless Goldstone mode and the massive Higgs mode.

Fig. [4.6], compared to that in the Higgs mode, ρ_H where

$$\rho_{tot} = \rho_H + \rho_G = |\dot{\phi}|^2 + |\nabla\phi|^2 + V(\phi) \tag{4.17}$$

for $\phi = f \exp i\alpha$ gives

$$\rho_H = \dot{f}^2 + (\nabla f)^2 + V(f) \tag{4.18}$$

$$\text{and} \quad \rho_G = f^2(\dot{\alpha}^2 + (\nabla\alpha)^2). \tag{4.19}$$

We have not ascertained the confinement of the energy density that is associated with the string but assume that a large proportion of the massless energy density will be able to radiate. Significant emission of massless radiation contributes to the higher rate of string decay in the Goldstone model and has the potential to mimic the massless gravitational back reaction effect. We use these simulations to approach the massless radiation backreaction problem. We compare the evolution of Abelian Higgs strings in a field theory to the global strings where there is a massless mode for radiation. We have established that the radiative effects of strings are realised in the simulations and will proceed to compare any additional effects that are due to the backreaction from a massless mode mode being introduced.

Chapter 5

Small scale structure

To understand the behaviour of small scales on cosmic strings we apply data from field theory simulations of Abelian Higgs and global strings to the predictions of analytic models. The main object of the study will be

$$\mathrm{corr}_{\mathrm{x}}(\sigma,\tau) \equiv \frac{\langle \mathbf{X}'(\sigma_1)\cdot\mathbf{X}'(\sigma_2)\rangle}{\langle \mathbf{X}'(0)\cdot\mathbf{X}'(0)\rangle}$$

where $\sigma = \sigma_1 - \sigma_2$, and a dependence on τ is implied where not explicitly stated. We calculate the exponent for the power law expected for gauge strings [70, 26]on scales from the string core width up to the horizon. To understand the effects of back reaction from radiation we also look at the tangent vector correlation function for global strings which emit massless radiation in the form of Goldstone modes. We find we can account for the modifications to the correlation function as due to the self force found which we model on the 'local back-reaction approximation' [11].

To begin, we review the models for the tangent vector correlation function as formulated for gauge strings and present our results for Abelian Higgs strings. Then we introduce the modifications for global strings and demonstrate a new scaling power law which quantifies the damping due to radiation reaction.

5.1 Gauge String Tangent Vector Correlators

The Nambu-Goto equations of motion

$$\ddot{\mathbf{X}} + 2\frac{\dot{a}}{a}(1-\dot{\mathbf{X}}^2)\dot{\mathbf{X}} - \frac{1}{\epsilon}\left(\frac{\mathbf{X}'}{\epsilon}\right)' = 0 \tag{5.1}$$

and

$$\dot{\epsilon} = -2\frac{\dot{a}}{a}(1-\dot{\mathbf{X}}^2)\epsilon \tag{5.2}$$

can be reformulated using left and right moving unit vectors which we will call $\mathbf{p}$ and $\mathbf{q}$. Defined in terms of the position vector $\mathbf{X}(\sigma,\tau)$ where σ is the string coordinate;

$$\mathbf{p}(\sigma,\tau) = \dot{\mathbf{X}} + \tfrac{1}{\epsilon}\mathbf{X}' \text{ and } \mathbf{q}(\sigma,\tau) = \dot{\mathbf{X}} - \tfrac{1}{\epsilon}\mathbf{X}'. \tag{5.3}$$

Dots are derivatives with respect to τ, primes with respect to σ and in the transverse gauge where $\mathbf{X}'\cdot\dot{\mathbf{X}} = 0$,

$$\epsilon^2 = \frac{\mathbf{X}'^2}{1-\dot{\mathbf{X}}^2}. \tag{5.4}$$

The equations of motion then become [4]

$$\dot{\mathbf{p}} - \frac{1}{\epsilon}\mathbf{p}' = -\frac{\dot{a}}{a}(\mathbf{q} - (\mathbf{p}\cdot\mathbf{q})\mathbf{p}) \tag{5.5}$$

$$\dot{\mathbf{q}} + \frac{1}{\epsilon}\mathbf{q}' = -\frac{\dot{a}}{a}(\mathbf{p} - (\mathbf{p}\cdot\mathbf{q})\mathbf{q}). \tag{5.6}$$

For consistency with notation used elsewhere [70, 61] we denote

$$\mathrm{corr}_{\mathrm{x}}(\sigma,\tau) \equiv \frac{\langle \mathbf{X}'(\sigma_1)\cdot\mathbf{X}'(\sigma_2)\rangle}{\langle \mathbf{X}'(0)\cdot\mathbf{X}'(0)\rangle}. \tag{5.7}$$

where the angle brackets denote averaging over an ensemble of strings, which is assumed to be equivalent to averaging over the string spatial coordinate. Since $\mathbf{X}'_1 = \frac{\epsilon_1}{2}(\mathbf{p}_1 - \mathbf{q}_1)$ from the definitions of Eq. (5.3), with the subscript indicating evaluation at σ_1, we have

$$\mathrm{corr}_{\mathrm{x}}(\sigma,\tau) = \frac{\frac{1}{4}\langle\epsilon_1\epsilon_2[(\mathbf{p}_1\cdot\mathbf{p}_2) - (\mathbf{p}_1\cdot\mathbf{q}_2) - (\mathbf{q}_1\cdot\mathbf{p}_2) + (\mathbf{q}_1\cdot\mathbf{q}_2)]\rangle}{\langle\epsilon^2(1-\dot{\mathbf{X}}^2)\rangle}. \tag{5.8}$$

By symmetry,

$$\langle\mathbf{p}_1\cdot\mathbf{p}_2\rangle = \langle\mathbf{q}_1\cdot\mathbf{q}_2\rangle \text{ and } \langle\mathbf{p}_1\cdot\mathbf{q}_2\rangle = \langle\mathbf{q}_1\cdot\mathbf{p}_2\rangle$$

and to first order in the fluctuations we can replace epsilon by its average. Thus,

$$\mathrm{corr}_{\mathrm{x}}(\sigma,\tau) \simeq \frac{\langle\mathbf{p}_1\cdot\mathbf{p}_2\rangle - \langle\mathbf{p}_1\cdot\mathbf{q}_2\rangle}{2(1-\langle\dot{\mathbf{X}}^2\rangle)}. \tag{5.9}$$

Correlations for opposite moving modes $\langle\mathbf{p}(\sigma_1)\cdot\mathbf{q}(\sigma_2)\rangle$ will be subdominant to those moving in the same direction along the string $\langle\mathbf{p}(\sigma_1)\cdot\mathbf{p}(\sigma_2)\rangle$. Identifying that $-\mathbf{p}(\sigma)\cdot\mathbf{q}(\sigma) = 1 - 2\dot{\mathbf{X}}^2$, allows an approximation to first order of $-\langle\mathbf{p}(\sigma)\cdot\mathbf{q}(0)\rangle = 1 - 2\langle\dot{\mathbf{X}}^2\rangle$ for σ small compared with the correlation length. Then

$$\mathrm{corr}_{\mathrm{x}}(\sigma,\tau) \simeq \frac{\langle\mathbf{p}(\sigma)\cdot\mathbf{p}(0)\rangle - 1}{2(1-\langle\dot{\mathbf{X}}^2\rangle)} + 1 \tag{5.10}$$

and thus

$$2(1-\langle\dot{\mathbf{X}}^2\rangle)(1-\mathrm{corr}_{\mathrm{x}}(\sigma,\tau)) \simeq 1-\langle\mathbf{p}(\sigma)\cdot\mathbf{p}(0)\rangle. \tag{5.11}$$

By changing the string coordinates σ , τ to new variables u, $\tilde{\tau}$ such that $\tilde{\tau}=\tau$ and $\dot{u}=\frac{1}{\epsilon}u'$, we see that

$$\frac{\partial}{\partial\tau}\mathbf{p}(\tilde{\tau},u)=\frac{\partial}{\partial\tilde{\tau}}\mathbf{p}(\tilde{\tau},u)+\frac{u'}{\epsilon}\frac{\partial\mathbf{p}}{\partial u}=\frac{\partial}{\partial\tilde{\tau}}\mathbf{p}(\tilde{\tau},u)+\frac{1}{\epsilon}\frac{\partial\mathbf{p}}{\partial\sigma} \tag{5.12}$$

and hence

$$\frac{\partial}{\partial\tilde{\tau}}\mathbf{p}=-\frac{\dot{a}}{a}(\mathbf{q}-(\mathbf{p}\cdot\mathbf{q})\mathbf{p}). \tag{5.13}$$

Dropping the tilde and using our approximation $\langle\mathbf{p}(\sigma)\cdot\mathbf{q}(0)\rangle\simeq 2\langle\dot{\mathbf{X}}^2\rangle-1$, we find

$$\partial_\tau\langle 1-\mathbf{p}(\sigma)\cdot\mathbf{p}(0)\rangle=-\frac{2\dot{a}}{a}(1-2\langle\dot{\mathbf{X}}^2\rangle)\langle 1-\mathbf{p}(\sigma)\cdot\mathbf{p}(0)\rangle \tag{5.14}$$

which integrates to the form

$$\langle 1-\mathbf{p}(s)\cdot\mathbf{p}(0)\rangle=f(u)\tau^{-2\nu(1-2\langle\dot{\mathbf{X}}^2\rangle)} \tag{5.15}$$

with ν defined as scale factor $a\propto\tau^\nu$.

The correlator must be a function of s/τ, where s is the comoving distance along the string, if it is to also exhibit scaling. Given that $s=\epsilon\sigma$, we need the time dependence of of ϵ, (Eq. (5.4))

$$\frac{\dot{\epsilon}}{\epsilon}=-2\frac{\dot{a}}{a}\dot{\mathbf{X}}^2\Rightarrow\epsilon\propto\tau^{-2\nu\langle\dot{\mathbf{X}}^2\rangle}.$$

to show that

$$\frac{s}{\tau}=\frac{\epsilon\sigma}{\tau}\propto\sigma\tau^{-1-2\nu\langle\dot{\mathbf{X}}^2\rangle}.$$

Given that Eq. (5.15) has a power law form

$$\langle 1-\mathbf{p}(s)\cdot\mathbf{p}(0)\rangle\propto\left(\frac{s}{\tau}\right)^{2\chi}$$

we find that in order to satisfy the scaling hypothesis, the exponent is

$$2\chi=\frac{2\nu(1-2\langle\dot{\mathbf{X}}^2\rangle)}{1+2\nu\langle\dot{\mathbf{X}}^2\rangle}. \tag{5.16}$$

The tangent vector correlator should also scale, thus

$$1-\mathrm{corr}_{\mathrm{x}}(s,\tau)=\mathrm{A}\left(\frac{s}{\tau}\right)^{2\chi}. \tag{5.17}$$

Having established the power law form for $\langle \mathbf{p} \cdot \mathbf{p} \rangle$, we can determine a form for the small fluctuation approximation which was used in Sec. [2.3.3] to estimate the back reaction scale. Where left and right movers, $\mathbf{p}$ and $\mathbf{q}$, are dominated by a large part, $\mathbf{P}$ and $\mathbf{Q}$ so that $\mathbf{P^2}(\tau) = \mathbf{1}$, we can define a small fluctuation $\mathbf{w}$ such that $\mathbf{P} \cdot \mathbf{w} = \mathbf{0}$. $\mathbf{p}$ is expressed as an expansion in the small scale fluctuation;

$$\mathbf{p}(\sigma, \tau) = \mathbf{P}(\tau) + \mathbf{w}(\sigma, \tau) - \frac{\mathbf{1}}{\mathbf{2}}\mathbf{P}(\tau)\mathbf{w^2}(\sigma, \tau) + \cdots$$

so the product

$$\langle \mathbf{p}(\sigma) \cdot \mathbf{p}(\sigma') \rangle \simeq \mathbf{1} - \frac{\mathbf{1}}{\mathbf{2}} \langle [\mathbf{w}(\sigma) - \mathbf{w}(\sigma')]^{\mathbf{2}} \rangle$$

and we see from Eq. (5.17) $\langle [\mathbf{w}(\sigma) - \mathbf{w}(\sigma')]^2 \rangle \propto \left(\frac{s}{\tau}\right)^{2\chi}$ scales in the same way as the tangent vector correlation function.

5.2 3 Scale Model

Much of the model follows in essence from the lengthy analysis of a 3 scale model by Austin, Copeland and Kibble [6], based on the foundations of a two scale model [51, 28], with length scales ξ, the mean inter-string distance and $\bar{\xi}$, the persistence length of correlations in direction where

$$\xi = \sqrt{l/V} \tag{5.18}$$

$$\bar{\xi} = a \int \mathrm{d}s \, \langle q(s) \cdot q(s') \rangle = a \int_0^\infty \frac{\langle \mathbf{X}'(s) \cdot \mathbf{X}'(s') \rangle}{\langle \mathbf{X}'^2 \rangle}. \tag{5.19}$$

The two scale model depends on parameters k, determining the excess of kinks on loops compared to long string and c, the efficiency of chopping a loop from the network. It also relies on loops being chopped from long string in regions of high kink density, reducing the overall kinkiness of long string and that loops would be high in kink density. It was determined that both ξ and $\bar{\xi}$ were of similar orders of magnitude and both scaled, growing proportional to time but that there was a smaller length scale ζ that remains small unless gravitational radiation smoothed the strings, [6, 7].

While the parameter k, essentially defined by

$$k = \frac{\text{kinks on loops}}{\text{kinks on long string}} - 1,$$

remains small with long string almost as kinky as loops, it is expected that the ratio $\zeta/\bar{\xi}$ will remain small and shrink compared to the horizon size until it becomes of order the gravitational radiation scale. At scales where backreaction has an effect, the string is smoothed and k becomes large so that $\zeta \sim \xi$, $\bar{\xi}$ and scales. In this context, a build up of small scale structure implies a small k and that the effects of gravitational radiation have not made an effect. In Abelian Higgs networks the emission of massive radiation will also suppress the build up of structure.

By comparing their model to that of Polchinski et al in [26] they show that there should be a critical scale s_c below which there is only one kink contributing to $\langle \mathbf{p}(0) \cdot \mathbf{p}(s) \rangle$ in the correlation function which is described by a kink probability distribution function such that

$$1 - \mathrm{corr_x} \propto \left(\frac{s}{\tau}\right), \tag{5.20}$$

below s_c. The power law of Eq. (5.17) is expected to hold down to s_c and it is suggested that Nambu-Goto strings may not be scaling on length scales below this as there is no radiative mechanism for smoothing the string.

5.3 Calculating the Correlator from Simulated String

From the coordinate locations of the string extracted from LAH it is simple to compare the Euclidean distance between 2 points on the string and the separation along the string coordinate.

The longest string at a set of equally spaced times throughout the scaling epoch in the simulation is isolated for analysis in both the radiation and matter dominated eras. The comoving distance along the string $s = \int \epsilon \mathrm{d}\sigma$ along a string coordinate length $\sigma = \sigma_1 - \sigma_2$ is compared to the Euclidean distance, r, between $\mathbf{X}(\sigma_1)$ and $\mathbf{X}(\sigma_2)$. Around each loop, the coordinates are averaged over 10 lattice steps along the string coordinate to smooth the lattice effect in addition of perpendicular segments. The mean square Euclidean distance is then averaged over many starting points a few string segments apart around the loop, thus creating a 2-point function,

$$\langle r^2(\sigma, \tau) \rangle = \int_0^\sigma \int_0^\sigma \mathrm{d}\sigma_1 \mathrm{d}\sigma_2 \, \langle \mathbf{X}'(\sigma_1) \cdot \mathbf{X}'(\sigma_2) \rangle. \tag{5.21}$$

Recalling the definition

$$\mathrm{corr_x}(\sigma,\tau) \equiv \frac{\langle \mathbf{X}'(\sigma_1)\cdot\mathbf{X}'(\sigma_2)\rangle}{\langle \mathbf{X}'(0)\cdot\mathbf{X}'(0)\rangle}$$

and the analytic form of Polchinski et al, [70, 35, 71] Eq. (5.17)

$$\mathrm{corr_x}(s,\tau) = 1 - \mathrm{A}\Big(\frac{s}{\tau}\Big)^{2\chi},$$

we can compare the two point function calculated from the simulation with the predicted scaling form by taking its second derivative.

$$\frac{1}{2}\frac{\partial^2\langle r^2\rangle}{\partial\sigma^2} = \langle \mathbf{X}'\cdot\mathbf{X}'\rangle\Big(1-\mathrm{A}\Big(\frac{s}{\xi}\Big)^{2\chi}\Big). \tag{5.22}$$

In order to test the prediction, the second derivative of the 2-point function $\langle r^2(s,\tau)\rangle$ is taken numerically. A least squares fit is used to optimise the parameters in the function for

$$1-\mathrm{corr_x} = 1 - \frac{1}{2\langle \mathbf{X}'\cdot\mathbf{X}'\rangle}\frac{\partial^2\langle r^2\rangle}{\partial\sigma^2} = \mathrm{A}\Big(\frac{s}{\xi}\Big)^{2\chi}$$

taking a nominal standard deviation equivalent to the length s to weight smaller s appropriately on the logarithmic scale. Noise is reduced by averaging the main results for the Abelian Higgs and Goldstone models over 20 simulations with different initialisations of the Gaussian random field. It should be noted that the smoothing process of averaging the coordinates was not found to alter the parameters or the shape of the $1-\mathrm{corr_x}$ function, notably at small s, but allowed the least squares fit to converge more quickly. Other smoothing methods were tested but this method is most consistent with the averages taken in the definition of the tangent vector correlator. As the strings become a random walk on horizon scales, the correlation function vanishes. The gradient of the correlation function demonstrates full scaling below the correlation length. The results are shown in Fig. [5.1] for the radiation era and Fig. [5.2] for the mater era and the average values found from the least square fit for the parameters 2χ, $\langle \mathbf{X}'\cdot\mathbf{X}'\rangle$ and A are listed in Table. [5.1]. Once established that $\langle \mathbf{X}'\cdot\mathbf{X}'\rangle = 1$ to a high degree of accuracy, the fit to the data can more quickly be made by finding just the two remaining parameters and these values are also given in Table. [5.1].

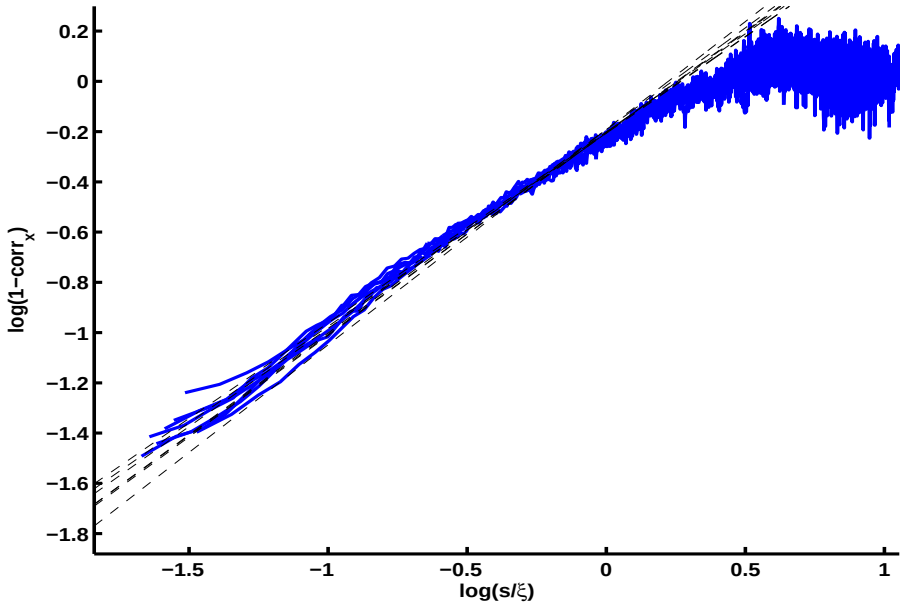

Figure 5.1: Solid lines indicate 2 point tangent vector correlation functions for Abelian Higgs string on a 512^3 lattice in the radiation era for 7 equally spaced times throughout the scaling epoch ($\tau \in [64, 128]$) with dashed lines showing the 3 parameter fits. The parameters are calculated by fitting the data from the smallest scales up to $\log(s/\xi) = 0$.

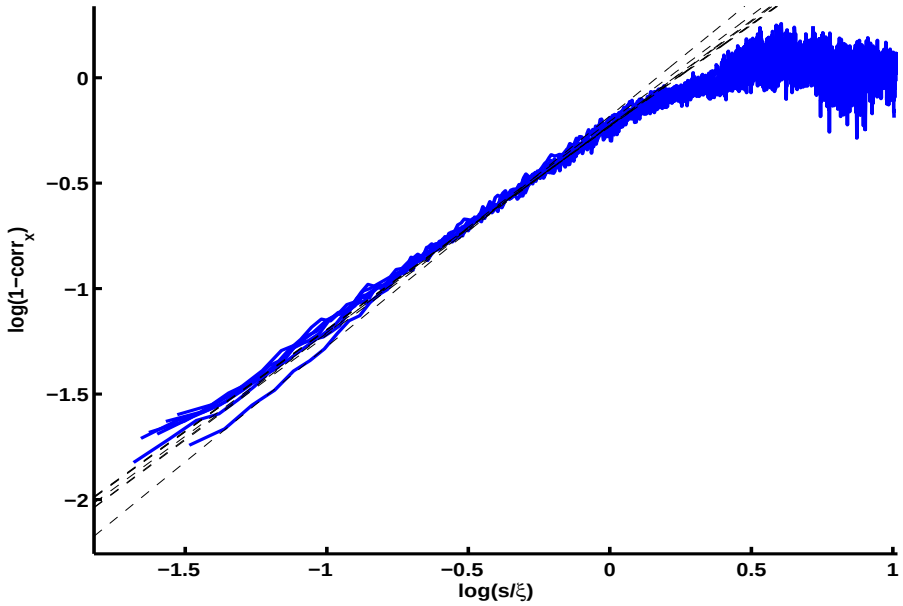

Figure 5.2: Tangent vector correlations and fit for Abelian Higgs string in the matter era as in Fig. [5.1].

Era (ν)	Fitting Procedure	2χ	A	$\langle \mathbf{X}' \cdot \mathbf{X}' \rangle$
1 (Rad)	Fit to $1 - \text{corr}_x$:			
	3 Parameter Fit	0.80 ± 0.03	0.63 ± 0.01	1.03 ± 0.02
	2 Parameter Fit	0.83 ± 0.04	0.62 ± 0.01	fixed to 1
	Fit to Fractal Dimension:			
	$-0.7 < \log(s/\xi) < 0.4$	1.03 ± 0.03		
	$-1.4 < \log(s/\xi) < -0.7$	1.36 ± 0.03		
	Fit to Velocity:			
	$\langle \dot{\mathbf{X}}^2 \rangle_{\text{G}}$	1.07		
	$\langle \dot{\mathbf{X}}^2 \rangle_{\text{Y}}$	0.35		
1.5	Fit to $1 - \text{corr}_x$:			
	2 Parameter Fit	0.93		
	Fit to Fractal Dimension:	1.06		
	Fit to Velocity:			
	$\langle \dot{\mathbf{X}}^2 \rangle_{\text{G}}$	1.63		
	$\langle \dot{\mathbf{X}}^2 \rangle_{\text{Y}}$	0.74		
2 (Matter)	Fit to $1 - \text{corr}_x$:			
	3 Parameter Fit	0.99 ± 0.04	0.60 ± 0.03	1.01 ± 0.003
	2 Parameter Fit	1.01 ± 0.03	0.61 ± 0.02	fixed to 1
	Fit to Fractal Dimension			
	$-1.4 < \log(s/\xi) < -0.4$	1.20 ± 0.03		
	Fit to Velocity:			
	$\langle \dot{\mathbf{X}}^2 \rangle_{\text{G}}$	2.05		
	$\langle \dot{\mathbf{X}}^2 \rangle_{\text{Y}}$	0.78		

Table 5.1: Summary of parameters fitting the correlation function for Abelian Higgs string averaged over 7 times throughout the scaling epoch with standard deviation between times quoted. The 3 parameter fit follows Eq. (5.17) and the 2 parameter fit is found setting $\langle \mathbf{X}' \cdot \mathbf{X}' \rangle = 1$. These are both fitted up to the correlation length, $\log(s/\xi) < 0$. The fractal dimension fit follows Eq. (5.25). The velocity estimates $\langle \dot{\mathbf{X}}^2 \rangle_{\text{G}}$ and $\langle \dot{\mathbf{X}}^2 \rangle_{\text{Y}}$ are defined in Section 5.5 and given in Table [5.3].

5.3.1 Fractal Dimension

We can further verify these results by calculating the fractal dimension of the string d_f defined

$$\frac{1}{d_f} = \frac{1}{2}\frac{d\log\langle r^2\rangle}{d\log s} \tag{5.23}$$

which measures the smoothness of the string. For a perfectly smooth string $d_f = 1$ and a string following a random walk where $s \propto \langle r^2\rangle$, $d_f = 2$.

By integrating the model for the 2-point function $\langle r^2\rangle$, Eq. (5.21) we see that

$$\langle r^2\rangle = s^2\left(1 - \frac{A}{(2\chi+1)(2\chi+2)}\left(\frac{s}{\tau}\right)^{2\chi}\right) \tag{5.24}$$

and arrive at a model for the fractal dimension for small s in terms of the 2χ parameter

$$d_f \simeq 1 + \frac{A\chi}{(2\chi+1)(2\chi+2)}\left(\frac{s}{\tau}\right)^{2\chi} + \mathcal{O}\left(\frac{s}{\tau}\right)^{4\chi}. \tag{5.25}$$

As such 2χ can be thought of as parameterising the deviation of the string from straightness.

Although Eq. (5.25) relies on an expansion to approximate, this method for calculating 2χ is advantageous as only one numerical differentiation of our data is required. As such, noise is minimal and no further 'smoothing' is required. The scaling exhibited is clear and unambiguous and, as shown in Fig. [5.4], extends beyond the correlation length to larger s up to horizon scales. Values for 2χ calculated using this method are summarised in Table. [5.1]. At very small scales, Eq. (5.25) fails to provide a consistent value for 2χ but this is reasonable given its definition as s and r approach zero, neither does it lend much support to the hypothesis of Ref. [26] that $2\chi \sim 1$ for $s < s_c$ despite the change in gradient evident in the radiation era correlation function.

5.3.2 Validity Tests

Gaussianity

The 4-point correlation functions $\langle r^2(s,\tau)\rangle^2$ and $\langle (r^2(s,\tau))^2\rangle$ are also calculated to test for gaussianity.

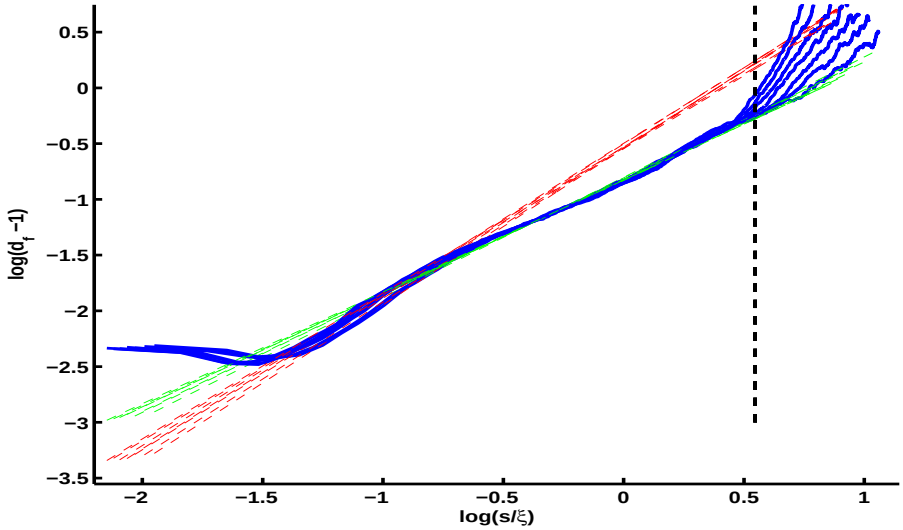

Figure 5.3: 2χ calculated from the fractal dimension model Eq. (5.25) for radiation era simulations of Abelian Higgs string where 2χ is the gradient of the slope shown. The fractal dimension model appears to scale beyond the correlation length, right up to horizon length scales $\sim \tau$, indicated with dashed line. There is a feature at $\log(s/\xi) \sim -0.7$ where the gradient changes.

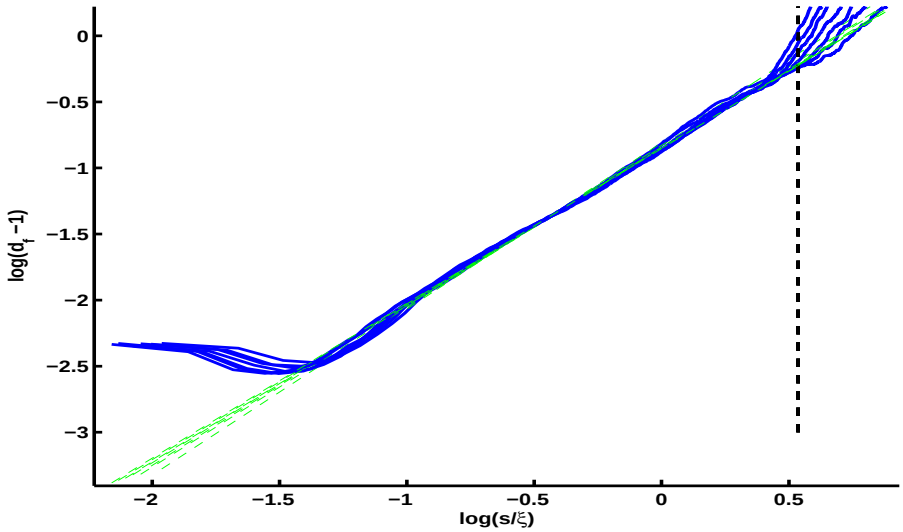

Figure 5.4: 2χ calculated from the fractal dimension model Eq. (5.25) for matter era simulations of Abelian Higgs string.

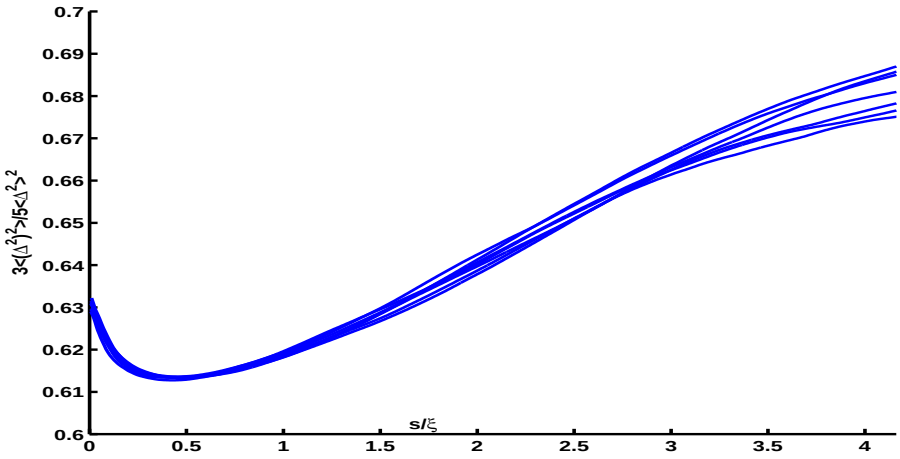

Figure 5.5: The ratio of the four-point correlation functions to the Gaussian prediction in the radiation-dominated era is shown against the dimensionless parameter s/ξ for a spread of times throughout the scaling epoch. A Gaussian four-point correlation would be indicated by this ratio being 1: Gaussianity is therefore not evident at any scale.

Denoting each spatial component of r as $\Delta_i \equiv \mathbf{X}_i(\sigma_1) - \mathbf{X}_i(\sigma_2)$, with σ_1 some initial base point for the measurement, the fourth moments formula is written

$$\begin{aligned} \langle (r^2(s,\tau))^2 \rangle &= \langle (\Delta \cdot \Delta)^2 \rangle \\ &= \delta_{ij}\delta_{kl}(\langle \Delta_i \Delta_j \rangle \langle \Delta_k \Delta_l \rangle + \langle \Delta_i \Delta_k \rangle \langle \Delta_j \Delta_l \rangle + \langle \Delta_i \Delta_l \rangle \langle \Delta_j \Delta_k \rangle) \end{aligned}$$

Then gaussianity would allow contraction on all pairs from Wick's Theorem so that $\langle (\Delta_i \Delta_j) \rangle = \frac{1}{3}\delta_{ij}\langle \Delta^2 \rangle$ and the ratio of the 4 point functions should behave as

$$\langle (r^2(s,\tau))^2 \rangle = \frac{5}{3}\langle r^2(s,\tau) \rangle^2 \tag{5.26}$$

Fig. [5.5] shows for the radiation era that on all scales the ratio of the 4 point correlations is not constant and not 5/3. The 4-point correlators in the matter era (not plotted) behave in a similar way, as do both radiation and matter era simulations of global strings. In the model for loop production proposed by Polchinski and collaborators [70, 35, 71], it is argued that non-gaussianity does not affect the power laws derived for the 2-point correlation function or the loop production function. We have confirmed that the 2-point correlation function is in accord with their model, but in the next section we will see that the loop production function is not. If we

accept the arguments of Polchinski et al, which are based on scaling, another reason must be found to account for the difference.

It has further been argued [89, 90] that the tangent vector correlation function will not obey a power law but should infact be exponential at very small scales. The explanation for this model relies explicitly on the gaussianity of the tangent vectors which is refuted here.

Growing core width

Simulations conducted in the radiation era are possible with the true equations of motion using $\kappa = 1$ in Eqs. (4.4)-(4.5) where the string width does not grow with the lattice. Correlation function results for an average of 5 simulations with $\kappa = 1$ are tested against our standard results for simulations with a comoving core width using $\kappa = 0$ in the equations of motion. Fig. [5.6] shows a comparison of the correlations at two different times in the simulation for both the $\kappa = 0$ and the $\kappa = 1$ cases, using the smoothing technique of Ref. [44]. The difference in the results is surprisingly insignificant for this calculation and no correction is felt necessary.

Initial Conditions

It is important to test for any dependence of our results upon the initial conditions chosen and to fully explore the approach to scaling. To achieve these two goals we have performed additional simulations of Abelian Higgs strings with an initial phase in which the Hubble damping term $2\dot{a}/a$ in Eqs. (4.4) and (4.5) is replaced by a constant, which we set to unity. This initial phase of artificial damping continues until a time when the Hubble damping would have been far smaller and hence string velocities are heavily reduced by the time we switch over to normal Hubble damping to complete the simulation. This gives us an alternative initial condition in which the string network is smooth and slowly moving, while radiation is negligible. The effects on the network length scale ξ for simulations on 512^3 lattices, seen in Fig. [5.7], shows the rate of growth of ξ is heavily retarded during the initial phase with $\xi \propto \tau^{1/2}$ as expected for over-damped motion [60] and observed in condensed matter defect networks.

In the velocity one scale (VOS) model a frictional damping term is introduced to

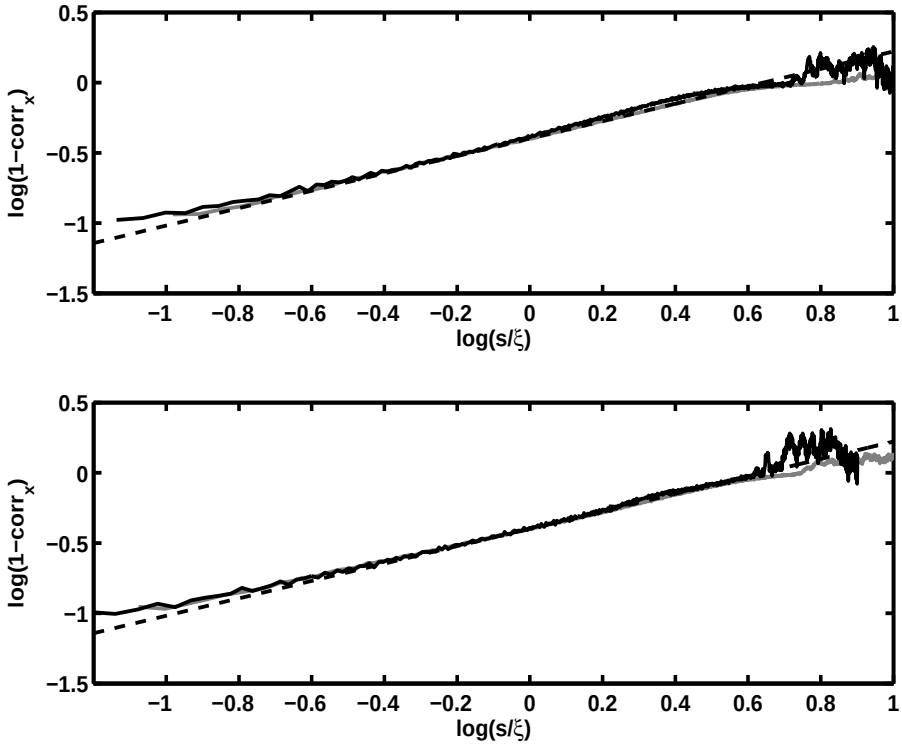

Figure 5.6: Testing the string core width approximation shows that the correlation function is not sensitive to the value of κ. The string coordinate averaging procedure used to calculated the tangent vector correlation function for this figure follows that used in Ref. [44]. The top figure shows the difference in $1 - \mathrm{corr_x}$ at time $\tau = 85$ and the lower figure at time $\tau = 115$ with grey plotting the usual $\kappa = 0$ comoving width approximation and black plotting the true $\kappa = 1$ version.

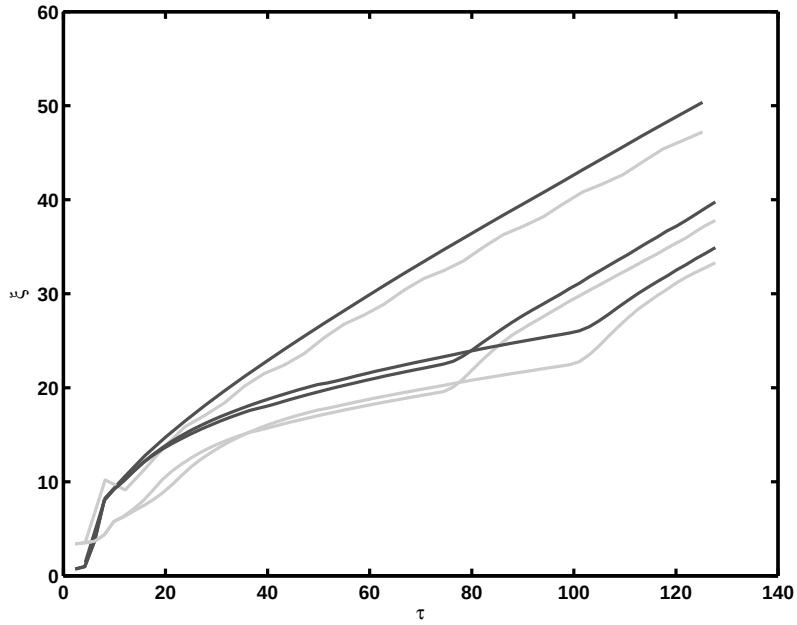

Figure 5.7: Network length scale ξ, showing linear behaviour with conformal time once the network settles into a scaling regime and memory of initial conditions is lost. ξ (black) and $\xi_{\mathcal{L}}$ (grey) are shown for radiation era simulations according to Eqs. (4.4) and (4.5) with parameters as stated in Sec. [4.1.1]. Curves for smaller ξ from simulations with a constant damping term which is not switched off until $\tau = 75$ and $\tau = 100$ respectively showing the speed with which the network length scale resumes the same scaling evolution with $d\xi/d\tau = 0.3$.

the Nambu-Goto equations of motion countering the acceleration due to curvature, [60]. The frictional force, [94]

$$F = -\frac{\mu}{l_f}\frac{\nu}{\sqrt{1-v^2}}$$

of a network moving at velocity defined by

$$v^2 = \langle\, \dot{\mathbf{x}}^2\rangle = \frac{\int \dot{\mathbf{x}}^2 \epsilon \mathrm{d}\sigma}{\int \epsilon \mathrm{d}\sigma} \tag{5.27}$$

at a damping length scale

$$l_f = \begin{cases} \dfrac{\mu}{\beta T^3} & \text{... gauge} \\ \dfrac{\mu}{\beta T^3}\ln^2(T\delta) & \text{... global} \end{cases}$$

at some background temperature T, introduces the friction term and the equations of motion in a FRW cosmology become

$$\ddot{\mathbf{X}} + \left(2\frac{\dot{a}}{a} + \frac{a}{l_f}\right)\left(1-\dot{\mathbf{X}}^2\right)\dot{\mathbf{X}} = \frac{1}{\epsilon}\left(\frac{\mathbf{X}'}{\epsilon}\right)' \tag{5.28}$$

$$\dot{\epsilon} + \left(2\frac{\dot{a}}{a} + \frac{a}{l_f}\right)\dot{\mathbf{X}}^2\epsilon = 0 \tag{5.29}$$

for gauge string.[1] Then the evolution of the energy density $\rho \propto E/a^3$ for string with energy $E = \mu a \int \epsilon \mathrm{d}\sigma$ and thus the correlation length $\xi^2 = \mu/\rho$ can be determined to evolve as

$$2\frac{d\xi}{dt} = 2\frac{\dot{a}}{a}\xi(1+v^2) + \frac{\xi}{l_f}v^2 + \tilde{c}v^2, \tag{5.30}$$

where the last term accounts for energy lost due to loop production.

As pointed out in [58], the effects of damping on a cosmological network of strings would only be relevant soon after production and the scaling regime in the damped epoch a transient. Once the constant damping used in our simulations to set up the alternative initial conditions is switched back to Hubble damping, the evolution of ξ quickly transitions to the same growth rate seen in the primary simulations.

In the damped epoch, strings are expected to be smooth. The lower velocities are expected to reduce intercommutation, suppressing the production of kinks, and the formation of cusps. The tangent vector correlation functions for radiation era gauge string simulations on a 768^3 lattice with an initial constant damping term are shown

[1] For global string in a homogeneous background $H^{ijk}_{\rm ext} = \sqrt{\rho_h}\epsilon^{ijk}$ induces a relativistic magnus force, adding a further term proportional to $\frac{\sqrt{\rho_h}}{\epsilon\mu}\dot{\mathbf{X}}\times\mathbf{X}'$ to the left hand side of Eq. (5.28).

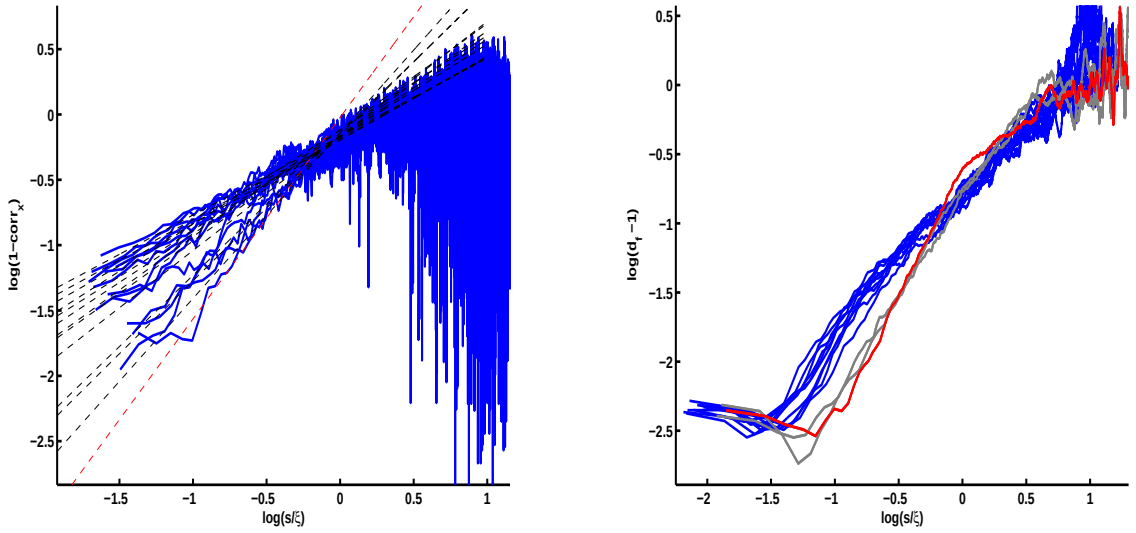

Figure 5.8: Correlation functions for a $(768\Delta x)^3$ simulation in the radiation era with constant damping term added to the equations of motion until $\tau = 100$ shown at times $\tau = 84$ (before Hubble damping resumes, red) and then at evenly spaced times throughout the evolution until $\tau = 192$. The gradients of the plots shown indicate the parameter 2χ and we see the change from a steep slope whilst the strings are heavily damped to a flatter slope as the string relaxes into the usual regime. The values for 2χ are plotted in Fig. [5.9]

in Fig. [5.8]. Whilst the strings are damped, they are smoother corresponding to a higher value of 2χ, but once the damping is removed at $\tau = 100$, the strings quickly develop small scale structure. The time-scale of relaxation to the scaling regime is depicted in Fig. [5.9] where we show the change in the 2χ parameter with time for a set of simulations with the constant damping term reverted back to Hubble damping after different periods of time, $\tau_{\rm off}$.

5.3.3 Between Eras

It is of interest to discuss the transition from radiation to matter dominated eras especially in the context of calculating cosmological phenomena. Although a contrived and oversimplified estimate, we calculate the tangent vector correlation function for simulations in 'intermediate eras' by setting the scale factor to scale with τ as $a \propto \tau^{\nu}$ $\nu = 1.5$. The average parameter values for the fit to Eq. (5.17) are given in Table. [5.1] and the comparison to the squared network velocities are shown in Fig. [5.13].

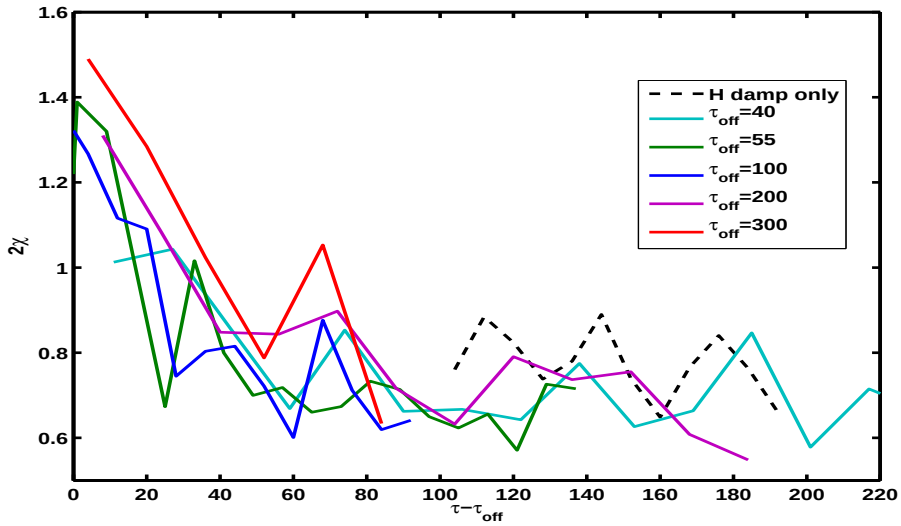

Figure 5.9: 2χ changes over time once damped simulations of abelian Higgs strings on a 768^3 lattice have their constant damping term turned off. Shown for simulations with different lengths of damping period $\tau_{\rm off}$.

5.4 Small Scale Structure and Backreaction on Global Strings

Due to backreaction, the equations of motion for global strings as defined by the Kalb-Ramond effective action Sec. [2.2.2], have additional interaction terms such that

$$\ddot{\mathbf{X}} + \frac{\dot{a}}{a}(1-\dot{\mathbf{X}})\dot{\mathbf{X}} - \frac{1}{\epsilon}\left(\frac{\mathbf{X}'}{\epsilon}\right)' = \frac{\mathbf{f}}{\mu} \tag{5.31}$$

$$\frac{\dot{\epsilon}}{\epsilon} = -2\frac{\dot{a}}{a}\dot{\mathbf{X}} + \frac{1}{\epsilon}\frac{f^{0,\rm rad}}{\mu}. \tag{5.32}$$

where μ is the effective tension and $\mathbf{f}$ is the string self energy per unit length as outlined in Sec. [2.4.1] but now in an expanding background. In Ref.[11] it is shown that

$$\mathbf{f}^{\rm rad} \simeq \mathbf{f}^{\rm rad}_{\rm flat} + \frac{\dot{a}}{a}\mathbf{g} \tag{5.33}$$

$$f^{0,\rm rad} \simeq f^{0,\rm rad}_{\rm flat} + \frac{\dot{a}}{a}g^0 \tag{5.34}$$

where $(g^0, \mathbf{g})$ is a correction to the self force due to the expansion in both radiation and matter eras.

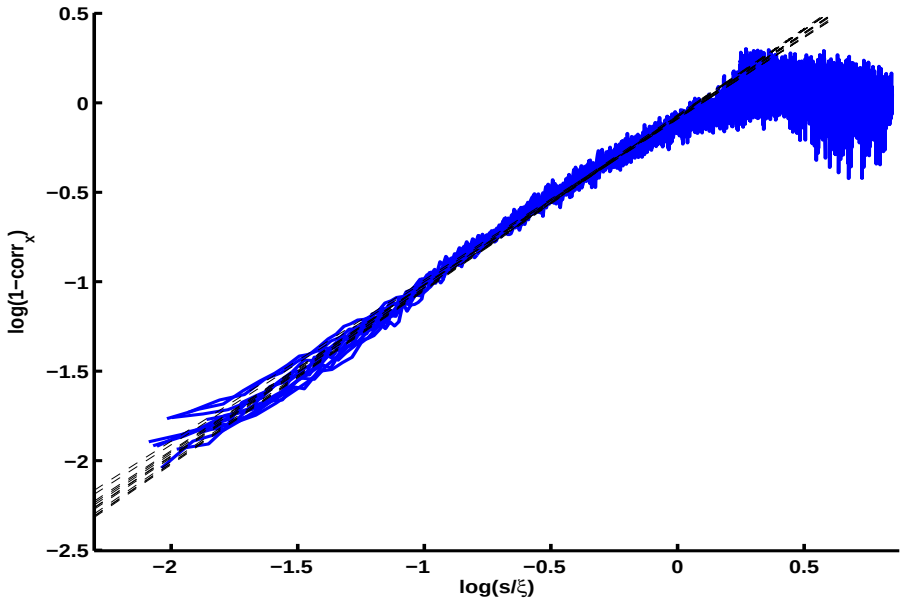

Figure 5.10: Tangent vector correlation function for $768\Delta x^3$ simulation of global strings in the radiation era.

By rewriting the equations of motion Eq. (5.31) in terms of the unit left and right moving vectors $\mathbf{p}$ and $\mathbf{q}$

$$\dot{\mathbf{p}} - \tfrac{1}{\epsilon}\mathbf{p}' = -\tfrac{\dot{a}}{a}(\mathbf{q} - (\mathbf{p}\cdot\mathbf{q})\mathbf{p}) + \tfrac{\mathbf{f}_p}{\mu} \tag{5.35}$$

$$\dot{\mathbf{q}} - \tfrac{1}{\epsilon}\mathbf{q}' = -\tfrac{\dot{a}}{a}(\mathbf{q} - (\mathbf{q}\cdot\mathbf{q})\mathbf{q}) + \tfrac{\mathbf{f}_q}{\mu} \tag{5.36}$$

where

$$\mathbf{f} = \frac{1}{2\mu}(\mathbf{f}_p + \mathbf{f}_q),$$

we see that the evolution of the correlation function $1 - \mathrm{corr_x} \propto 1 - \langle \mathbf{p}(\sigma_1)\cdot\mathbf{p}(\sigma_2)\rangle$ for the tangent vectors should take the form

$$\frac{\partial}{\partial\tau}(1-\mathrm{corr_x}) = -\frac{\dot{a}}{a}(1 - 2\langle\dot{\mathbf{X}}^2\rangle)(1-\mathrm{corr_x}) - \frac{1}{\mu}\left[\langle\mathbf{f}_p(\sigma_1)\cdot\mathbf{p}(\sigma_2)\rangle + \langle\mathbf{f}_p(\sigma_2)\cdot\mathbf{p}(\sigma_1)\rangle\right]. \tag{5.37}$$

However the tangent vector correlator for global string appears to be strongly consistent with a power law of the original form (Eq. (5.17)) as evident from Figs. [5.10] and [5.11] for the radiation and matter dominated eras respectively and Fig. [5.12] for the fractal dimension model. In view of this, we note that if the self force has a scaling form

$$\frac{1}{\mu}\left[\langle\mathbf{f}_p(\sigma_1)\cdot\mathbf{p}(\sigma_2)\rangle + \langle\mathbf{f}_p(\sigma_2)\cdot\mathbf{p}(\sigma_1)\rangle\right] \propto \frac{1}{\tau}(1-\mathrm{corr_x}) \tag{5.38}$$

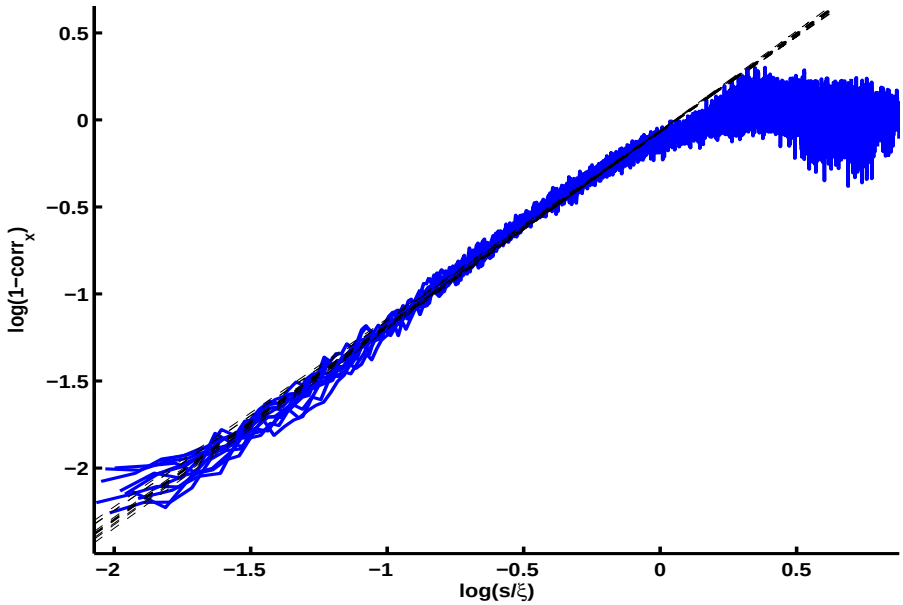

Figure 5.11: Tangent vector correlation function for $768\Delta x^3$ simulation of global strings in the matter era.

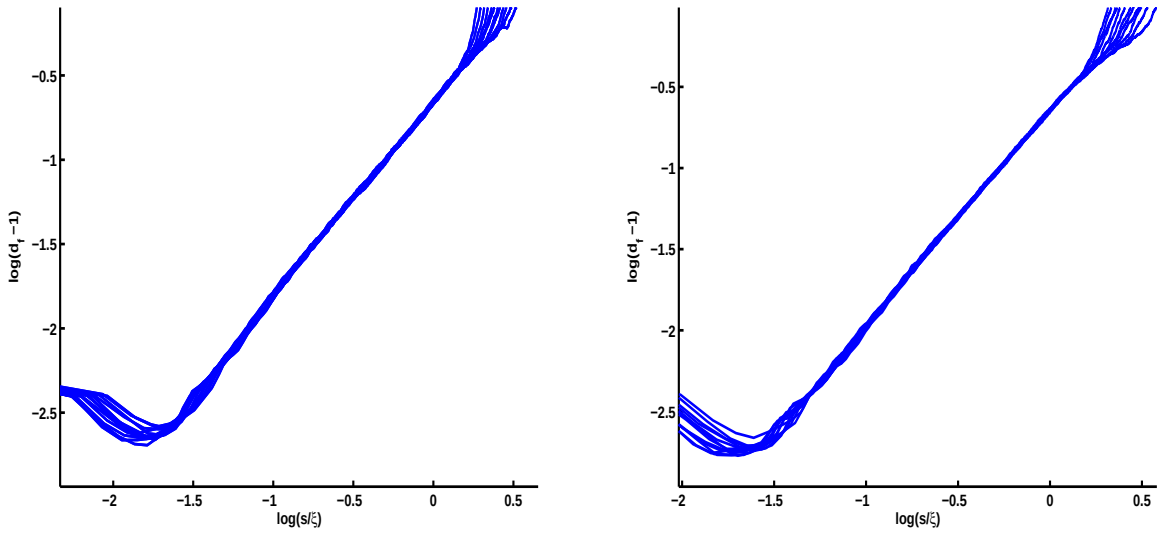

Figure 5.12: 2χ calculated from the fractal dimension model Eq. (5.25) for global string in the radiation era (left) and matter era (right) where 2χ is the gradient of the slope. Values for 2χ are summarised in Table. [5.2].

then on integrating Eq. (5.37), the effect is to change the expression for the exponent 2χ, which will now be demonstrated.

We will first neglect the correction, $(g^0, \mathbf{g})$ due to expansion, so we can use the local backreaction approximations for the force density provided in Eqns. (2.48-2.51). Then for ϵ as defined in Eq. (5.4), $\Delta \propto$ radius of curvature cut-off and δ of order the string width, $\mathbf{f}$ of Eq. (5.31) is given by

$$\begin{aligned} \frac{\mathbf{f}^{\rm rad}}{\mu(\Delta)} &\simeq \frac{2}{3}\frac{\Delta}{\ln\frac{\Delta}{\delta}}\left[\epsilon\dddot{\mathbf{X}} - \frac{1}{\epsilon}\left(\frac{(\mathbf{X}'\cdot\dddot{\mathbf{X}})}{1-\dot{\mathbf{X}}^2}\right)\mathbf{X}'\right] \\ &= \frac{2}{3}\frac{\Delta}{\ln\frac{\Delta}{\delta}}\epsilon\left[\dddot{\mathbf{X}} - \frac{(\mathbf{X}'\cdot\dddot{\mathbf{X}})}{\mathbf{X}'^2}\mathbf{X}'\right] \end{aligned} \tag{5.39}$$

and

$$\frac{f^{0,\rm rad}}{\mu(\Delta)} = \frac{2}{3}\frac{\Delta}{\ln\frac{\Delta}{\delta}}\left[\epsilon^2\left(\frac{(\dot{\mathbf{X}}\cdot\ddot{\mathbf{X}})}{1-\dot{\mathbf{X}}^2}\right)\right] \tag{5.40}$$

where the evolution of ϵ is altered by the string self energy loss f^0 according to Eq. (2.54).

We can validate the the emergence of the power law form for the tangent vector correlations by firstly making some assumptions about $\mathbf{f}$. First we observe that that

$$\frac{\mathbf{f}}{\mu} = \frac{2}{3}\frac{\Delta}{\ln\frac{\Delta}{\delta}}\epsilon\left[\dddot{\mathbf{X}} - \frac{(\mathbf{X}'\cdot\dddot{\mathbf{X}})}{\mathbf{X}'^2}\mathbf{X}'\right] \tag{5.41}$$

takes the part of $\ddot{\mathbf{X}}$ is orthogonal to $\mathbf{X}'/\epsilon$ and thus writing $\mathbf{u} = \dot{\mathbf{X}}\wedge\mathbf{X}'/\epsilon = 2\mathbf{p}\wedge\mathbf{q}$ for an unnormalised basis vector orthogonal to $\mathbf{X}'/\epsilon$ and $\dot{\mathbf{X}}$,

$$\frac{\mathbf{f}}{\mu} \simeq \frac{2}{3}\frac{\Delta}{\ln\frac{\Delta}{\delta}}\epsilon\left[\frac{(\dot{\mathbf{X}}\cdot\ddot{\mathbf{X}})}{\dot{\mathbf{X}}^2}\dot{\mathbf{X}} + \frac{(\mathbf{u}\cdot\dddot{\mathbf{X}})}{\mathbf{u}^2}\mathbf{u}\right], \tag{5.42}$$

We will assume we can drop the part proportional to $\mathbf{u}$, as we will be taking the scalar product with $\mathbf{p}(0)$ when calculating the equations of motion of the correlation functions, which gives zero as $\sigma\to 0$. Hence

$$\frac{\mathbf{f}}{\mu} \simeq \frac{2}{3}\frac{\Delta}{\ln\frac{\Delta}{\delta}}\epsilon\left[\frac{(\dot{\mathbf{X}}\cdot\ddot{\mathbf{X}})}{\dot{\mathbf{X}}^2}\dot{\mathbf{X}}\right]. \tag{5.43}$$

We now proceed to identify the components of the forces acting on $\mathbf{p}$ and $\mathbf{q}$. Differentiating the definitions of the unit vectors Eq. (5.3) and substituting into the

equations of motion Eq. (5.31) to find

$$\frac{1}{2\mu}(\mathbf{f}_p - \mathbf{f}_q) = \frac{\dot{\epsilon}}{\epsilon}\frac{\mathbf{X}'}{\epsilon} - 2\frac{\dot{a}}{a}\frac{\mathbf{X}'\dot{\mathbf{X}}^2}{\epsilon} \tag{5.44}$$

$$= -\left(\frac{\mathbf{X}'}{\epsilon}\right)\frac{f^0}{\epsilon\mu} \tag{5.45}$$

$$= -\left(\frac{\beta}{2\tau}\right)(\mathbf{q} - \mathbf{p} + \mathbf{q}\cdot\mathbf{p}(\mathbf{q} - \mathbf{p})) \tag{5.46}$$

where we define

$$\beta = \frac{\tau}{3}\frac{\Delta}{\ln\frac{\Delta}{\delta}}\epsilon\left[\frac{(\dot{\mathbf{X}}\cdot\ddot{\mathbf{X}})}{\dot{\mathbf{X}}^2(1-\dot{\mathbf{X}}^2)}\right] \tag{5.47}$$

β is dimensionless, so if the string is scaling it will on average be constant. With Eq. (5.43) we also have

$$\frac{1}{2\mu}(\mathbf{f}_p + \mathbf{f}_q) = \frac{\mathbf{f}}{\mu} \tag{5.48}$$

$$= \left(\frac{\beta}{2\tau}\right)(1-\dot{\mathbf{X}}^2)\dot{\mathbf{X}} \tag{5.49}$$

$$= \left(\frac{\beta}{2\tau}\right)(1-\mathbf{p}\cdot\mathbf{q})(\mathbf{p}+\mathbf{q}), \tag{5.50}$$

leading to

$$\frac{\mathbf{f}_p}{\mu} = \left(\frac{\beta}{2\tau}\right)(\mathbf{q} - \mathbf{p}(\mathbf{p}\cdot\mathbf{q})). \tag{5.51}$$

Hence the equation of motion for the correlation function with local back-reaction becomes

$$\frac{\partial}{\partial\tau}(1-\mathrm{corr_x}) = -\left(\frac{\dot{a}}{a} + \frac{\beta}{\tau}\right)(1 - 2\langle\dot{\mathbf{X}}^2\rangle)(1-\mathrm{corr_x}) \tag{5.52}$$

whose solution can again be written

$$1 - \mathrm{corr_x} = A\left(\frac{s}{\tau}\right)^{2\chi} \tag{5.53}$$

where now the exponent is modified

$$2\chi = \frac{2\nu_{\mathrm{eff}}(1 - 2\langle\dot{\mathbf{X}}^2\rangle)}{1 + 2\nu_{\mathrm{eff}}\langle\dot{\mathbf{X}}^2\rangle} \tag{5.54}$$

with

$$\nu_{\mathrm{eff}} = \nu + \beta. \tag{5.55}$$

Thus backreaction has the same effect on the correlation function as Hubble damping.

Era (ν)	Fitting Procedure	2χ	A	$\langle \mathbf{X}' \cdot \mathbf{X}' \rangle$
1 (Rad)	Fit to $1 - \text{corr}_x$:			
	3 Parameter Fit	0.94 ± 0.02	0.83 ± 0.01	1.01 ± 0.01
	2 Parameter Fit	0.99 ± 0.01	0.85 ± 0.01	fixed to 1
	Fit to Fractal Dimension:			
	$-1.5 < \log(s/\xi) < 0.2$	1.15 ± 0.01		
2 (Matter)	Fit to $1 - \text{corr}_x$:			
	3 Parameter Fit	1.11 ± 0.02	0.86 ± 0.01	1.00 ± 0.004
	2 Parameter Fit	1.16 ± 0.01	0.89 ± 0.01	fixed to 1
	Fit to Fractal Dimension:			
	$-1.5 < \log(s/\xi) < 0.2$	1.32 ± 0.01		

Table 5.2: Summary of mean parameters fitting the tangent vector correlation function and fractal dimension expansion for global string networks taken at 12 times in the scaling epoch and the standard deviation between times quoted.

Taking account of the correction to the self force due to expansion, we should in principle recalculate with the additional terms proportional to the Hubble parameter which appear in the expressions for $(f^0, \mathbf{f})$ and ϵ. This involves multiplying a complicated expression with string coordinates and their derivatives to obtain a consistent expression for Eq. (5.51). However, scaling tells us that the result will also be proportional to $1/\tau$. Hence it is reasonable to assert that the general form of ν_{eff} should be

$$\nu_{\text{eff}} = \nu(1 + \gamma) + \beta. \tag{5.56}$$

where γ is a constant.

Calculating $\dddot{\mathbf{X}}$ is a hugely difficult computational task and we have not quantified this value but we can compare the fixed value of ν with ν_{eff} as calculated from 2χ for global strings and their network velocities $\langle \dot{\mathbf{X}}^2 \rangle$. We discuss the calculation of network velocity in the next section and return to this point later.

5.5 Velocities

The parameter 2χ provides an estimate for the average network velocity squared $\langle\dot{\mathbf{X}}^2\rangle$ via Eq. (5.16) and its value can be cross-checked with that calculated directly from the simulation Fig. [5.5].

Due to the difficulty in estimating the network velocity, we apply a number of methods. One uses the electric $\mathbf{E}$ and magnetic $\mathbf{B}$ components from the field strength tensor and the other the canonical momentum and spatial gradients of the field, $\Pi = \dot{\phi}$ and $\mathbf{D}\phi = \nabla + i\mathbf{A}\phi$. Denoting the estimators $\langle\dot{\mathbf{X}}^2\rangle_{\rm F}$ and $\langle\dot{\mathbf{X}}^2\rangle_{\rm G}$, we have

$$\gamma_F^2\langle\dot{\mathbf{X}}^2\rangle_{\rm F} = \frac{\mathbf{E}_{\mathcal{L}}^2}{\mathbf{B}_{\mathcal{L}}^2} \tag{5.57}$$

and

$$\gamma_G^2\langle\dot{\mathbf{X}}^2\rangle_{\rm G} = \frac{\Pi_{\mathcal{L}}^2}{(\mathbf{D}\phi)_{\mathcal{L}}^2}, \tag{5.58}$$

where γ_F^2 and γ_G^2 are the Lorentz factors calculated using $\langle\dot{\mathbf{X}}^2\rangle_{\rm F}$ and $\langle\dot{\mathbf{X}}^2\rangle_{\rm G}$ respectively, and the subscript $\mathcal{L}$ denotes a Lagrangian weighting of a field Y according to

$$Y_{\mathcal{L}} = \frac{\int {\rm d}^3x\ Y\ \mathcal{L}}{\int {\rm d}^3x\ \mathcal{L}}. \tag{5.59}$$

Applying this weighting ensures points on the lattice containing string are selected since the Lagrangian density is negative where there is string and vanishes for small amplitude radiation, as outlined in Sec. [4.1.2]. The consistency between the Lagrangian weighting method and the average over winding sites method is demonstrated in the results shown in Fig. [5.13]. Alternatively one can calculate the the velocity at sites of non-trivial winding and average over sites which we will refer to as a plaquette weighting.

The third method is to calculate the velocity averaged over the sites of non-trivial winding in the network according to the velocity operator [102]

$$\langle\dot{\mathbf{X}}\rangle_Y = \frac{\Pi\nabla\phi^* - \Pi^*\nabla\phi}{|\nabla\phi\times\nabla\phi^*|} \tag{5.60}$$

Fig. [5.13] shows that the measured velocities in Abelian Higgs simulations agree with those inferred from the slope of the correlation function, with the exception of the velocity operator (5.60), which is higher and fluctuates wildly. The rest of the

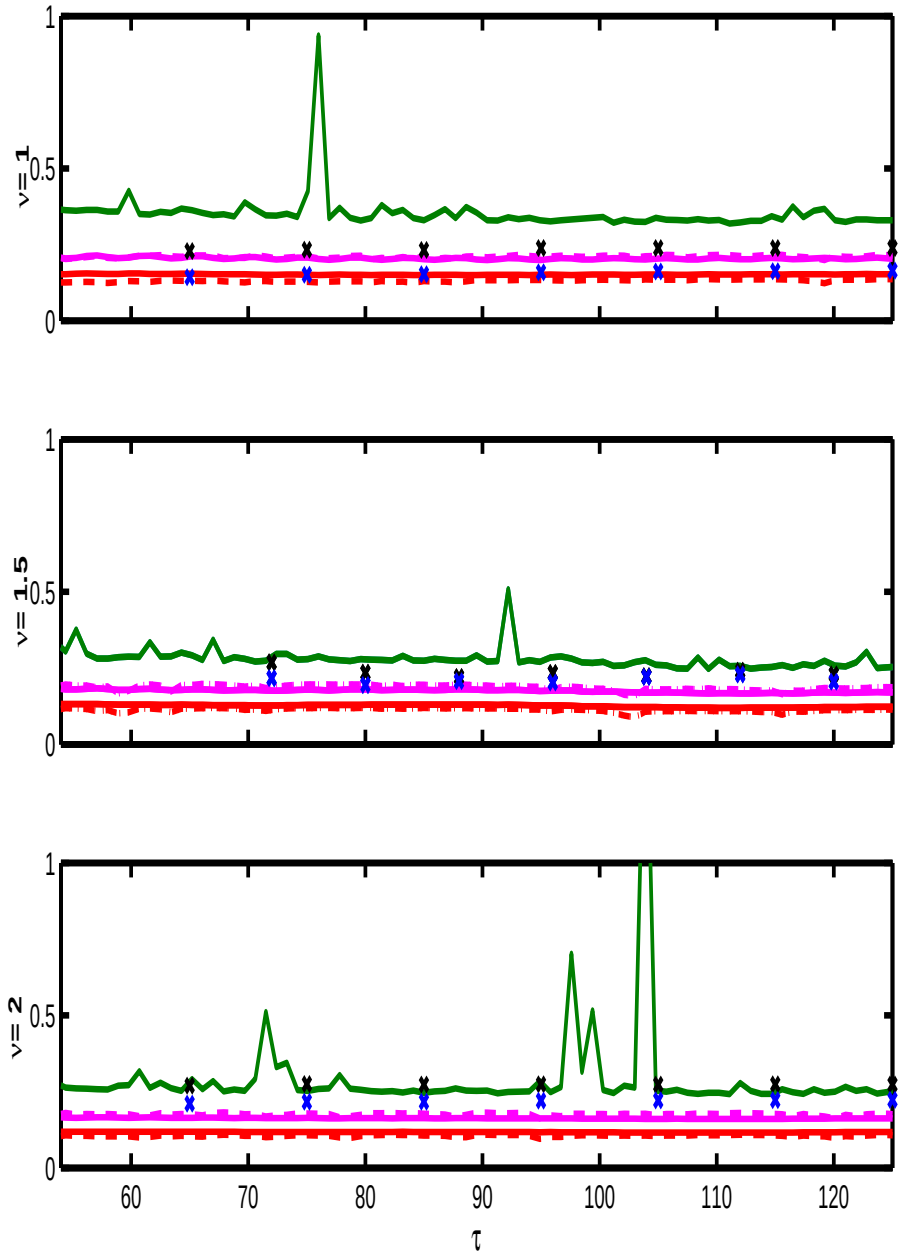

Figure 5.13: Mean square velocities $\langle \dot{\mathbf{X}}^2 \rangle$ of Abelian Higgs string networks. 'Gradient' velocity calculated via Eq. (5.58), (red; dotted lines for Lagrangian weighted and solid lines for winding plaquette weighted). 'Gauge' velocity calculated via Eq. (5.57), (magenta; solid and dashed as above). 'Operator' velocity calculated via Eq. (5.60), (green). Velocities from 2χ found according to Eq. (5.16) as derived from the tangent vector correlation function (black $\mathbf{x}$) and the fractal dimension model (blue $\mathbf{x}$) at the times during scaling for which they have been calculated.

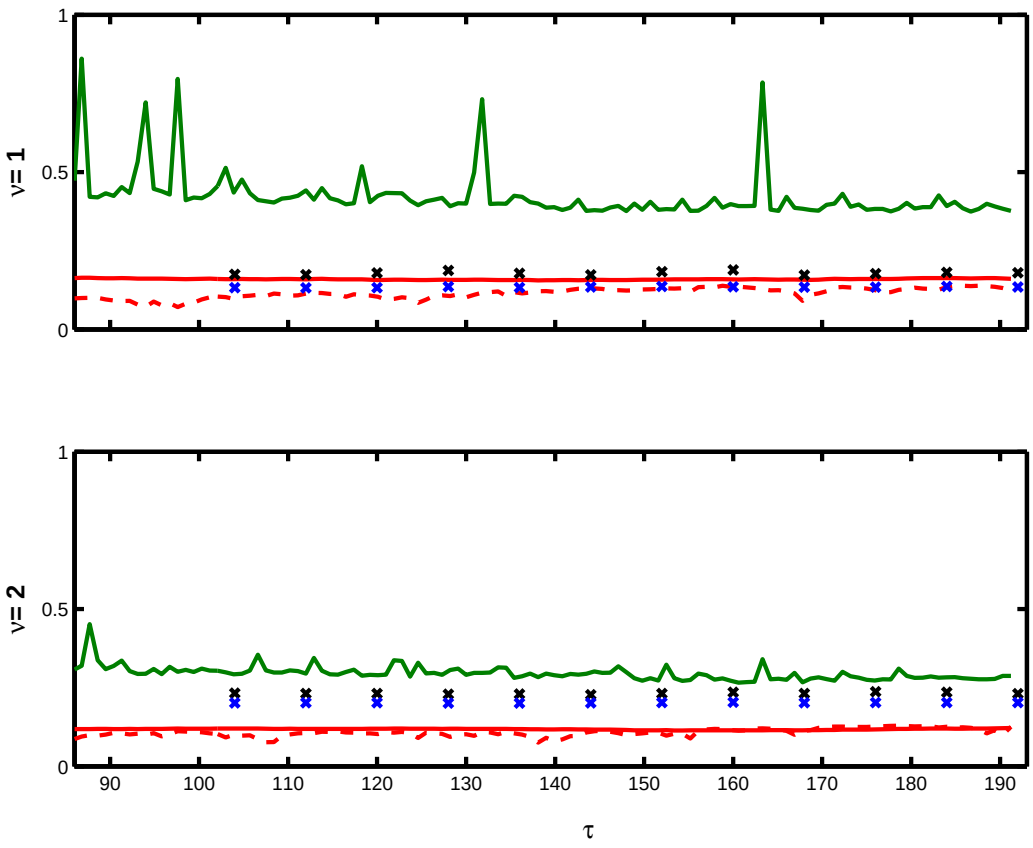

Figure 5.14: Mean square velocities $\langle \dot{\mathbf{X}}^2 \rangle$ of global string networks calculated from field gradients via Eq. (5.58) in red (dashed red indicates Lagrangian weighted), from the velocity operator via Eq. (5.60) in green and from 2χ according to Eq. (5.16) marked as $\mathbf{x}$ at times during scaling for which the tangent vector correlation function (black) and the fractal dimension expansion model (blue) are calculated by fixing $\nu = 1$ for the radiation era and $\nu = 2$ in the matter era.

data is good evidence that the model of [70] describes the dynamics of long string in the Abelian Higgs model well.

We also note that the plaquette weighted RMS velocities are approximately 0.4 for both the radiation and the matter era. These are significantly lower than measured in Nambu-Goto simulations, about 0.66 in the radiation era and 0.61 in the matter era. This is likely to be a result of backreaction from massive radiation, not included in Nambu-Goto simulations. Global string network velocities have been calculated using the velocity operator of Eq. (5.60). Ref. [103], finds $\langle \dot{\mathbf{X}}^2 \rangle = 0.5$ in the radiation era for field theory simulations on an Eulerian mesh. Our results are

shown in Fig. [5.14] and consistently find the velocity operator giving much higher values for the RMS velocity than those found by taking gradients of the Higgs field. We were interested to learn that the ratio of Lagrangian weighted gradients gave a very similar velocity to finding the gradient velocity at the zeroes. This apparent localisation of the Lagrangian density near the global string core would be interesting to follow up on at a later date.

The relationship between 2χ, the velocity and ν is non-linear but simplistically in some fixed era, increasing smoothness of the string and resulting increase in 2χ should be observed as a decrease in mean square velocity. Fig. [5.14] shows the mean square velocities of the network if no correction is made to the expression for 2χ under the local back reaction damping model of Sec. [5.4] but it is not apparent from the disparate values of the velocity calculated by different means as to the nature ν_{eff}.

The results of these numerous velocity calculations are summarised in Table. [5.3] and indicates the difficulty in calculating a consistent value for the velocity of the network. As expected the network velocity calculated from the actual simulation of a string network in the matter era is less than in the radiation era - due to additional background damping. The additional damping and smoothing is replicated in an increasing value for 2χ; though we should note care should be taken in comparing across eras. The trend in velocities for increasing ν, as calculated from the value of 2χ, is to increase which is inconsistent with both global and gauge network velocities. Global strings are expected to have substantial back reaction damping but there seems to be evidence of sufficient back reaction in the gauge string networks for a correction to be necessary. We can compare the velocities and calculate a ν_{eff} in each case. We will compare to both the gradient velocity and the operator velocity to try to determine which is the better estimate. In general the gradient velocity tells us that the network is slower than predicted by 2χ and the operator velocity comes out faster. The values are computed according to

$$\nu_{\text{eff}} = \frac{\chi}{1 - 2\langle \dot{\mathbf{X}}^2 \rangle (1 + \chi)} \tag{5.61}$$

and tabulated in Table. [5.4]. We see that the velocity operator estimate for the RMS velocity gives nonsensical results, casting doubt on its utility.

	Gauge Strings			Global Strings	
	$\nu = 1$	$\nu = 1.5$	$\nu = 2$	$\nu = 1$	$\nu = 2$
$\langle \dot{\mathbf{X}}^2 \rangle_{\rm cx}$	0.24	0.23	0.27	0.18	0.23
$\langle \dot{\mathbf{X}}^2 \rangle_{\rm df}$	0.17	0.21	0.22	0.13	0.20
$\langle \dot{\mathbf{X}}^2 \rangle_{\rm G}$ (Lag)	0.13	0.11	0.11	–	–
$\langle \dot{\mathbf{X}}^2 \rangle_{\rm G}$ (Plq)	0.15	0.13	0.12	0.16	0.12
$\langle \dot{\mathbf{X}}^2 \rangle_{\rm F}$ (Lag)	0.21	0.19	0.18	–	–
$\langle \dot{\mathbf{X}}^2 \rangle_{\rm F}$ (Plq)	0.20	0.17	0.16	–	–
$\langle \dot{\mathbf{X}}^2 \rangle_{\rm Y}$	0.35	0.28	0.29	0.41	0.29

Table 5.3: Summary of velocities. $\langle \dot{\mathbf{X}}^2 \rangle_{\rm cx}$ and $\langle \dot{\mathbf{X}}^2 \rangle_{\rm df}$ are inferred from the values of 2χ found by fitting the tangent vector correlation function to $1 - corr_{\rm x}$, Eq. (5.17) and the fractal dimension expansion, Eq. (5.25), respectively. The rest are calculated from the simulation directly as described in Sec. [5.5]. With (Lag) denoting Lagrangian weighting and (Plq) denoting velocities are found only at plaquettes threaded by string.

		$\nu_{\rm eff}$	
		$\langle \dot{\mathbf{X}}^2 \rangle_{\rm G}$	$\langle \dot{\mathbf{X}}^2 \rangle_{\rm Y}$
AH radiation	$\chi_{\rm cx} = 0.40$	0.69	19.4
	$\chi_{\rm df} = 0.52$	0.96	−7.8
AH matter	$\chi_{\rm cx} = 0.50$	0.78	3.8
	$\chi_{\rm df} = 0.60$	0.97	8.3
G radiation	$\chi_{\rm cx} = 0.47$	0.89	−2.3
	$\chi_{\rm df} = 0.58$	1.16	−2.0
G matter	$\chi_{\rm cx} = 0.56$	0.89	5.7
	$\chi_{\rm df} = 0.66$	1.09	17.4

Table 5.4: Values for $\nu_{\rm eff}$ for gauge (AH) and global (G) string in matter and radiation eras calculated from Eq. (5.61) using observed network velocities from field gradients Eq. (5.58) and from the operator velocity Eq. (5.60).

5.6 Summary

The two point tangent vector correlation function Eq. (5.17) and fractal dimension expansion model Eq. (5.25) are predicted in Ref. [70] to obey a power law form. We calculate the functions for cosmic string networks formed in local and gauge field theories and find strong evidence of a power law. There is general agreement between the power law and the predicted form of the exponent, Eq. (5.16) which is calculated from the average network velocity and the scale factor's exponent with time, ν.

Taking into account a radiation field creating a back reaction effect on the string we show that the scaling principle behind the form for the tangent vector correlation function can be reconciled with a smoothing of the string that behaves in the same way as Hubble damping so that the exponent for the power law can be redefined in terms of an effective ν. Numerical simulations are performed for both local and global strings, but the velocity measurements are not reliable enough to demonstrate an effect.

Chapter 6

Loops

In the standard lore, a network of strings with scaling energy density $\rho \propto t^{-2}$ that loses energy by the production of loops at a typical size of order the horizon, t, must produce those loops at a rate $\dot{n} \propto t^{-4}$ [86]. But loop production in cosmic string networks is still a subject of some debate despite a number of recent numerical investigations using the Nambu-Goto approximation [75, 67, 61], taking advantage of improvements in computational facilities and algorithms, and focusing on small scale structure and loop production rates.

The crucial quantities in question are the loop (length) distribution function and the loop production function. Unfortunately, different groups measure different quantities, and emphasise different features, so the results are difficult to compare.

Those that measure the loop production function [67, 61] find that it peaks at a small scale, with a power law rise [67], and a less prominent feature at about a tenth of the horizon length, t. The identity of the small scale peak is not clear, but on inspection of the data [61, 67], it appears to be related to (and at least no greater than) the initial comoving correlation length. Full scaling requires that the only scale in the distribution and production functions should be t: the peak therefore does not scale. Furthermore, it is found that the amplitude of the power law does not scale either [67].

Measurements of the loop distribution function on the other hand [75], show a peak at the initial numerical cut-off, and scaling at intermediate scales. The peak is understandable as a transient from the initial evolution, but as the distribution function is essentially the time integral of the production function, the intermediate

range scaling is a puzzle.

It has been suggested that the non-scaling of the loop production function is a transient effect [61, 67], and that the peak should eventually disappear altogether [67] or start scaling if only a large enough simulation could be performed [61]. However, the evidence that a power law with a small scale cutoff is a real feature of Nambu-Goto string networks has been strengthened thanks to the agreement with Polchinski and collaborators' model of loop production [70, 71, 35]. There is also no evidence for scaling of the peak in the loop production function from visual inspection of the graphs in Refs. [61, 67].

Accepting the emergence of a power law form for the loop production function, a small scale cut-off is required to keep the total energy loss finite. The conventional string scenario demands full scaling, and invokes gravitational radiation reaction to change the loop production scale to a constant fraction of the horizon size, which is $(G\mu)^{1+2\chi}t$, according to Ref. [71] and outlined in Sec. [2.3.3]. However, there are no network simulations including gravitational radiation reaction so this is still a conjecture. It could equally well be that loop production really does not scale as the Nambu-Goto simulations suggest; this does not prevent the energy density of the long string network from scaling. Furthermore, if the small scale cut-off is the string width [97], it is necessary to perform field theory simulations in order to include the true small scale physics.

Previous field theory simulations of the Abelian Higgs model [95, 62] have not studied the loop distributions in any detail, but it is already clear that their properties are very different from the Nambu-Goto versions. The number of loops in the simulation volume is substantially less, which prompted the suggestion [95] that the network could lose energy to classical radiation directly rather than via the production and eventual decay of loops. Arguing in favour of loop production, it was pointed out in [62] that even if all the energy is lost to "core" or "proto"-loops (loops whose length is of order the string width) that the number density would be very low anyway, approximately t^{-3}. It was also conjectured that these protoloops would eventually grow if a large enough simulation could be performed.

Global strings in field theory simulations [100, 103, 102] have been found to

produce loops at horizon scale according to the one-scale model with

$$n = \frac{v}{t^2(l + \kappa t)^2}$$

in the matter era with $\kappa \sim 0.48$ and

$$n = \frac{v}{t^{3/2}(l + \kappa t)^{5/2}}$$

in the radiation era with $\kappa \sim 0.5$. Initially it was argued that horizon scale loops produced by global string networks would have to fragment in order to preserve scaling as their higher velocities due to the long range force would cause reconnection probabilities to be high. It was found however that the timescale of boson emission causes parent loops to shrink before the need to fragment and scaling is maintained. Lack of fragmentation is evident from our results outlined below.

6.1 Protoloop Distributions

The Polchinski model shows how the small scale structure accounts for the production of loops at the small scale cut off in Nambu-Goto simualtions. We are led to investigate loop distributions in field theory simulations also, and to try to connect small scale structure and energy loss by looking for core width sized protoloops.

In the first part of this section we test the hypothesis that a substantial fraction of the energy loss from long strings is in the form of protoloops. The impression given by visualisations such as Fig. [2.2] is that direct radiation appears to be very important, although it is very difficult to tell the difference between a large amplitude excursion by the Higgs field and a core loop. However, if energy loss into protoloops is important we would expect to find protoloops near long strings, and our first test is to look for these correlations.

We define a protoloop to be made from the minimum number of lattice segments to create a closed loop (i.e. 4 linked segments, located as described in Sec. [4.1.2]. With the choice of constants for our theory as given in Sec. [4.1.1], the protoloop length is approximately the string width. We then measure the distance from protoloops to the closest point on a neighbouring piece of string and the length of the string to which it is closest. The results are shown in Fig. [6.1]. Interestingly, for Abelian Higgs networks, it is seen that protoloops lie close to other very small loops

and that these clusters or isolated protoloops lie at distances of order half the correlation length from long string; between two long strings. As loops collapse they appear to fragment into clusters of very small loops but the lack of protoloops close to long strings argues against small loop production being a significant source of energy loss from long strings.

In contrast with it particularly clear in the radiation era, the protoloops in global string simulations are local to other small loops but also found near long string. This indicates that both energy loss channels are at play. If massive radiation is somehow suppressed in global string decay since they are smoother, it may be that the wiggles on the strings are of large enough amplitude to form small loops.

We can also check the hypothesis by looking at the number distribution of loops in field theory simulations, using a large number of runs. The length scales of interest are the string width (protoloops) and the network correlation length, ξ, defined as Eq. (4.16). Fig. [6.2] shows cumulatively the number densities of loops per horizon in the radiation era of Abelian Higgs simulations over the conformal time range $64 < \tau < 128$ when the network is scaling. The loops are divided into those of length 4 links (protoloops), those up to length ξ, and those longer than ξ. In each of these classes the number density of loops per horizon appears to be constant with protoloops seen to occupy a very small fraction, of order 0.1.

We can estimate whether this is consistent with protoloops being a significant channel of energy loss for long strings. If an Abelian Higgs network with comoving length scale $\xi = \beta\tau$ decays into loops of size $\bar{l}$, then their lifetime should also be $\bar{l}$, given the shrinking mechanism outlined in Ch.4. By conservation of energy $-\frac{d}{dt}(\xi^{-2}) \sim n(\tau, \bar{l})$, so the number of loops per horizon volume $n(\tau, \bar{l})\tau^3$ should be $\sim \beta^{-2}$. Given that $\beta \sim 0.3$ (Fig. [4.1]), there are roughly 100 times too few protoloops if they were to take a significant amount of energy away from long strings in Abelian Higgs networks.

Our result seems to be in contradiction to Ref. [62], who use a fit to the Velocity-dependent One-Scale model [59] to argue that loop production is significant in their field theory simulations. However, their algorithm for the equations of motion differ from ours in the rescaling of the coupling constants plus they do not give absolute values of the loop distribution function, so it is not possible to compare the results

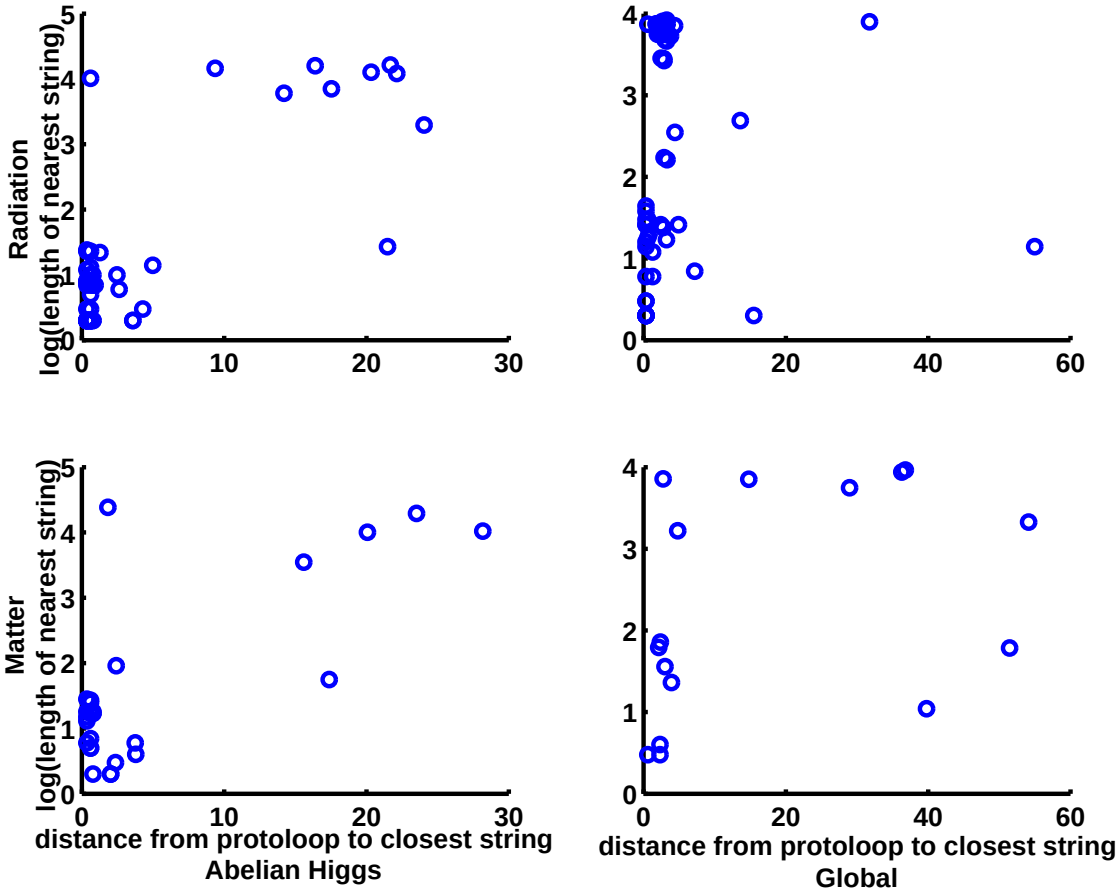

Figure 6.1: Distance of protoloops to other Abelian Higgs string (left) in the radiation era in the top plot and matter era in the lower plot. Small loops lie close together in clusters in the voids between long strings at about half the average interstring distance, $\sim \xi/2$. Emission of protoloops directly from long string is not evident. In contrast, particularly for the radiation era, Global string protoloops (right) are located near string of all lengths indicating no preference for direct production, shrinking or fragmentation.

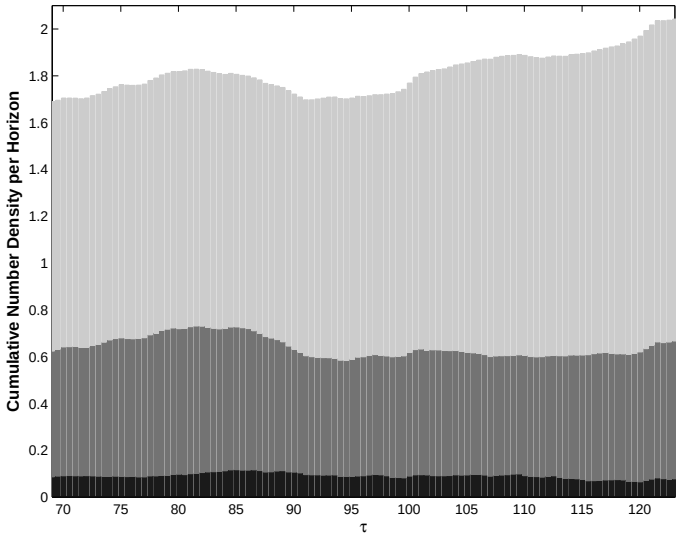

Figure 6.2: Number of abelian-Higgs string loops per horizon volume (shown cumulatively) in the radiation era over the scaling epoch $64 < \tau < 128$ of $512^3\Delta x$ simulations (average of 20 runs) with data smoothed by further averaging results over blocks of 10τ. Black represents proportion by number of protoloops of size the order of the string core width, δ; dark grey represents loops up to the size of the average interstring distance, $\xi(\tau)$; light grey represents all string that is greater in length than ξ and considered to be infinite string.

directly. One possible resolution, explored in more detail below, is that horizon-size loops with lifetime $\sim t$ are carrying away an appreciable fraction of the energy.

Fig. [6.3] shows the number density distribution of global string loops, again in the radiation era. These simulations are comfortably performed on a larger lattice as no gauge fields are required so we observe the same 3 length scales of loops over the longer conformal time range $96 < \tau < 192$. We see that there are significantly fewer strings in global string simulations, of order 1 per horizon in total, but the density of protoloops per horizon is still of order 0.1.

Global string loops shrink faster than Abelian Higgs loops due to Goldstone boson emission and have a decay rate $\mathcal{O}(10)$, as verified in Sec. [4.2]. By the conservation of energy argument above with $\beta \sim 0.6$ for global string, the production of protoloops is potentially another significant energy loss mechanism. It is possible that the importance of protoloops could be coupling constant dependant as global string networks are an extreme case of the coupling constant ratio. This scenario

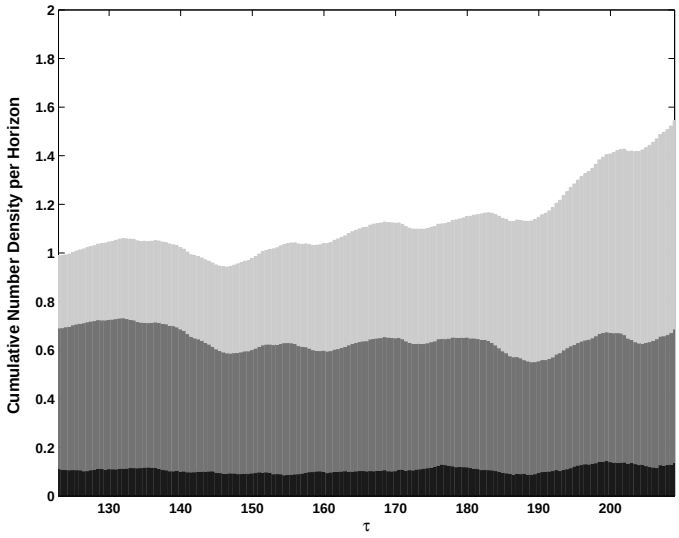

Figure 6.3: Number of global string loops per horizon volume in the radiation era over the scaling epoch $96 < \tau < 192$ of $(768\Delta x)^3$ simulations (average of 6 runs) with data smoothed by averaging results over blocks of 10τ. The colour grading is the same as in Fig. [6.2] for the 3 bands of loop lengths.

has been explored by Ref. [2].

6.2 Loop Distribution Function

6.2.1 Gauge Strings

To study the loop distribution and production functions in more detail, we must model both the production and shrinking of loops. We denote the loop distribution function in terms of the cosmic time t and physical length l_p as $n_p(t, l_p)$, where $l_p = a(t)l$ and l is the comoving loop length, which is given in terms of the string variables ϵ and σ by $l = \int \epsilon \mathrm{d}\sigma$. We denote the comoving loop distribution function in conformal time as $n(\tau, l)$. Then the number density of loops $n_p(t, l_p)\mathrm{d}l_p$ in physical length interval $[l_p, l_p + \mathrm{d}l_p]$ is related to the comoving number density of loops $n(\tau, l)\mathrm{d}l$ in interval $[l, l + \mathrm{d}l]$ by

$$\begin{aligned} n(\tau, l)\mathrm{d}l &= a^3 n_p(t, l_p)\mathrm{d}l_p \\ \Rightarrow \quad n(\tau, l) &= a^4 n_p(t, l_p) \end{aligned} \tag{6.1}$$

The equation governing the loop distribution function, [3] is

$$\frac{\partial n_p}{\partial t} + 3Hn_p + \frac{\partial l_p}{\partial t}\frac{\partial n_p}{\partial l_p} = P_p(t, l_p) \tag{6.2}$$

where $H = \frac{1}{a}\frac{\mathrm{d}a}{\mathrm{d}t}$ and we introduce the loop production function in physical units P_p. We also take into account energy loss from loops which we shall assume takes place at a constant rate such that $\frac{\partial l_p}{\partial t} = -\lambda$. We estimate $\lambda \sim \mathcal{O}(1)$ for Abelian Higgs string from the properties of the energy loss mechanism outlined in Sec. 2.3.2[1]. Using Eq. (6.1) we can relate the comoving number density distribution and the loop production function in comoving units

$$\frac{\partial n}{\partial \tau} - \frac{\dot{a}}{a}n - \lambda\frac{\partial n}{\partial l} = P(\tau, l) \tag{6.3}$$

where $P(\tau, l) = a^5 P_p(t, l_p)$.

Assuming scaling, the comoving loop production function and number density distribution behave as [92]

$$n(\tau, l) = \tfrac{1}{\tau^4}N(x) \text{ and } P(\tau, l) = \tfrac{1}{\tau^5}f(x)$$

for functions N and f of the dimensionless ratio of loop length to horizon size $x = l/\tau$. Rewriting Eq. (6.3) in terms of N and f one obtains (with $a \propto \tau^\nu$),

$$(x + \lambda)N'(x) + (\nu + 4)N(x) = -f(x)$$

with solution

$$N(x) = (x + \lambda)^{-(\nu+4)} \int_x^\infty f(x')(x' + \lambda)^{\nu+3}\, dx'. \tag{6.4}$$

Numerical simulations suggest a power law for loop production, $f \propto x^\alpha$ below $x \sim 1$. If radiative effects can be neglected ($x \gg \lambda$), and making the reasonable assumption that f vanishes for $x \gg 1$, we have from Eq. (6.4)

$$N \propto f \propto x^\alpha. \tag{6.5}$$

For length scales where radiative effects are strong ($x \ll \lambda$)

$$N \propto x^{\alpha+1}. \tag{6.6}$$

[1] Gravitational radiation would give $\lambda \sim \Gamma G\mu$ were it to be included

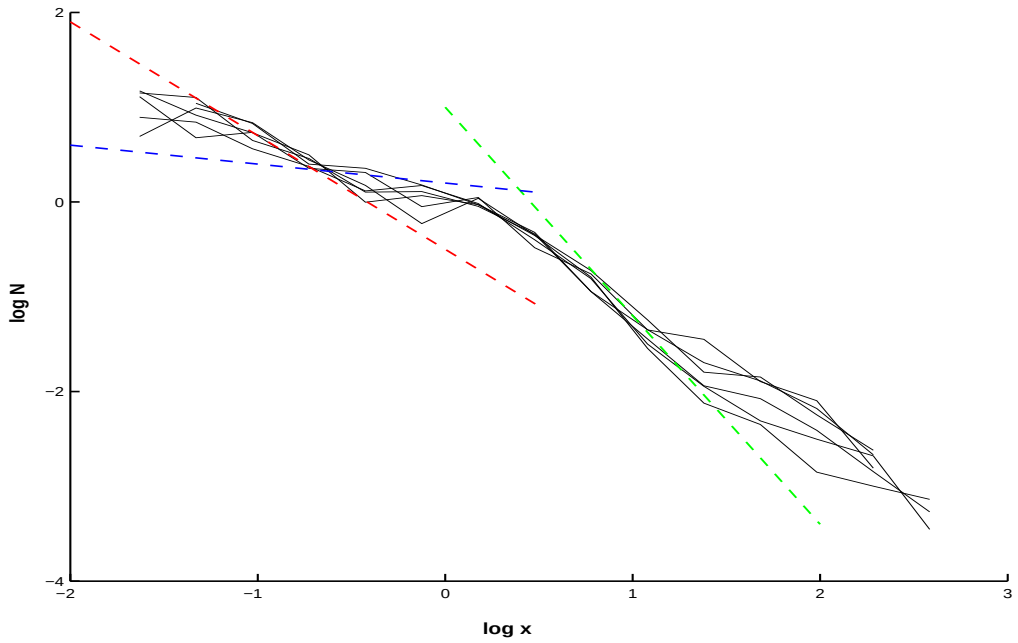

Figure 6.4: Number density distribution of loop lengths, N, against $x \propto l/\tau$ for Abelian Higgs strings in the radiation era. The slope predicted by the model of Ref. [35], $\alpha = 2\chi - 3$, including radiative effects at small scales as in Eq. (6.6) is shown with $\alpha + 1 = 2\chi - 2 = -1.2$ in red, where α is the power of the loop production function. At longer length scales where radiative effects can reasonably be ignored we show the slope $\alpha = -2.2$ in green. Combining the model of Ref. [54] at small scales the power for the loop production function becomes $\alpha' = 2\chi - 2$. With radiative effects included we show the slope of $\alpha' + 1 = -0.2$ in blue. Values for 2χ taken from the 3 parameter fit to the correlation function given in Table. 5.1.

To make our measurement we define the comoving loop number density in a length interval $\Delta l = l$

$$\Delta n = \int_{l}^{2l} n(\tau, l')\mathrm{d}l'.$$

Figs. [6.4] and [6.5] show an estimate for

$$N(x) = \tau^4 \frac{\Delta n}{\Delta l}$$

taken from the average of 20 runs in radiation and matter eras respectively. The solid black line in Fig. [6.6] shows the initial loop distribution function, in good agreement with the expected power law of slope $-5/2$, [87]. For a network that has reached scaling, the analytic model of Ref. [70], further refined by Dubath et al

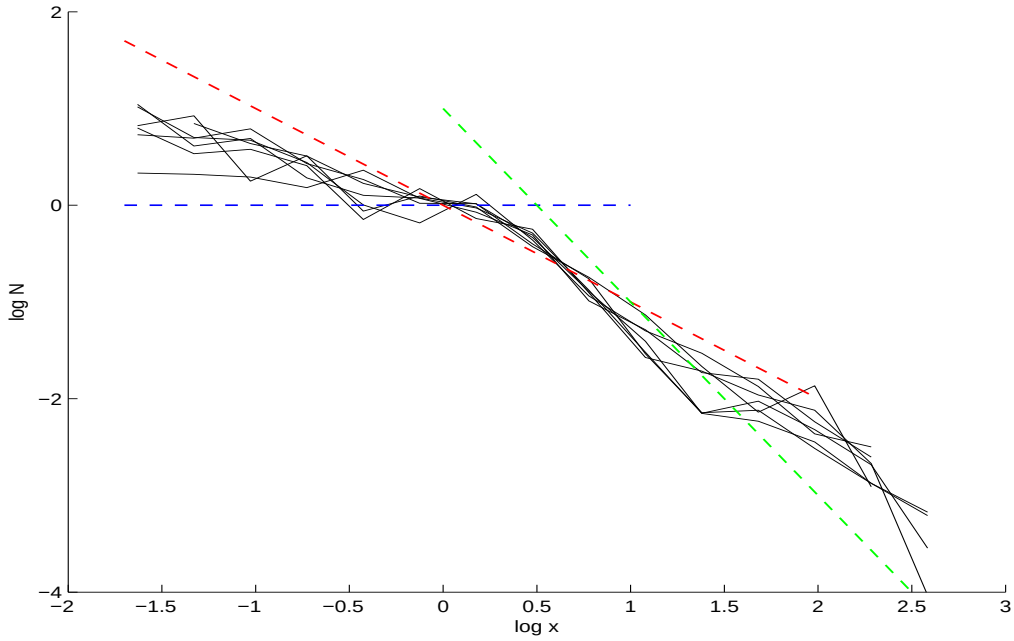

Figure 6.5: Number density of loops, N, of Abelian Higgs string in the matter era with slope $\alpha + 1 = -1$ (red) predicted by the model of Ref. [35] including radiative effects at small scales as in Eq. (6.6). Without radiative effects, at longer length scales, we show $\alpha = -2$ (green). Ref. [54] predicts $N^{\alpha'}$ with $\alpha' = 2\chi - 2$ at small length scales and we show comparison to $\alpha' + 1 = 0$ (blue) for when radiative effects are also added.

in [35], proposes that loop density is dominated by recently produced loops. They derive a function for loop production which they extrapolate to loop number density distribution under the assumption that radiative effects can be ignored and obtain

$$f \propto \left(\frac{l}{\tau}\right)^{2\chi-3} \tag{6.7}$$

with χ defined in Eq. (5.16). If radiative effects are considered the exponent for the number density distribution function will be higher by +1 at small length scales by the arguments from Eqs. (6.4) and (6.6). This is also consistent with the analytic findings of Rocha in Ref. [76] where the loop distribution model is enhanced by including of the effects of gravitational radiation. From the values of 2χ calculated from our simulation results and given in Table. 5.1, this would give exponents of $\alpha_{\rm R} + 1 \sim -1.2$ in the radiation era and $\alpha_{\rm M} + 1 \sim -1.0$ in the matter era which are compared to our data in Figs. [6.4] and [6.5]. The agreement remains less than convincing, particularly for the radiation era.

Olum et al [67] calculate the loop production function $f(x)$ from their Nambu-Goto simulations. The function drops from a small scale peak with a power law consistent with the model proposed by Dubath et al [35]: $f \propto x^{2\chi-3}$. The exponent is calculated using Eq. (5.16) with velocities taken from simulations of Ref. [62]; $v_R = 0.63$ and $v_M = 0.57$. No fit values for the gradient of $\log f$ are quoted in Ref. [67] but pictures showing average gradients of their loop production function in the matter and radiation era are used in Ref. [35] to demonstrate their model. Exponents are listed in Table. 6.1.

Number densities can also be compared with Nambu-Goto simulations of Ref. [75] who quote a length distribution,

$$xN(x) \propto x^p \tag{6.8}$$

They find a consistent power law over the whole range of their Nambu-Goto simulation with exponents $p = -1.6$ for the radiation dominated era and $p = -1.4$ in the matter era. Given that there is no radiative decay mechanism in Nambu-Goto simulations we can infer slopes for the loop production function of $\alpha = -2.6$ and $\alpha = -2.4$ for radiation and matter eras respectively, in good agreement with the values predicted by the model [35] for Nambu-Goto strings. However, even if radiative effects are taken into consideration these results are steeper than those predicted

for our Abelian Higgs strings, (see Table. 6.1), which are already too steep to fit our data.

The flatter power law for loop distributions found in the field theory examination Figs. [6.4] and [6.5] can be better explained by invoking loop production and fragmentation at horizon scales combined with energy loss at small scales. From Ref. [78] it is predicted that unusual power laws for the production of loops can be explained by loop fragmentation probabilities, q, with $f \propto l^{-2q}$. For small loops where radiative effects are strong, number density distribution functions will take the form $N \propto x^{-2q+1}$. Then the steepest slope possible at these small length scales would be -1 when the fragmentation probability is of order unity.

We also see evidence of loop production at the horizon scale in the small feature visible in the loop distribution function at $\log x \simeq 0.5$, which has some similarity to the Nambu-Goto simulations of [67]. It is straightforward to check that the production of one such loop per horizon volume per Hubble time is sufficient to remove a significant fraction of the energy in long strings. Given that these loops are losing length at a rate of order 1 as well as fragmenting, this is consistent with our observation of order one loop per horizon volume at any time. The correlation of protoloops with other small loops shown Fig. [6.1] can also be explained by loop fragmentation.

A further explanation for the flatter distribution has been put forward by Ref. [54]. They construct a continuous number density distribution function which exhibits different scaling over 3 domains of x. The power $\alpha = 2\chi - 3$ has been shown to be reasonable on scales $x \gg x_d = -\frac{dl}{d\tau}$. In the length scale range from the gravitational cutoff, x_c, to x_d the power law for the number density distribution has been shown to follow

$$N_{(x_c<x\ll x_d)} \propto \frac{x^{2\chi-2}}{x_d} \tag{6.9}$$

Since our lower cutoff for the smallest loops produced can be taken as the string width and for our simulations $x_d = \mathcal{O}(1)$, this coincides with the range of scales where radiative effects are also strong so overall our number density power law should then be consistent with $\alpha + 2$. This value is shown in Figs. [6.4] and [6.5] against the measured number density distributions in Abelian Higgs simulations.

Finally, we note that the large $x = l/\tau$ behaviour in our number density analysis

	α_R	α_M
Abelian Higgs Prediction	-2.2	-2.0
Nambu-Goto Prediction	-2.8	-2.5
Nambu-Goto Measurement	-2.6	-2.4

Table 6.1: Table to show comparison of simulation results for the exponent α obtained for a power law model for loop production as Eq. (6.7) in both radiation (R) and matter (M) eras. The first line shows our values calculated using the velocities $\langle \dot{\mathbf{x}}^2 \rangle_{2\chi}$ from Table 5.3. The second line shows the exponent predictions calculated using velocities obtained from Ref. [61] which fits well to Nambu-Goto simulations of Ref. [67]. The last line shows exponents derived from measured length distributions in Nambu-Goto simulations by Ref. [75].

remains a puzzle, as it departs from the -2.5 slope expected outside the horizon. It may be that the loop distribution at these much longer length scales is quite sensitive to the finite volume of the simulation [8].

6.2.2 Global Strings

For global string networks the loop number density distribution function is shown in Fig. [6.7]. The distribution becomes very flat at small scales but the power law seems steeper and more consistent over a wider range of scales than for Abelian Higgs networks. That the power law is constant to longer length scales is reasonable since according to our model for including radiation effects in the number density distribution Eq.(6.6), the lengthscales in question are $x \ll \lambda$ and for global strings we have found that $\lambda \sim \mathcal{O}(10)$. Like Abelian Higgs strings though, since there are so few loops, a fit to our data is unreliable. A comparison to slopes calculated from the 2χ model are shown as an indicator and shows this model with radiation taken additionally into consideration to have reasonable success.

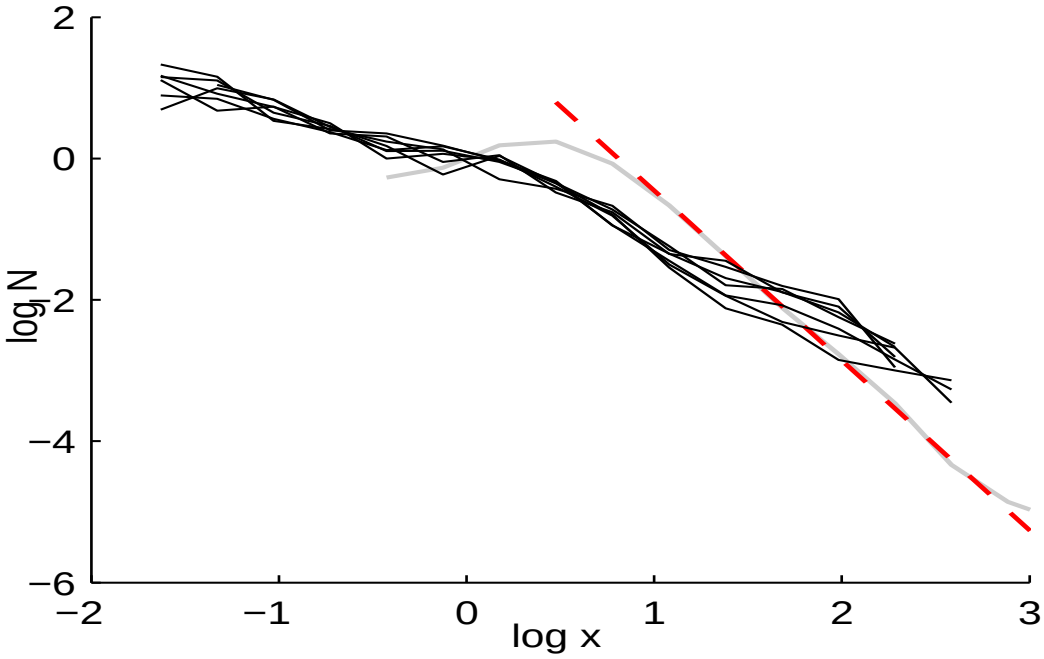

Figure 6.6: The loop number density $N = \tau^4 \Delta n/\Delta l$, per comoving logarithmic bin length Δl is shown for 7 equally spaced times throughout the scaling epoch of the radiation era against the dimensionless ratio $l/\xi \propto x$. This is compared with the very early time $\tau = 10$ case in solid black which is compatible for $l \gg \tau$ with slope -5/2 (shown dashed) as predicted in [87].

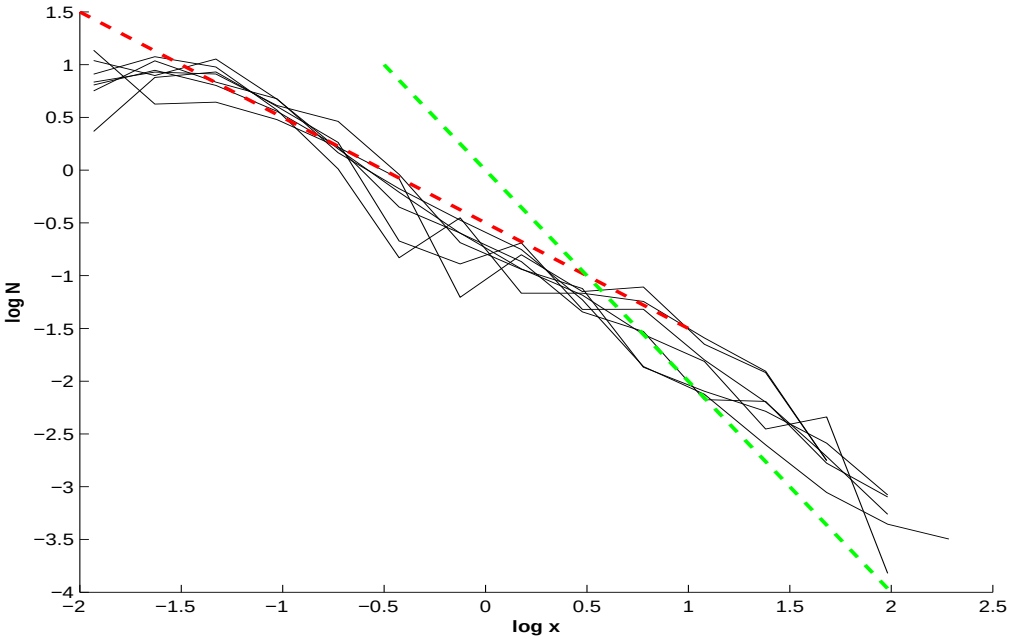

Figure 6.7: The loop number density distribution for global string networks in the radiation era. Using the value for 2χ taken from the 3 parameter fit to the correlation function given in Table. 5.2 we show the slopes for $\alpha = 2\chi - 3$ (green) and $\alpha + 1 = 2\chi - 2$ (red).

Chapter 7

Summary and Conclusions

We have analysed cosmic string networks from Abelian Higgs and Goldstone field theory simulations in order to establish the significance of small scale structure on their dynamics. A cosmic string network settles into to a scaling evolution whereby the mean interstring distance, ξ, remains a fixed fraction of the horizon size $\mathcal{O}(\tau)$, where τ is conformal time.

By continuing the efforts made in Kibble's 3 scale model [6] in terms of correlations in the tangent vectors along the string, Polchinski et al [70] reveal that a power law can be expected for scaling evolutions of gauge string in a correlation function defined by

$$1 - \mathrm{corr_x}(\sigma, \tau) = \mathrm{A}\left(\frac{s}{\xi}\right)^{2\chi}$$

We confirm that this correlation function is valid and scales for string networks in both the Abelian Higgs and Goldstone models with non-guassianity of the systems not seeming to effect the qualitative agreement. The parameter 2χ is evaluated and, despite the difficulties in measuring network velocities $\langle \dot{x}^2 \rangle$, the formula

$$2\chi = \frac{2\nu(1 - 2\langle \dot{\mathbf{x}}^2 \rangle)}{1 + 2\nu\langle \dot{\mathbf{x}}^2 \rangle}$$

is found to be generally consistent with our data for ν defined by scale factor $a = \tau^\nu$. Scaling in the tangent vector correlator is an attractor solution as evident from an over-damped system rapidly relaxing to a scaling evolution once additional damping is removed and there is no evidence of memory of initial conditions with the value for 2χ settling to the same value in spite of the length of the interval of over-damping.

The fractal dimension of long string can also be formulated in terms of a power

law in 2χ

$$d_f \simeq 1 + \frac{A\chi}{(2\chi+1)(2\chi+2)}\left(\frac{s}{\tau}\right)^{2\chi} + \mathcal{O}\left(\frac{s}{\tau}\right)^{4\chi}.$$

making the relationship between 2χ and 'smoothness' clear. We find a clear indication of scaling in this definition though the values for 2χ and A are slightly elevated for a match to the correlation function.

For global strings the correlation function also scales according to the same formula with the value for 2χ greater than for Abelian Higgs strings indicating they are indeed smoother, as expected. We calculate the effect due to backreaction from a radiation field using the local backreaction approximation of Battye et al [11] and under the scaling assumption, we find that the power law will change rather than necessarily introduce a small scale cut off in the correlation function. We demonstrate how the power, 2χ, is changed due to the additional damping by radiative back reaction from the Goldstone field, finding that the effect behaves in a similar way to Hubble damping that can be incorporated into the formula with an effective ν. Due to construction using an anti-symmetric tensor field in the Kalb-Ramond action is it reasonable to expect that gravitational radiation damping will also act like a Hubble damping.

Small scale structure is significant in determining the size of loops emitted from the long string network which is a key contributor to cosmic strings achieving the scaling regime. The loop production function is linked to the correlation function by the proposed model of Polchinski and collaborators via a power law distribution for the number density of loops in terms of the parameter 2χ

$$N \propto \left(\frac{s}{\tau}\right)^{2\chi-3}.$$

The observed power law for loop distributions for our field theory simulations do not agree well with the prediction from this model, even taking into account the radiative decay channel open to field theory strings for which we make a simple modification and show the power law is decreased by 1 on scales where radiative effects will be significant. An enhancement to the model by Ref. [54] suggests that the power for small scales should be $2\chi - 2$ even for Nambu strings, but this still provides a less than convincing fit to our data.

A further mechanism effecting decay of loops is their fragmentation to smaller loops as they continue to self intersect until they are small enough to evaporate.

Evidence shows that core sized protoloops in Abelian Higgs networks are not located near long strings but are likely produced in fragmentation of horizon sized loops. Further, there are not enough of them, roughly 0.1 per horizon volume, to be a significant direct energy loss channel for the long string network. A model for loop distributions with a flat fragmentation probability q explored by Sherrer et al [78]

$$N \propto l^{-2q}$$

is more consistent with our loop production data.

Since Abelian Higgs strings are not found to directly produce many small loops, the graviational radiation from string networks will be suppressed so that it is unlikely that the gravitational wave signatures from the early universe will be influenced to any great extent by the presence of strings. It would appear that detecting strings will rely on the analysis of cosmic ray signals however the types of particle produced by strings is model dependant.

In global string networks we find that there is a spatial correlation between long string and protoloops plus an appreciable amount of energy is lost to loops of the smallest length scales. We conclude that the smoothness of global strings, evident from a higher 2χ, could be enough to raise the amplitude of small scale structure to allow the formation of recognisable loops instead of energy being released into massive radiation as favoured by gauge strings.

The results presented in Chapter 5 can be used to provide an explanation to the scale separation problem: how massive radiation of frequency around the inverse string width is produced from fields which are apparently changing with a frequency of about the Hubble rate. It was established from the tangent vector correlation function that there is small-scale structure on all scales between the Hubble length and the string width. This means that strings are not smooth on scales near the string width, and hence there are oscillation modes with frequency of order the inverse string width, which is sufficient to generate massive radiation. For smoother strings where the small amplitude fluctuations are damped, recognisable loops at the string width scale can be formed. We also explain why the correlation function and loop production functions for string networks scale without including the effects from radiative back reaction in that he value for 2χ incorporates the damping effects of a massless radiation field which behaves like Hubble damping. To quantify the

effect requires a technically difficult calculation of the third derivative of the position vector and we leave this as an open question for future investigation.

Bibliography

[1] UK National Cosmology Supercomputer: SGI Altix 3700 containing 152 Intel Itanium II CPUs. 40

[2] A. Achucarro and G. J. Verbiest. Higher order intercommutations in Cosmic String Collisions. 2010. 81

[3] A. Albrecht and N. Turok. Evolution of cosmic strings. *Phys. Rev. Lett.*, 54(16):1868–1871, Apr 1985. 82

[4] Andreas Albrecht and Neil Turok. Evolution of Cosmic String Networks. *Phys. Rev.*, D40:973–1001, 1989. 20, 48

[5] B. Allen and E. P. S. Shellard. Cosmic string evolution: A numerical simulation. *Phys. Rev. Lett.*, 64:119–122, 1990. 20

[6] Daren Austin, Edmund J. Copeland, and T. W. B. Kibble. Evolution of cosmic string configurations. *Phys. Rev.*, D48:5594–5627, 1993. 50, 90

[7] Daren Austin, Edmund J. Copeland, and T. W. B. Kibble. Characteristics of cosmic string scaling configurations. *Phys. Rev.*, D51:2499–2503, 1995. 50

[8] Daren Austin, Edmund J. Copeland, and R. J. Rivers. The Statistical mechanics of strings on periodic lattices. *Phys. Rev.*, D49:4089–4093, 1994. 87

[9] R. A. Battye and E. P. S. Shellard. Global string radiation. *Nucl. Phys.*, B423:260–304, 1994. 27

[10] R. A. Battye and E. P. S. Shellard. String radiative back reaction. *Phys. Rev. Lett.*, 75:4354–4357, 1995. 27

[11] R. A. Battye and E. P. S. Shellard. Radiative back reaction on global strings. *Phys. Rev.*, D53:1811–1826, 1996. 27, 47, 63, 91

[12] R. A. Battye and E. P. S. Shellard. Spectrum of radiation from axion strings. *Nucl. Phys. Proc. Suppl.*, 72:88–93, 1999. 27

[13] Daniel Baumann. TASI Lectures on Inflation. 2009. 10

[14] David P. Bennett and Francois R. Bouchet. HIGH RESOLUTION SIMULATIONS OF COSMIC STRING EVOLUTION. 1. NETWORK EVOLUTION. *Phys. Rev.*, D41:2408, 1990. 20

[15] Neil Bevis and Mark Hindmarsh. 40

[16] Neil Bevis, Mark Hindmarsh, Martin Kunz, and Jon Urrestilla. Cmb polarization power spectra contributions from a network of cosmic strings. *Phys. Rev.*, D76:043005, 2007. 31

[17] Neil Bevis, Mark Hindmarsh, Martin Kunz, and Jon Urrestilla. Cmb power spectrum contribution from cosmic strings using field-evolution simulations of the abelian higgs model. *Phys. Rev.*, D75:065015, 2007. 23, 36, 37, 38, 39, 40, 41

[18] Neil Bevis, Mark Hindmarsh, Martin Kunz, and Jon Urrestilla. Fitting CMB data with cosmic strings and inflation. *Phys. Rev. Lett.*, 100:021301, 2008. 31

[19] Neil Bevis, Mark Hindmarsh, Martin Kunz, and Jon Urrestilla. CMB power spectra from cosmic strings: predictions for the Planck satellite and beyond. 2010. 31

[20] Neil Bevis and Paul M. Saffin. Cosmic string Y-junctions: a comparison between field theoretic and Nambu-Goto dynamics. *Phys. Rev.*, D78:023503, 2008. 41

[21] Pijushpani Bhattacharjee and Gunter Sigl. Origin and propagation of extremely high energy cosmic rays. *Phys. Rept.*, 327:109–247, 2000. 34

[22] J. J. Blanco-Pillado and Ken D. Olum. The form of cosmic string cusps. *Phys. Rev.*, D59:063508, 1999. 20

[23] E.B. Bogomol'nyi. *Sov. J. Nucl. Phys.*, 24:449, 1976. 15, 39

[24] Szabolcs Borsanyi and Mark Hindmarsh. Semiclassical decay of topological defects. *Phys. Rev.*, D77:045022, 2008. 23

[25] David F. Chernoff and S. H. Henry Tye. Cosmic String Detection via Microlensing of Stars. 2007. 33

[26] E. J. Copeland and T. W. B. Kibble. Kinks and small-scale structure on cosmic strings. *Phys. Rev.*, D80:123523, 2009. 4, 47, 51, 55

[27] Edmund J. Copeland, D. Haws, and M. Hindmarsh. Classical theory of radiating strings. *Phys. Rev.*, D42:726–730, 1990. 27

[28] Edmund J. Copeland, T. W. B. Kibble, and Daren Austin. Scaling solutions in cosmic string networks. *Phys. Rev.*, D45:1000–1004, 1992. 50

[29] A. Dabholkar and J. M. Quashnock. Global strings and the axion mass bound. In *Cambridge 1989, Proceedings, The formation and evolution of cosmic strings* 179-194. (see HIGH ENERGY PHYSICS INDEX 29 (1991) No. 7720). 27

[30] Atish Dabholkar and Jean M. Quashnock. PINNING DOWN THE AXION. *Nucl. Phys.*, B333:815, 1990. 27

[31] Thibault Damour and Alexander Vilenkin. Gravitational wave bursts from cosmic strings. *Phys. Rev. Lett.*, 85:3761–3764, 2000. 20

[32] Thibault Damour and Alexander Vilenkin. Gravitational wave bursts from cusps and kinks on cosmic strings. *Phys. Rev.*, D64:064008, 2001. 20

[33] R. L. Davis and E. P. S. Shellard. Global strings and superfluid vortices. *Phys. Rev. Lett.*, 63(19):2021–2024, Nov 1989. 27

[34] Matthew R DePies and Craig J Hogan. Harmonic Gravitational Wave Spectra of Cosmic String Loops in the Galaxy. 2009. 32

[35] Florian Dubath, Joseph Polchinski, and Jorge V. Rocha. Cosmic String Loops, Large and Small. *Phys. Rev.*, D77:123528, 2008. 3, 20, 23, 52, 57, 76, 83, 84, 85

[36] Sergei Dyda and Robert H. Brandenberger. Cosmic Strings and Weak Gravitational Lensing. 2007. 34

[37] Allen E. Everett. COSMIC STRINGS IN UNIFIED GAUGE THEORIES. *Phys. Rev.*, D24:858, 1981. 22

[38] J. Richard Gott, III. Gravitational lensing effects of vacuum strings: Exact solutions. *Astrophys. J.*, 288:422–427, 1985. 31

[39] Ruth Gregory. Effective actions for bosonic topological defects. *Phys. Rev. D*, 43(2):520–525, Jan 1991. 17

[40] C. Hagmann and P. Sikivie. Computer simulations of the motion and decay of global strings. *Nucl. Phys.*, B363:247–280, 1991. 27

[41] Mark Hindmarsh. Gravitational radiation from kinky infinite strings. *Phys. Lett.*, B251:28–33, 1990. 19, 25, 26

[42] Mark Hindmarsh, Christophe Ringeval, and Teruaki Suyama. The CMB temperature bispectrum induced by cosmic strings. *Phys. Rev.*, D80:083501, 2009. 32

[43] Mark Hindmarsh, Christophe Ringeval, and Teruaki Suyama. The CMB temperature trispectrum of cosmic strings. *Phys. Rev.*, D81:063505, 2010. 32

[44] Mark Hindmarsh, Stephanie Stuckey, and Neil Bevis. Abelian Higgs Cosmic Strings: Small Scale Structure and Loops. *Phys. Rev.*, D79:123504, 2009. 34, 58, 59

[45] Rachel Jeannerot, Jonathan Rocher, and Mairi Sakellariadou. How generic is cosmic string formation in susy guts. *Phys. Rev.*, D68:103514, 2003. 6

[46] Nick Kaiser and A. Stebbins. Microwave Anisotropy Due to Cosmic Strings. *Nature*, 310:391–393, 1984. 31

[47] K. Kajantie, M. Karjalainen, M. Laine, J. Peisa, and A. Rajantie. Thermodynamics of gauge-invariant u(1) vortices from lattice monte carlo simulations. *Phys. Lett.*, B428:334–341, 1998. 40

[48] Michael Kalb and P. Ramond. Classical direct interstring action. *Phys. Rev. D*, 9(8):2273–2284, Apr 1974. 18

[49] T. W. B. Kibble. Topology of cosmic domains and strings. *J. Phys.*, A9:1387–1398, 1976. 18

[50] T. W. B. Kibble. Some Implications of a Cosmological Phase Transition. *Phys. Rept.*, 67:183, 1980. 18

[51] T. W. B. Kibble and Edmund J. Copeland. Evolution of small scale structure on cosmic strings. *Phys. Scripta*, T36:153–166, 1991. 50

[52] E. Komatsu et al. Seven-Year Wilkinson Microwave Anisotropy Probe (WMAP) Observations: Cosmological Interpretation. *Astrophys.J.Suppl.*, 192:18, 2011. 57 pages, 20 figures. Accepted for publication in ApJS. (v2) References added. The SZ section expanded with more analysis. The discrepancy between the KS and X-ray derived profiles has been resolved. (v3) New analysis of the SZ effect on individual clusters added (Section 7.3). The LCDM parameters have been updated using the latest recombination history code (RECFAST version 1.5). 11

[53] Konrad Kuijken, Xavier Siemens, and Tanmay Vachaspati. Microlensing by Cosmic Strings. 2007. 33

[54] Larissa Lorenz, Christophe Ringeval, and Mairi Sakellariadou. Cosmic string loop distribution on all length scales and at any redshift. 2010. 4, 83, 84, 86, 91

[55] Fernando Lund and Tullio Regge. Unified Approach to Strings and Vortices with Soliton Solutions. *Phys. Rev.*, D14:1524, 1976. 18

[56] David H. Lyth and Andrew R. Liddle. The primordial density perturbation: Cosmology, inflation and the origin of structure. 2009. 8

[57] Katherine J. Mack, Daniel H. Wesley, and Lindsay J. King. Observing cosmic string loops with gravitational lensing surveys. *Phys. Rev.*, D76:123515, 2007. 33

[58] C. J. A. P. Martins and E. P. S. Shellard. Quantitative String Evolution. *Phys. Rev.*, D54:2535–2556, 1996. 61

[59] C. J. A. P. Martins and E. P. S. Shellard. Quantitative string evolution. *Phys. Rev. D*, 54(4):2535–2556, Aug 1996. 78

[60] C. J. A. P. Martins and E. P. S. Shellard. String evolution with friction. *Phys. Rev.*, D53:575–579, 1996. 58, 61

[61] C. J. A. P. Martins and E. P. S. Shellard. Fractal properties and small-scale structure of cosmic string networks. *Physical Review D (Particles, Fields, Gravitation, and Cosmology)*, 73(4):043515, 2006. 21, 48, 75, 76, 87

[62] J. N. Moore, E. P. S. Shellard, and C. J. A. P. Martins. On the evolution of abelian-higgs string networks. *Phys. Rev.*, D65:023503, 2002. 21, 22, 23, 38, 41, 76, 78, 85

[63] K. J. M. Moriarty, Eric Myers, and Claudio Rebbi. DYNAMICAL INTERACTIONS OF FLUX VORTICES IN SUPERCONDUCTORS. *Phys. Lett.*, B207:411, 1988. 39

[64] Holger Bech Nielsen and P. Olesen. Vortex-line models for dual strings. *Nucl. Phys.*, B61:45–61, 1973. 15

[65] S. Olmez, V. Mandic, and X. Siemens. Gravitational-Wave Stochastic Background from Kinks and Cusps on Cosmic Strings. *Phys. Rev.*, D81:104028, 2010. 32

[66] Ken D. Olum and J. J. Blanco-Pillado. Radiation from cosmic string standing waves. *Phys. Rev. Lett.*, 84(19):4288–4291, May 2000. 22

[67] Ken D. Olum and Vitaly Vanchurin. Cosmic string loops in the expanding universe. *Phys. Rev.*, D75:063521, 2007. 21, 40, 75, 76, 85, 86, 87

[68] Levon Pogosian, S. H. Henry Tye, Ira Wasserman, and Mark Wyman. Cosmic Strings as the Source of Small-Scale Microwave Background Anisotropy. *JCAP*, 0902:013, 2009. 31

[69] Levon Pogosian and Mark Wyman. B-modes from Cosmic Strings. *Phys. Rev.*, D77:083509, 2008. 31

[70] Joseph Polchinski and Jorge V. Rocha. Analytic study of small scale structure on cosmic strings. *Phys. Rev.*, D74:083504, 2006. 3, 4, 23, 47, 48, 52, 57, 71, 74, 76, 83, 90

[71] Joseph Polchinski and Jorge V. Rocha. Cosmic string structure at the gravitational radiation scale. *Phys. Rev.*, D75:123503, 2007. 21, 23, 26, 52, 57, 76

[72] M. S. Pshirkov and A. V. Tuntsov. Local constraints on cosmic string loops from photometry and pulsar timing. *Phys. Rev.*, D81:083519, 2010. 32

[73] Jean M. Quashnock and David N. Spergel. GRAVITATIONAL SELFINTERACTIONS OF COSMIC STRINGS. *Phys. Rev.*, D42:2505–2520, 1990. 19

[74] D. M. Regan and E. P. S. Shellard. Cosmic String Power Spectrum, Bispectrum and Trispectrum. 2009. 32

[75] Christophe Ringeval, Mairi Sakellariadou, and Francois Bouchet. Cosmological evolution of cosmic string loops. *JCAP*, 0702:023, 2007. 21, 40, 75, 85, 87

[76] Jorge V. Rocha. Scaling solution for small cosmic string loops. *Phys. Rev. Lett.*, 100:071601, 2008. 85

[77] M. Sakellariadou. Gravitational waves emitted from infinite strings. *Phys. Rev.*, D42:354–360, 1990. 25, 26

[78] R. J. Scherrer and W. H. Press. COSMIC STRING LOOP FRAGMENTATION. *Phys. Rev.*, D39:371–378, 1989. 86, 92

[79] Robert J. Scherrer and Alexander Vilenkin. Lattice effects in simulations of topological defect formation. *Phys. Rev.*, D58:103501, 1998. 41

[80] Xavier Siemens and Ken D. Olum. Gravitational radiation and the small-scale structure of cosmic strings. *Nucl. Phys.*, B611:125–145, 2001. 20

[81] Xavier Siemens and Ken D. Olum. Cosmic string cusps with small-scale structure: Their forms and gravitational waveforms. *Phys. Rev.*, D68:085017, 2003. 20

[82] Xavier Siemens, Ken D. Olum, and Alexander Vilenkin. On the size of the smallest scales in cosmic string networks. *Phys. Rev.*, D66:043501, 2002. 26

[83] M. Srednicki and S. Theisen. *Phys. Rev. Lett. B 189*, page 379, 1987. 20

[84] Daniel B. Thomas, Carlo R. Contaldi, and Joao Magueijo. Rotation of galaxies as a signature of cosmic strings in weak lensing surveys. *Phys. Rev. Lett.*, 103:181301, 2009. 34

[85] A. V. Tuntsov and M. S. Pshirkov. Quasar variability limits on cosmological density of cosmic strings. *Phys. Rev.*, D81:063523, 2010. 33

[86] Neil Turok and Pijushpani Bhattacharjee. STRETCHING COSMIC STRINGS. *Phys. Rev.*, D29:1557, 1984. 75

[87] Tanmay Vachaspati and Alexander Vilenkin. Formation and Evolution of Cosmic Strings. *Phys. Rev.*, D30:2036, 1984. 83, 88

[88] Tanmay Vachaspati and Alexander Vilenkin. Gravitational Radiation from Cosmic Strings. *Phys. Rev.*, D31:3052, 1985. 19

[89] Vitaly Vanchurin. Non-linear dynamics of cosmic strings with non-scaling loops. *Phys. Rev.*, D82:063503, 2010. 58

[90] Vitaly Vanchurin. Semi-scaling cosmic strings. 2010. 58

[91] A. Vilenkin. Cosmic Strings. *Phys. Rev.*, D24:2082–2089, 1981. 18

[92] Alexander Vilenkin and Edward P. Shellard. *Cosmic Strings and Other Topological Defects*. Cambridge: Cambridge University Press, 1994. 82

[93] Alexander Vilenkin and Tanmay Vachaspati. Radiation of goldstone bosons from cosmic strings. *Phys. Rev. D*, 35(4):1138–1140, Feb 1987. 18

[94] Alexander Vilenkin and Tanmay Vachaspati. RADIATION OF GOLDSTONE BOSONS FROM COSMIC STRINGS. *Phys. Rev.*, D35:1138, 1987. 61

[95] Graham Vincent, Nuno D. Antunes, and Mark Hindmarsh. Numerical simulations of string networks in the abelian-higgs model. *Phys. Rev. Lett.*, 80(11):2277–2280, Mar 1998. 21, 22, 23, 41, 76

[96] Graham R. Vincent, Mark Hindmarsh, and Mairi Sakellariadou. Correlations in cosmic string networks. *Phys. Rev. D*, 55(2):573–581, Jan 1997. 41

[97] Graham R. Vincent, Mark Hindmarsh, and Mairi Sakellariadou. Scaling and small scale structure in cosmic string networks. *Phys. Rev.*, D56:637–646, 1997. 21, 76

[98] S. Weinberg. *Gravitation and Cosmology*. New York: Wiley, 1972. 19

[99] Edward Witten. Cosmic Superstrings. *Phys. Lett.*, B153:243, 1985. 18

[100] Masahide Yamaguchi. Scaling property of the global string in the radiation dominated universe. *Phys. Rev.*, D60:103511, 1999. 27, 76

[101] Masahide Yamaguchi, M. Kawasaki, and Jun'ichi Yokoyama. Evolution of axionic strings and spectrum of axions radiated from them. *Phys. Rev. Lett.*, 82:4578–4581, 1999. 27

[102] Masahide Yamaguchi and Jun'ichi Yokoyama. Quantitative evolution of global strings from the Lagrangian view point. *Phys. Rev.*, D67:103514, 2003. 27, 69, 76

[103] Masahide Yamaguchi, Jun'ichi Yokoyama, and M. Kawasaki. Evolution of a global string network in a matter dominated universe. *Phys. Rev.*, D61:061301, 2000. 27, 71, 76

Appendix A

Leap-Frog Algorithm

The algorithm for the equations of motion of the Abelian Higgs model are found from variation of the discretised action

$$
\begin{aligned}
S \;=\; \Delta\tau\,(\Delta x)^3 \sum_{\tau}\sum_{\mathbf{x}}\Bigg(& -\frac{1}{2e_{\tau}^{2}\,(\Delta x)^4}\sum_{i}\sum_{j}\left[1-\cos(\Delta_{ij}^{x+\frac{1}{2}i+\frac{1}{2}j,\tau})\right] \\
& +\frac{1}{2e_{\tau+\frac{1}{2}}^{2}(\Delta x)^2(\Delta\tau)^2}\sum_{i}\left(\theta_i^{x+\frac{1}{2}i,\tau+1}-\theta_i^{x+\frac{1}{2}i,\tau}\right)^2 \\
& +a_{\tau+\frac{1}{2}}^{2}\left|\frac{\phi^{\mathbf{x},\tau+\mathbf{1}}-\phi^{\mathbf{x},\tau}}{\Delta\tau}\right|^2-a_{\tau}^{2}\sum_{i}\left|\frac{\phi^{x+i,\tau}e^{i\theta_i^{x+\frac{1}{2}i},\tau}-\phi^{\mathbf{x},\tau}}{\Delta x}\right|^2 \\
& -a_{\tau}^{4}\frac{\lambda_{\tau}}{4}\left(|\phi^{\mathbf{x},\tau}|^2-\eta^2\right)^2\Bigg). \qquad \text{(A.1)}
\end{aligned}
$$

where ϕ is the Higgs field and θ is the phase associated with the gauge field.

From the Euler-Lagrange equations of motion we calculate the evolution of each field from one time step to the next where Π is the time derivative of ϕ, and ϵ the time derivative of θ and Δ_{ij} is defined in Eq. 4.12

$$\phi^{\mathbf{x},\tau+\mathbf{1}} = \phi^{\mathbf{x},\tau} + \Delta\tau\Pi^{\mathbf{x},\tau+\frac{\mathbf{1}}{\mathbf{2}}} \tag{A.2}$$

$$\begin{aligned}\Pi^{\mathbf{x},\tau+\frac{\mathbf{1}}{\mathbf{2}}} &= \left(\frac{a_{\tau-\frac{1}{2}}}{a_{\tau+\frac{1}{2}}}\right)^2 \Pi^{\mathbf{x},\tau-\frac{\mathbf{1}}{\mathbf{2}}} - \Delta\tau\left(\frac{a_\tau^2}{a_{\tau+\frac{1}{2}}}\right)^2 \frac{\lambda_\tau}{2}\left(|\phi^{\mathbf{x},\tau}|^2-\eta^2\right)\phi^{\mathbf{x},\tau} \\ &+ \frac{\Delta\tau}{(\Delta x)^2}\left(\frac{a_\tau}{a_{\tau+\frac{1}{2}}}\right)^2 \sum_j \left(\phi^{\mathbf{x}+\mathbf{j},\tau}\exp(i\theta^{\mathbf{x}+\frac{\mathbf{1}}{\mathbf{2}}\mathbf{j},\tau}) - 2\phi^{\mathbf{x},\tau} + \phi^{\mathbf{x}-\mathbf{j},\tau}\exp(-i\theta^{\mathbf{x}-\frac{\mathbf{1}}{\mathbf{2}}\mathbf{j},\tau})\right)\end{aligned} \tag{A.3}$$

$$\theta_i^{\mathbf{x}+\frac{\mathbf{1}}{\mathbf{2}}\mathbf{i},\tau+\mathbf{1}} = \theta_i^{\mathbf{x}+\frac{\mathbf{1}}{\mathbf{2}}\mathbf{i},\tau} + \Delta\tau\epsilon_i^{\mathbf{x},\tau+\frac{\mathbf{1}}{\mathbf{2}}} \tag{A.4}$$

$$\begin{aligned}\epsilon_i^{\mathbf{x},\tau+\frac{\mathbf{1}}{\mathbf{2}}} &= \left(\frac{e_{\tau+\frac{1}{2}}}{e_{\tau-\frac{1}{2}}}\right)^2 \epsilon_i^{\mathbf{x},\tau-\frac{\mathbf{1}}{\mathbf{2}}} + 2\Delta\tau a_\tau^2 e_{\tau+\frac{1}{2}}^2 \mathcal{I}\Updownarrow\left[\left(\phi^{\mathbf{x}+\mathbf{i},\tau}\right)^* \exp(-i\theta^{\mathbf{x}+\mathbf{i},\tau})\phi^{\mathbf{x},\tau}\right] \\ &- \frac{\Delta\tau}{(\Delta x)^2}\left(\frac{e_{\tau+\frac{1}{2}}}{e_\tau}\right)^2 \sum_{j\neq i}\left[\sin\left(\Delta_{ij}^{\mathbf{x}+\frac{\mathbf{1}}{\mathbf{2}}\mathbf{i}+\frac{\mathbf{1}}{\mathbf{2}}\mathbf{j},\tau}\right) - \sin\left(\Delta_{ij}^{\mathbf{x}+\frac{\mathbf{1}}{\mathbf{2}}\mathbf{i}-\frac{\mathbf{1}}{\mathbf{2}}\mathbf{j},\tau}\right)\right].\end{aligned} \tag{A.5}$$